

2

REPORT DOCUMENTATION PAGE

AD-A199 811

2b. DECLASSIFICATION/DOWNGRADING SCHEDULE OCT 06 1988		1b. RESTRICTIVE MARKINGS	
4. PERFORMING ORGANIZATION REPORT NUMBER(S)		3. DISTRIBUTION/AVAILABILITY OF REPORT Approved for public release; distribution unlimited.	
6a. NAME OF PERFORMING ORGANIZATION Drexel University ECE Department		5. MONITORING ORGANIZATION REPORT NUMBER(S) AFOSR-TR- 88-1012	
6b. ADDRESS (City, State and ZIP Code) Philadelphia, PA 19104		7a. NAME OF MONITORING ORGANIZATION AFOSR	
8a. NAME OF FUNDING/SPONSORING ORGANIZATION AFOSR		7b. ADDRESS (City, State and ZIP Code) Bldg 410 Bolling AFB DC	
8b. OFFICE SYMBOL (If applicable) LIE		9. PROCUREMENT INSTRUMENT IDENTIFICATION NUMBER AFOSR-84-0125	
8c. ADDRESS (City, State and ZIP Code) Bldg 410 Bolling Air Force Base, D.C. 20332		10. SOURCE OF FUNDING NOS. PROGRAM ELEMENT NO. 61102F PROJECT NO. 2306 TASK NO. A3 WORK UNIT NO.	
11. TITLE (Include Security Classification) Research on the Statistics of Grain Voltage Echoes and their use in Grain Size Estimation and Grain Echo Suppression			
12. PERSONAL AUTHOR(S) F. Karpur, V.L. Newhouse (Principal Investigator)			
13a. TYPE OF REPORT Final		13b. TIME COVERED FROM 6/84 TO 3/88	
		14. DATE OF REPORT (Yr., Mo., Day) 8/19/88	
		15. PAGE COUNT 154	
16. SUPPLEMENTARY NOTATION			
17. COSATI CODES FIELD GROUP SUB GR.		18. SUBJECT TERMS (Continue on reverse if necessary and identify by block number)	
19. ABSTRACT (Continue on reverse if necessary and identify by block number) <p>Split spectrum processing (SSP) was developed in the late-Seventies for ultrasonic applications as a convenient method of introducing frequency diversity in ultrasonic signals for the purpose of the reduction of coherent material noise. Although the technique is very powerful, the use of SSP remained somewhat limited because of the ambiguity that prevailed in the selection of suitable processing parameters. The ambiguity was mainly because of the lack of a physical model of the spectral splitting process. The need for such a physical modeling has been fulfilled in the course of this investigation. An ultrasonic signal has been modeled as a time-limited process which facilitates the use of the frequency sampling theorem to describe the frequency splitting process. Further,</p> <p style="text-align: right;">(cont)</p>			
20. DISTRIBUTION/AVAILABILITY OF ABSTRACT UNCLASSIFIED/UNLIMITED <input checked="" type="checkbox"/> SAME AS RPT. <input type="checkbox"/> DTIC USERS <input type="checkbox"/>		21. ABSTRACT SECURITY CLASSIFICATION UNCLASSIFIED	
22a. NAME OF RESPONSIBLE INDIVIDUAL Scholer		22b. TELEPHONE NUMBER (Include Area Code) (202) 767-4931	
		22c. OFFICE SYMBOL LIE	

the theory of Fourier integrals is used to determine the bandwidth of the theoretical SINC filters obtained as per the frequency sampling theorem. Experimental results have been provided to corroborate the theory.

Another aspect of SSP addressed here is a detailed theoretical analysis of a newly developed algorithm called the Polarity Thresholding (PT) algorithm. An elaborate analysis of such a newly developed algorithm is essential for an understanding of the operation of the algorithm, to predict the signal-to-noise ratio (SNR) enhancement obtainable for different input and processing parameters, as well as to develop the receiver operating characteristics (ROC) of the algorithm. The analysis will also provide the limits of operation of the algorithm. The PT algorithm has been analyzed here by first developing the probability density function (pdf) of the output of the algorithm. From this the SNR enhancement curves, the probabilities of detection and false alarm, and hence the ROC of the algorithm have been derived. Experimental SNR enhancement results are also provided to demonstrate the effectiveness of the PT algorithm in SNR enhancement.

Yet another important aspect of SSP addressed in this report is the demonstration of the utility of SSP in many engineering materials, such as centrifugally cast stainless steel (CCSS), composites, and interface between bimetallic alloys. The potential of SSP as a tool for material characterization is also experimentally demonstrated.

Accession For	
NTIS GRA&I	<input checked="" type="checkbox"/>
DTIC TAB	<input type="checkbox"/>
Unannounced	<input type="checkbox"/>
Justification	
By	
Date	
Distribution	
Availability	
Notes	
A-1	



2000 FILE COPY
AFOSR-TR- 88-1012

Grant No. AFOSR-84-0125

Research on the Statistics of Grain Lattice Echoes
and their use in
Grain Size Estimation and Grain Echo Suppression

Final Report for the Period
June 1, 1984 - March 31, 1988

by

Prasanna Karpur, Ph.D.
Department of Electrical and Computer Engineering
Drexel University

and

V.L. Newhouse, Ph.D.
Robert C. Disque Professor of
Electrical and Computer Engineering
Drexel University

Project Director: V.L. Newhouse

August 1988

TABLE OF CONTENTS

LIST OF TABLES.....	vi
LIST OF ILLUSTRATIONS.....	vii
ABSTRACT.....	xiv
1. INTRODUCTION.....	1
Methods of NDE.....	1
Acoustic Emission.....	1
Eddy Current.....	1
Leak Testing.....	2
Liquid Penetrant Test.....	2
Magnetic Particle Test.....	2
Radiography.....	2
Visual Examination.....	3
Ultrasonic Testing.....	3
Material Noise in Ultrasonic Signals.....	3
Methods of Noise Suppression.....	4
Synopsis of the following chapters.....	7
2. ULTRASONIC SPECKLE, SPECKLE SUPPRESSION AND SPLIT SPECTRUM PROCESSING.....	9
Ultrasonic Speckle and Speckle Suppression.....	9
Split Spectrum Processing (SSP).....	15
3. PROBLEM STATEMENT, OBJECTIVES AND METHODOLOGY.....	20
Problem Statement.....	20
Objectives and Contributions of this Dissertation.....	21
Methodology.....	23
Process Modeling.....	23
Performance evaluation of the Polarity Thresholding Algorithm	23

	iv
Utility of Split Spectrum Processing in Ultrasonic NDE.....	24
4. PROCESS MODELING AND PARAMETER SELECTION.....	25
Split Spectrum Processing Methodology..	25
Number of Filters and Their Bandwidth.....	27
Theory.....	28
Experimental Results.....	31
Discussion.....	40
Considerations for the Estimation of the Available Bandwidth of the Received Signal for Spectral Splitting.....	41
Experiments to Evaluate the Usable Bandwidth of the Spectrum of the Received Signal.....	45
Discussion.....	46
Summary.....	53
5. POLARITY THRESHOLDING ALGORITHM: AN EVALUATION OF PERFORMANCE.....	54
Introduction.....	54
Theory.....	55
Mathematical model of the signal.....	56
Polarity Thresholding algorithm.....	58
Density function of Polarity Thresholding.....	59
Results of theoretical analysis.....	64
SNR enhancement curves.....	64
SNR enhancement for the signal in the total range of T sec.....	64
SNR enhancement at a time delay in the presence and in the absence of a target.....	69
Probabilities of false alarm and detection.....	78
Receiver Operating Characteristics (ROC).....	82
Receiver Operating Characteristics when no threshold is set to the processed output.....	82
ROC of the algorithm by Neyman-Pearson Criterion.....	82
Summary.....	93

6. UTILITY OF SPLIT SPECTRUM PROCESSING IN ULTRASONIC NDE.....	94
Introduction.....	94
Algorithms of SSP.....	95
Minimization.....	96
Polarity Thresholding.....	96
Experimental Results.....	98
Signal-to-noise Ratio Enhancement in 1-D RF Signals.....	98
Centrifugally Cast Stainless Steel.....	98
Composite Material.....	110
Zircalloy-Zirconium Tubing.....	110
Speckle Reduction in 2-D B-scan Images.....	119
Potential of SSP as a tool for material characterization....	122
Theory.....	122
Experiments.....	124
Discussion.....	138
Summary.....	140
7. SUMMARY, CONCLUSIONS AND FUTURE RESEARCH.....	142
Summary.....	142
Conclusions.....	143
Process modeling and parameter selection.....	143
Performance of the Polarity Thresholding algorithm.....	144
Utility of Split Spectrum Processing.....	145
Future Research.....	146
Hardware implementation of SSP.....	146
Split spectrum processing and SAFT.....	147
SSP as a Tool for material characterization.....	147
LIST OF REFERENCES.....	148
VITA.....	155

LIST OF TABLES

Table		Page
4.1	Table showing the relationship between the optimum filter bandwidth and the bandwidth of the transducer.....	42

LIST OF ILLUSTRATIONS

Figure	Page
4.1 Filtering scheme for split spectrum processing.....	26
4.2 a Signal obtained from a welded joint between two 1020 steel plates.....	32
4.2 b Graph of SNR (RMS) vs. total number of filters used for the signal in Figure 4.2a.....	32
4.2 c Performance curves showing the SNR as a function of the filter bandwidth for different number of filters.....	33
4.2 d Graph showing the optimum filter bandwidth and the optimum SNR as a function of the total number of filters used.....	34
4.3 a A signal obtained from an equiaxed CCSS test block showing the backwall echo. The signal from a cylindrical hole is completely obscured by grain noise.....	35
4.3 b Graph of SNR (RMS) vs. total number of filters used for the signal in Figure 4.3a.....	35
4.3 c Performance curves showing the SNR as a function of the filter bandwidth for different number of filters.....	36
4.3 d Graph showing the optimum filter bandwidth and the optimum SNR as a function of the total number of filters used.....	37
4.4 a Signal obtained from a Carbon-Epoxy composite material.....	38
4.4 b Graph of SNR (RMS) vs. total number of filters used for the signal in Figure 4.4 a.....	38

4.5 a	An impulse response of a 5 MHz nominal center frequency transducer in a standard reference stepped block.....	43
4.5 b	The magnitude - frequency spectrum of the impulse response shown in Figure 4.5a.....	43
4.6 a	An ultrasonic signal obtained from an equiaxed CCSS test block using the transducer having an impulse response as shown in as shown in Figure 4.5a.....	44
4.6b	The magnitude - frequency spectrum of the signal shown in Figure 4.6a.....	44
4.7	Signal-to-noise ratio enhancement curve due to split spectrum processing the signal in 4.6a using minimization followed by polarity thresholding algorithms. The echo from the flat back surface of the sample has been used as a target	47
4.8	A hypothetical transducer spectrum and the grain scattering response shown on the same frequency axis to demonstrate the influence of grain scattering on the performance of a transducer.....	48
4.9	Signal_to_noise ratio enhancement plotted as a function of the number of filters used for spectral splitting. Minimization followed by polarity thresholding algorithms are used for the processing. The target echo is from a cylindrical hole of 3 mm diameter.....	51
5.1	An ultrasonic signal obtained from a centrifugally cast stainless steel block with a side drilled hole. The figure illustrates the various time delays used in the theoretical analysis.....	57
5.2	Theoretical signal-to-noise ratio curves showing the SNR enhancement of the whole signal when all the time delays are considered.....	66
5.3	Experimental signal-to-noise ratio curves using i. polarity thresholding alone ii. minimization and polarity thresholding used in tandem iii. minimization alone.....	68
5.4 a	The processor output signal for an input signal as shown in Figure 5.1. Filters with a half power bandwidth of 0.092 MHz are used for the	

processing.....	70
5.4 b The processor output for filters of half power bandwidth of 0.172 MHz.....	71
5.4 c The processor output for filters of half power bandwidth of 0.460 MHz.....	72
5.5 a Theoretical signal-to-noise ratio (variance) curves of the processor at a time delay where only the grain noise and no target exists.....	74
5.5 b Theoretical signal-to-noise ratio (variance) curves of the processor at a time delay where both the grain noise and a target signal exists.....	75
5.6 Theoretical signal-to-noise ratio curves showing the effect of processing on the mean of the output signal.....	77
5.7 Probability of False Alarm as a function of the number of windows used for the processing.....	80
5.8 Probability of detection curves plotted as a function of the number of filters used and the input signal-to-noise ratio.....	81
5.9 Receiver operating characteristics of the algorithm obtained for a case when no threshold is set to the output of the algorithm.....	83
5.10 An enlarged version of the curves in Figure 5.9.....	84
5.11 a Receiver operating characteristics of the Neyman-pearson criterion for a case of a simple thresholding of the input signal (without any processing).....	89
5.11 b Receiver operating characteristics of the Neyman-Pearson criterion for the output of the Polarity Thresholding algorithm when three filters are used.....	90
5.11 c Receiver operating characteristics of the Neyman-Pearson criterion for the output of the Polarity Thresholding algorithm when five filters are used.....	91
5.11 d Receiver operating characteristics of the Neyman-Pearson criterion	

for the output of the Polarity Thresholding algorithm when seven filters are used.....	92
6.1 Minimization algorithm applied to the split time domain signals. Only the first and the N^{th} split time domain signals are shown along with the minimized signal.....	97
6.2 a An ultrasonic signal obtained from an equiax grained CCSS sample showing the back wall echo. The signal from a side drilled hole is completely obscured by grain noise.....	99
6.2 b The frequency - magnitude spectrum of the signal shown in Figure 6.2 a.....	99
6.2 c The processed signal after applying minimization algorithm to the signal shown in Figure 6.2a.....	100
6.2 d The frequency - magnitude spectrum of the processed signal shown in Figure 6.2c.....	100
6.2 e The processed signal after a low frequency bandpass filtering of the spectrum shown in Figure 6.2d. The backwall echo and the signal from the cylindrical hole are seen.....	101
6.2 f The processed signal after applying minimization and polarity thresholding algorithms to the signal shown in Figure 6.2a.....	101
6.2 g The frequency - magnitude spectrum of the processed signal in Figure 6.2f.....	102
6.2 h The processed signal after a low frequency bandpass filtering of the spectrum shown in Figure 6.2g. The backwall echo, the signal from the cylindrical hole and the reverberating echoes are seen.....	102
6.3 a An ultrasonic signal obtained from an equiax grained CCSS sample showing echo signals from the backwall and a cylindrical hole.....	105
6.3 b Minimized and lowpass filtered signal.....	105
6.3 c Minimized, polarity thresholded and lowpass filtered signal.....	105

6.4 a	An ultrasonic signal obtained from a columnar grained sample. The angle of interrogation is zero degree with respect to the axis of orientation of the grains.....	106
6.4 b	Minimized and lowpass filtered signal.....	106
6.4 c	Minimized, polarity thresholded and lowpass filtered signal.....	106
6.5 a	An ultrasonic signal obtained from a columnar grained sample. The angle of interrogation is 15 degrees with respect to the axis of orientation of the grains.....	107
6.5 b	Minimized and lowpass filtered signal.....	107
6.5 c	Minimized, polarity thresholded and lowpass filtered signal.....	107
6.6 a	An ultrasonic signal obtained from a columnar grained sample. The angle of interrogation is 45 degrees with respect to the axis of orientation of the grains.....	108
6.6 b	Minimized and lowpass filtered signal.....	108
6.6 c	Minimized, polarity thresholded and lowpass filtered signal.....	108
6.7 a	An ultrasonic signal obtained from a columnar grained sample. The angle of interrogation is 75 degrees with respect to the axis of orientation of the grains.....	109
6.7 b	Minimized and lowpass filtered signal.....	109
6.7 c	Minimized, polarity thresholded and lowpass filtered signal.....	109
6.8	A pictorial cross section of the Carbon-Epoxy composite material used for the experiment.....	111
6.9 a	Unprocessed signal obtained from the Carbon-Epoxy Composite material shown in Figure 6.8.....	112
6.9 b	Minimized signal showing the echoes from the composite layers.....	112

6.10	A pictorial cross section of the Zircalloy tube showing the Zirconium lining and a grain abnormality causing an ultrasonic 'dead zone'.....	113
6.11 a	Signal obtained from a 'normal zone' of a zircalloy tubing. The signal shows the front wall echo and the backwall echo. Interface echo is not seen due to insufficient gain.....	115
6.11 b	Signal in Figure 6.11a after an additional 30 dB of amplification. The interface echo is seen. Front wall and the back echoes are distorted.....	115
6.11 c	A 'composite' signal obtained by superimposing the signal in gate A-B of Figure 6.11b on Figure 6.11a.....	115
6.12 a	Signal obtained from a 'dead zone' of a zircalloy tube. The signal shows the front wall and the back wall echoes. The interface echo is not seen due to insufficient gain.....	116
6.12 b	Signal in Figure 6.12a after an additional 30 dB of gain. The interface echo is obscured due to grain noise.....	116
6.12 c	Minimized and polarity thresholded output of the gated signal A-B in Figure 6.12 b.....	118
6.12 d	A 'composite' signal obtained by superimposing Figure 6.12c on to Figure 6.12a.....	118
6.13 a	An unprocessed B-scan image of an equiax grained CCSS block showing pronounced speckl pattern obscuring the signals from the backwall and the cylindrical hole.....	120
6.13 b	Processed B-scan image after applying polarity thresholding to the image shown in Figure 6.13a.....	121
6.14 a	A centrifugally cast stainless steel pipe.....	125
6.14 b	A section of the CCSS pipe shown in Figure 6.14a.....	125
6.14 c	A test sample prepared from the CCSS pipe section.....	126

6.15 a	Signal-to-noise ratio curves of the split time domain signals obtained for equiax grained CCSS for 0 degree wave incidence.....	128
6.15 b	Signal-to-noise ratio curves of the split time domain signals obtained for equiax grained CCSS for 15 degrees wave incidence.....	129
6.15 c	Signal-to-noise ratio curves of the split time domain signals obtained for equiax grained CCSS for 45 degrees wave incidence.....	130
6.15 d	Signal-to-noise ratio curves of the split time domain signals obtained for equiax grained CCSS for 75 degrees wave incidence.....	131
6.15 e	Signal-to-noise ratio curves of the split time domain signals obtained for equiax grained CCSS for 90 degrees wave incidence.....	132
6.16 a	Signal-to-noise ratio curves of the split time domain signals obtained for columnar grained CCSS for 0 degree wave incidence.....	133
6.16 b	Signal-to-noise ratio curves of the split time domain signals obtained for columnar grained CCSS for 15 degree wave incidence.....	134
6.16 c	Signal-to-noise ratio curves of the split time domain signals obtained for columnar grained CCSS for 45 degree wave incidence.....	135
6.16 d	Signal-to-noise ratio curves of the split time domain signals obtained for columnar grained CCSS for 75 degree wave incidence.....	136
6.16 e	Signal-to-noise ratio curves of the split time domain signals obtained for columnar grained CCSS for 90 degree wave incidence.....	137
6.17	Schematic diagram showing a possible plane of orientation of a defect with respect to the axis of the transducer.....	139

ABSTRACT

Split Spectrum Processing: Process Modeling and the Evaluation of Polarity Thresholding Algorithm for Material Noise Reduction in Ultrasonic NDE.

Author: Prasanna Karpur

Supervising Professors: J. L. Rose and V. L. Newhouse

Split spectrum processing (SSP) was developed in the late seventies for ultrasonic applications as a convenient method of introducing frequency diversity in ultrasonic signals for the purpose of the reduction of coherent material noise. Although the technique is very powerful, the use of SSP remained somewhat limited because of the ambiguity that prevailed in the selection of suitable processing parameters. The ambiguity was mainly because of a lack of a physical model of the spectral splitting process. The need for such a physical modeling has been fulfilled as a part of this dissertation. An ultrasonic signal has been modeled as a time limited process which facilitates the use of the frequency sampling theorem to describe the frequency splitting process. Further, the theory of Fourier integrals is used to determine the bandwidth of the theoretical SINC filters obtained as per the frequency sampling theorem. Experimental results have been provided to corroborate the theory.

Another aspect of SSP addressed by this thesis is a detailed theoretical analysis of a newly developed algorithm called the Polarity Thresholding (PT) algorithm. An elaborate analysis of such a newly developed algorithm is essential for an understanding of the operation of the algorithm, to predict the signal-to-noise ratio (SNR) enhancement obtainable for different input and processing parameters as well as to develop the receiver operating characteristics (ROC) of the algorithm. The analysis will also provide the limits of operation of the algorithm. The PT algorithm has been analyzed in this thesis by first developing the probability density function (pdf) of the output of the algorithm using which the theoretical SNR enhancement curves, the probabilities of detection and false alarm and hence the ROC of the algorithm have been derived. Experimental SNR enhancement results

are also provided to demonstrate the effectiveness of the PT algorithm in SNR enhancement.

Yet another important aspect of SSP addressed by this dissertation is the demonstration of the utility of SSP in many engineering materials such as centrifugally cast stainless steel (CCSS), composites and interface between bimetallic alloys. The potential of SSP as a tool for material characterization is also experimentally demonstrated.

1. INTRODUCTION

Nondestructive evaluation (NDE) is a very important aspect of assuring in-service reliability as well as manufacturing integrity of engineering products. It is the process of a complete evaluation of a material to determine any external or internal anomalies, their geometry, orientation, criticality etc., without affecting the functional usefulness of the material being tested. Nondestructive evaluation also includes the characterization of the material itself to determine the material properties such as grain type and size which often critically influence the detection and classification of the anomalies present in the material. The importance of the technique is obvious from the important role it plays in several industries such as utilities, nuclear industry, railways, aerospace, aviation, defense, automobile, metals, nonmetals, construction, chemical and petroleum etc. The multitude of the type of industries and the diversity of the end products which need NDE require the use of many methods of NDE.

1.1 Methods of NDE

The important methods of NDE are i) acoustic emission, ii) eddy current, iii) leak testing, iv) liquid penetrant, v) magnetic particle, vi) radiography, vii) visual examination and vii) ultrasonics. A brief description of each method follows.

1.1.1 Acoustic Emission

Acoustic emission is based on the principle that any imperfections within the material emit short bursts of high frequency sound energy when the material is stressed. The anomaly which is the source of the acoustic emission can be evaluated by studying the energy being emitted by the imperfection.

1.1.2 Eddy current

Eddy current testing is useful in materials which conduct electricity. A magnetic field is applied to the material being tested which results in the flow of electrical currents in the material. However, when imperfections are present in the material or if the properties of

the material change, the flow of the electric current is affected which in turn affects the applied magnetic field. The resultant changes in the magnetic field can be studied to evaluate the test object.

1.1.3 Leak Testing

Leak testing is the process of detecting any leaks in the components which are designed to carry (retain) high pressures. Leak testing can be achieved by various methods such as pressure gauge, pressurized air, high sensitivity listening devices, soap bubble test, etc.

1.1.4 Liquid Penetrant Test

Liquid penetrant method is used to detect surface cracks. A fluorescent (or visible) dye is coated on the surface of the material. The dye is allowed to penetrate any surface cracks. Any excess dye is wiped off and a 'developer' liquid is applied to the surface. The developer has an affinity to the penetrant liquid and hence draws the penetrant from any surface cracks. As a result, the surface cracks become clearly visible either under an ultraviolet source or ordinary light depending on the type of the penetrant used.

1.1.5 Magnetic Particle Test

The magnetic particle test is used to detect surface cracks and imperfections in ferromagnetic materials. A magnetic field is induced in the ferromagnetic material being tested and the surface of the material is dusted with iron particles. The iron particles get oriented along the magnetic field on the surface and thus enhance any surface imperfections which distort the magnetic field.

1.1.6 Radiography

Radiations such as X ray or gamma ray emitted from a radioactive isotope can be used to inspect the inside of materials. The object being tested is irradiated by an incident beam of radiation which passes through the material and falls on a photographic film

located on the other side. The film is then developed to find any imperfections inside the material.

1.1.7 Visual Examination

Visual testing is the simplest and the most extensively used method of NDE. Visual examiners inspect the material for any external imperfections in form, shape and function.

1.1.8 Ultrasonic Testing

Ultrasonics, as the name implies, makes use of sound energy in the inaudible frequency range, usually from several KHz to several MHz. In usual practice, short bursts of ultrasonic energy is transmitted into the material. The pulses of ultrasound travel through the material and are reflected when they encounter imperfections. The reflected echoes are received by a receiving transducer and are analyzed to detect, locate, classify and size the reflecting imperfection.

1.1.8.1 Material Noise in Ultrasonic Signals

One of the major limitations of ultrasonic techniques is the 'Coherent' ultrasonic noise produced by unresolvable scatterers present in the object being tested. The scatterers might be the randomly packed grains found in metals or fibrous texture of the tissue being tested. These scatterers are unresolvable by the interrogating ultrasonic pulse because of their size in relation to the pulse width as well as the interrogating wavelength. The incident ultrasonic wave is randomly scattered by the unresolvable scatterers. The scattered wavelets superimpose on one another producing interference patterns which manifest as coherent noise or clutter in A-mode signals and as speckle in B-mode images. Since clutter might be of equal or even larger amplitude than that of a target, it is quite frequent to come across situations where the coherent noise present in an ultrasonic signal has effectively masked the presence of an anomaly. Thus, it would be extremely difficult to even detect a target, let alone locate, characterize or size the anomaly.

Time variant random noise, like instrumentation noise, is also present in ultrasonic signals. However, since such noise is time variant, suppression of incoherent noise could

be easily achieved by simple signal processing techniques while it is much more difficult to suppress coherent noise. Usually more sophisticated techniques of signal processing techniques are required for coherent noise suppression.

1.1.8.2 Methods of Noise Suppression

There are various techniques available to reduce noise levels in ultrasonic signals. The choice of the technique is determined primarily by the type of noise being suppressed. The ease of application is also a determining factor in the choice of the noise reduction technique. Some of the useful methods of noise reduction are: 1. temporal averaging, 2. correlation reception, 3. spatial compounding, 4. synthetic aperture technique, 5. frequency agility technique, 6. split spectrum processing, etc. A brief description of some of these methods follows.

Temporal Averaging

Temporal averaging or time averaging [1] is an useful technique for the suppression of time variant random noise. Temporal averaging is usually performed by capturing the received signals by repeated transmissions of ultrasonic pulses and averaging these signals to suppress any incoherent noise in the signals. The procedure is usually carried out after A/D conversion and storage in a computer. The randomly varying incoherent noise could be suppressed by this procedure. However, noise produced by the scatterers present in the material being tested can not be reduced by temporal averaging due to time invariant property of such material noise.

Correlation Reception

The principle of operation of correlation receivers [2,3,4] is similar to matched filtering. The transmitted signal is used as a reference signal against which the received echoes are compared to determine how close they match the transmitted signal. The comparison is carried out by multiplying a series of time shifted reference signal and the received signal and finally integrated to find the correlation between the reference signal and the transmitted signal. The resulting autocorrelation function will show large peaks when

echoes from targets are present. The system effectively reduces time dependent noise. Details about such a correlation receiver can be found in the literature [2,3,4].

Spatial Compounding

Spatial compounding, also known as spatial averaging [1,5,6], makes use of the fact that noise present in an ultrasonic signal is produced by the interference of coherently scattered ultrasonic energy. The interference pattern can be altered if the transducer is moved to a new position such that the target of interest is still within the incident beam and, at the same time, a new ensemble of scatterers are insonified thereby creating 'uncorrelated' clutter. When several such uncorrelated signals are coherently averaged, the noise level is substantially reduced while the target signal is relatively unaltered resulting in a SNR enhancement.

Even though spatial compounding is simple and easy to implement, it is not without drawbacks. For a successful implementation of the technique, the plane of the transducer motion should be parallel to the plane of the target of interest. Otherwise, loss of resolution or, under severe conditions, a complete loss of the target signal occurs. The geometry of the test specimen should permit a suitable movement of the transducer.

Directional spatial averaging [5] is a modified version of spatial compounding technique and was introduced to overcome some of the drawbacks of spatial compounding. Directional spatial averaging is implemented by compounding the uncorrelated signals obtained by changing the angle of insonification by small angles. The technique is particularly useful when the surface of wave entry is not planar and/or when the target of interest has a known nonplanar surface (as in organs in medical applications). Again, the technique suffers from the limitation that an a priori knowledge of the location and shape of the target is essential for a successful implementation.

Synthetic Aperture Technique

The synthetic aperture technique has its roots in radar applications [7,8]. One of the modes of implementations in radars is by an aircraft carrying an imaging antenna. The antenna carried by the aircraft produces an image along its path of flight thereby 'synthesizing' a large aperture. The technique has been extended to ultrasonic imaging

[9,10,11,12,13] wherein a large aperture is obtained by either the motion of a single element transducer [12,13] or by a multi element transducer.

In principle, the synthetic aperture technique operates by sequential pulsing of the elements of a multi-element array transducer. One or more elements of the array can be pulsed at a time. The reflected echoes are received by the other elements in the array and coherently summed after suitably compensating for differences in arrival times from element to element. The process is repeated by pulsing each element or groups of elements of the array while listening with the others.

One of the foremost advantages of the technique is that the noise or speckle due to reverberating sound is reduced substantially when the signals received by the different elements are coherently summed. Also, because of a large synthesized aperture, lateral resolution is improved. However, the advantages are not obtained without a price: the hardware and/or the software required is very expensive and involved. Also, the material being tested should have constant velocity with respect to the angle of interrogation. On the other hand, if the velocity is variable with the angle of incidence, the various velocities should be known. Finally, beam skew, if any, will affect the results of the technique.

Frequency Agility Technique

The frequency agility technique of noise reduction was initially introduced in radar applications [8,14]. Uncorrelated speckle patterns in radar images can be achieved when the images used for compounding are obtained by a suitable frequency shift from one image to the other. When such frequency diverse images are compounded either before or after demodulation, the speckle noise is reduced and the target signal, being frequency independent, is unaffected. An extensive literature review of frequency agility in radars can be found in [2].

The frequency agility technique can be extended in principle to ultrasonic imaging also. One of the most successful frequency compounding methods was introduced by Newhouse et al [15]. A detailed literature review on ultrasonic speckle and SSP is contained in the second chapter of this dissertation. A synopsis of the remaining chapters of the thesis follows.

1.2 Synopsis of the following chapters

Chapter 2 Ultrasonic Speckle, Speckle Reduction and Split Spectrum Processing; A Literature Review

The first section of the second chapter contains a detailed literature review of speckle in ultrasonic imaging. The second section of the chapter contains a literature survey of SSP, covering the invention and development of Split Spectrum Processing (SSP). Any existing ambiguities will be pointed out during the literature review as a basis for establishing the need for the present Ph.D. research work.

Chapter 3 Problem Statement, Objectives and Methodology

A statement of the problem, developed with the literature review as the basis, will be presented which in turn will be the basis of the objectives of this research effort. Also, the methodology of research will be discussed.

Chapter 4 Process modeling and Parameter Selection

The parameter selection is formalized by modeling the ultrasonic signal as a time limited, band unlimited process. Analytical expressions to calculate the number of filters and their bandwidth are derived from the analytical physical model. Experimental corroboration is provided by using the minimization algorithm. A rationale based on the physical phenomenon of wave scattering and target geometry is developed to determine the location of the bank of filters used to split the spectrum.

Chapter 5 Polarity Thresholding Algorithm: A Performance Evaluation

This chapter contains a theoretical analysis of the Polarity Thresholding algorithm. A density function of the output of the algorithm is developed based on which SNR curves of various definitions are drawn. The probability of detection and false alarm are studied as functions of input SNR and the number of filters used for the processing. Also, the ROC of the algorithm are drawn. Some experimental results of the effect of using correlated

filters on the SNR enhancement are presented.

Chapter 6 Utility of Split Spectrum Processing

Utility of SSP in problems of engineering interest is demonstrated by experimentation. The potential of SSP as a tool for material characterization is explored. Results of SNR enhancement experiments in various types of engineering materials like centrifugally cast stainless steel and composite materials are also presented.

Chapter 7 Summary, Conclusions and Future Research

This chapter contains a summary of this dissertation, conclusions and possible future directions of the research effort.

2. ULTRASONIC SPECKLE, SPECKLE SUPPRESSION AND SPLIT SPECTRUM PROCESSING

One of the major limitations of ultrasonic techniques is the 'clutter' in A-mode signals which manifests as 'speckle' in B-mode images. Speckle is created due to the interference of ultrasonic energy coherently scattered by the ensemble of unresolvable scatterers found in the resolution cell of the ultrasonic transducer. Speckle is not specific to ultrasonic techniques alone and can be found in laser systems as well. Speckle in laser systems is a well studied and analyzed phenomenon [16]. Speckle can also be found in radar imaging since the radar techniques rely on the coherent property of the received signals [14]. Due to the fact that different fields of imaging are susceptible to speckle formation, the available literature on speckle and speckle reduction is too vast for an exhaustive review. Moreover, extensive reviews of laser speckle [16,17] and speckle in radars [2,14] can be found in the literature. As such, the rest of this chapter will be devoted to ultrasonic speckle phenomenon and methods of acoustical speckle suppression.

2.1 Ultrasonic Speckle and Speckle Suppression

The first major analysis of ultrasonic speckle was provided by Burckhardt, 1978 - [18]. He mentioned that ultrasound images obtained with simple linear or sector scan show a granular appearance which he called 'Speckle'. He analyzed the speckle by modelling the amplitude statistics by Rayleigh probability density function and proposed maximum amplitude writing as an alternate method of speckle reduction (the first method being simple averaging). He showed that if the transducer is moved by at least half its diameter for compounding purposes, the speckle amplitudes of the two images so obtained will be uncorrelated. Under such conditions, he showed that 'maximum amplitude writing' can give almost as much speckle reduction as averaging.

Parker, Pryer and Ridges, 1979 - [19], showed that speckle as well as artifacts in ultrasonic images is mainly due to poor lateral resolution of the system. They showed that the speckle and artifacts due to poor lateral resolution can be substantially reduced by lateral filtering instead of the conventional two dimensional filtering of images. Parker and Pryer, 1982 - [20], in their follow up paper, provided answer to the question of how much information is lost by the resolution limited lateral filtering. They made qualitative as well

as quantitative comparisons of images before and after processing. They concluded that, while processing reduces speckle, increases signal-to-noise ratio and improves continuity of targets, it blurs the image and loses some axial information.

Abbott and Thurstone, 1979 - [17], briefly reviewed the concept of laser speckle using which they explained the phenomenon of acoustic speckle. They discussed the similarities and differences between laser speckle and acoustic speckle and suggested summation of multiple frames of independent speckle patterns as an effective tool to suppress acoustical speckle. Abbott and Thurstone also experimentally showed in their paper that ultrasonic speckle is caused primarily due to phase changes and not amplitude changes across the face of the aperture. They addressed the question of how to generate images with independent speckle patterns and how to combine them into a single image. They concluded that frequency compounding and spatial compounding are feasible and effective approaches for speckle suppression.

Newhouse, Furgason, Bilgutay and Saniie, 1979 - [15], introduced a new and very effective frequency diversity method of ultrasonic speckle reduction. They named their technique 'Split Spectrum Processing (SSP)'. Split spectrum processing was implemented on the receive mode by splitting the spectrum of a received ultrasonic signal into several narrow frequency bands by using several Gaussian filters of different center frequencies. They also introduced an algorithm called Minimization for the purpose of compounding the frequency diverse signals obtained as a result of the frequency splitting process. They reported excellent SNR enhancement with simulated signals. Experimental results were also subsequently reported [2,42].

Wells and Halliwell, 1981 - [21], discussed speckle in ultrasonic imaging. They mentioned that, while speckle is a result of coherency, it does not represent resolvable structure in the tissue and hence is only an artifact. They concluded that speckle can be reduced by a factor of \sqrt{N} when N scans from different directions of interrogation are compounded. They also mentioned that no speckle reduction is achieved by compound scanners with 'last value memory'.

O'Donnell, 1982 - [22], proposed a phase insensitive detection technique to reduce speckle in B-mode images. The technique was implemented by a nonlinear processing of the detected output of an array of transducers. He compared images formed by his phase insensitive method with the images made by the conventional phase sensitive technique and found that the phase insensitivity reduces speckle in B-scan images.

Dickinson, 1982 - [23], processed simulated ultrasound B-scan images using a deconvolution filter. He tested his deconvolution algorithm for both low contrast (objects of low scattering level) and high contrast situations by using simulated B-scans. He found that the deconvolution filter can improve both low contrast and high contrast resolutions if applied to the scans before demodulation and if the deconvolution process includes the axial pulse.

Shattuck and von Ramm, 1982 - [24], studied compound scans made with a dynamically focussed, dynamically focussed, real time, phased array. They found that the compound scans improved echo acquisition from specular targets and reduced speckle while maintaining the high resolution of the phased array sector scanner. Compound images formed by four sector scans were found to provide increased near field view and reduced noise and target anomalies.

Magnin, von Ramm and Thurstone, 1982 - [25], investigated frequency compounding as a technique for speckle contrast reduction in ultrasonic images. They showed that frequency compounding using narrow bandwidth transmit excitation is an effective scheme for speckle suppression. Speckle suppression was found to increase with decrease in the transmitted bandwidth. The rate of decorrelation of speckle patterns with the change in frequency was found to be inversely related to the transmitted bandwidth. They also found that the rate of SNR enhancement was significantly lower for two dimensional images than for A-mode signals.

Wagner, Smith, Sandvik and Lopez, 1983 - [26], in the first of a two paper series, analysed the statistics of speckle in ultrasound B-scans. They showed that the statistics of ultrasound pressure field is Gaussian and that of the envelope detected image is Rayleigh. They concluded, following much theoretical analysis and experimentation, that texture or speckle in envelope detected images is characterized by Rayleigh probability density function. Also, speckle was found to carry information about only the transducer and its focussing pattern. They demonstrated that speckle size in the axial direction is inversely proportional to the pulse bandwidth and directly proportional to the beam width in the lateral direction.

Smith, Wagner, Sandrik and Lopez, 1982 - [27], in the second of their two paper series, applied the results of their previous paper [26] to statistical decision analysis of speckle noise limited detectability of focal lesions by an ideal observer. They provided a heuristic treatment supported by a rigorous discussion and corroborated by experimental

data. Smith et al showed that best performance (detectability) is achieved by integrating intensity over the lesion and comparing this to the integrated value over a background of the same size. They recommended use of broad banded, higher frequency transducers for the improvement of detectability and suppression of speckle. In addition, they suggested that spatial compounding, frequency compounding and image smoothing also would enhance the detectability and SNR. Smith and Wagner, 1984 - [28], followed up their earlier two paper sequence [26,27], by providing simulation and experimental data in support of their theoretical predictions. They showed that the simulation and experimental data closely match that of their theoretical predictions.

Patterson and Foster, 1983 - [29, 30, 31], developed an annular/conical hybrid transducer system which allowed them to utilize the high sensitivity of ceramic piezoelectric materials thereby providing a signal-to-noise ratio improvement of almost eight times over the conventional PVDF conical receivers. In addition, they evaluated two methods of signal processing - phase insensitive sector addition and multiplicative processing - for speckle reduction and found that while phase insensitive sector addition reduced speckle fluctuation by a factor of 2.5, lateral resolution was degraded by a factor of almost three times. Multiplicative processing showed lower speckle reduction, but also smaller degradation of lateral resolution. However, multiplicative processing also reduced artifacts due to off-axis scatterers/reflectors.

Melton and Magnin, 1984 - [32], modeled A-mode signals by a series of Poisson distributed impulses convolved with the transfer function of the transducer/electronics system. They analysed the cross correlation among signals of different frequency contents (both RF signals and their envelopes) and found that the frequency shift should be at least twice the transmitted bandwidth for a complete decorrelation to occur. Also, they found that the correlation decreases when signals of same center frequency but varying bandwidths are compounded. They also provided experimental data in support of their theoretical analysis. From the analysis and the experimental results provided by Melton and Magnin, it appears likely that speckle suppression could be very effective if signals of different center frequencies and varying, bandwidths are compounded.

Shankar and Newhouse, 1985 - [33], showed in their paper that completely decorrelated signals/images are not essential for speckle suppression. It had had been shown in the past by several authors that a signal-to-noise ratio improvement of \sqrt{N} could be achieved by either spatially compounding or frequency compounding N uncorrelated

signals. However, Shankar and Newhouse showed, through linear transformation methods, that a comparable improvement in signal-to-noise ratio could indeed be obtained by compounding N image frames (either space diverse or frequency diverse) with a correlation coefficient ρ provided the covariance matrix is positive definite (implying an upper limit on ρ).

Shankar, 1986 - [34], showed that spatial compounding with correlated signals/images can still provide an enhancement factor of \sqrt{N} (as if uncorrelated images are being compounded) by using linear transformation and weighted averaging. The value of the weighting factors are dependent on the correlation coefficient ρ and hence on the covariance matrix. Since this method allows the use of larger aperture without losing image quality, lateral resolution is better than simple compounding with uncorrelated images.

Wagner, Insana and Brown, 1985 - [35], demonstrated that the first order, second order and other higher order statistics of speckle does indeed contain information about the structure of the scatterers. This was in complete contradiction to the earlier stand by Wagner et al [28] wherein they had stated that speckle pattern carries information about only the transducer and its focusing pattern. However, Wagner et al [35] now showed that it is possible to extract information about the scatterers using higher order statistics in conjunction with computer assisted analysis. They found the variance and covariance of the second order statistics of speckle to be particularly useful to classify and grade image texture for tissue characterization. Wagner, Insana and Brown, 1983 - [36], further showed, based on speckle statistics, how the structure of the diffuse scatterers could be classified in three dimensional feature space by estimating two, three or four parameters using generalized Rician statistics. In a subsequent paper by Insana, Wagner, Garra, Brown and Shawkar [37], they provided some preliminary results of experiments conducted on phantoms and clinical volunteer patients. They were able to accurately measure average spacing between long range specular scatterers, the ratio of specular to diffuse backscatterer intensities and resolvability of specular targets. They segmented the image to discriminate between different normal tissues and to detect abnormal conditions based on three dimensional feature space.

Bamber and Daft, 1986 - [38], proposed an adaptive filtering scheme to reduce speckle in B-scan images. They proposed an adaptive two dimensional filter, which, using features like the ratio of speckle mean to local speckle variance, recognizes the presence of speckle alone and maximally smooths the image. At the same time, when the feature value

indicates the presence of specular targets, the filter reduces filtering effect by various degrees depending on the strength of the specular echo present in the image. They provided some preliminary experimental results in support of the effectiveness of their technique.

Trahey, Smith and von Ramm, 1986 - [39], conducted extensive studies to determine the effect of various parameters on the decorrelation of the speckle pattern by spatial compounding. They conducted experiments to measure the speckle correlation as a function of lateral aperture translation for different frequencies, range, aperture size, focus error and reflecting material. They concluded that independent speckle patterns are obtained with translation distances of about 40% of the aperture length and is independent of acoustic frequency and the target range. They also found that more rapid decorrelation occurs outside the focal range of the imaging system. They further showed that better signal-to-noise ratio could be obtained by compounding larger number of correlated images than that obtained by compounding fewer uncorrelated images. Thus, they found that an aperture translation of 0.2 times the aperture length is sufficient to produce best signal-to-noise ratio even though almost complete decorrelation occurs only at about 0.4 times the aperture length.

Trahey, Allison, Smith and von Ramm, 1986 - [40], reported on decorrelation of speckle by frequency diversity. They showed that decorrelation of speckle pattern could be achieved by variations in the center frequency of the transmitted pulse. They also showed, experimentally, that speckle pattern decorrelation is independent of the aperture size, target range and magnitude of focal error, but varies inversely as the pulse duration. They also predicted, based on the earlier theoretical work of Smith et al [29], that simple frequency compounding might reduce image quality in a fixed bandwidth system. However, they did not provide conclusive experimental evidence to show that image quality reduces by simple frequency compounding. They also mentioned that some form of 'more complex divisions of the available bandwidth' might be more successful.

In summary, speckle statistics has been extensively studied. The amplitude statistics has been modelled by Rayleigh pdf. There have been discussions about whether speckle contains information about the speckle producing scatterers. Even though initially it was believed that speckle statistics was related only to the instrumentation limits, it has been shown recently that speckle statistics does indeed carry information about the scatterers themselves.

Spatial compounding and frequency compounding methods have emerged as the

principal methods of speckle reduction; techniques like lateral filtering, multiplicative processing, phase insensitive summation have been suggested. Spatial compounding was initially thought to be effective only when the transducer is moved by at least 50% of the aperture size. However, it was later showed that, even though a translation of about 40% is essential for virtually a complete speckle decorrelation, a translation of only about 20% of the aperture size is enough to produce substantial speckle reduction.

Frequency agility and frequency compounding have been shown to be effective in achieving speckle decorrelation and speckle suppression. However, it has been suggested recently that a simple frequency compounding might not be sufficient to obtain substantial speckle suppression and that a special frequency compounding technique might be necessary to achieve a true speckle suppression. Split spectrum processing, introduced by Newhouse et al [15], is one such special frequency compounding technique and has been shown to be very effective in speckle suppression. A literature review of split spectrum processing is contained in the remaining part of this chapter.

2.2 Split Spectrum Processing (SSP)

The first mention of SSP in ultrasonic applications dates back to 1979. Newhouse, Furgason, Bilgutay and Saniie, 1979 - [15], proposed a new technique of introducing frequency diversity in ultrasonic signals and images. At about the same time when Abbott and Thurstone [17] were suggesting that frequency diversity (obtained by transmitting different frequency bandwidths) might help to decorrelate the speckle pattern, Newhouse et al arrived at the same conclusion and went on to show how frequency diverse signals could be obtained in receive-mode by splitting the wideband spectrum of the received signal. They called their newly conceived technique - "Split Spectrum Processing (SSP)".

Furgason, Bilgutay, Lee and Newhouse, 1980 - [41], showed experimental effectiveness of SSP technique. They provided some experimental results wherein SNR enhancement was obtained in Titanium and stainless steel samples. They utilized Gaussian filters to split the spectrum of the received signal. However, they mentioned nothing about the number of filters, their bandwidth and the frequency separation between the adjoining filters for a good performance of the technique.

A major research work in SSP was performed by Bilgutay, 1981 - [2], as a part of his Ph.D. dissertation. He provides an extensive literature review of frequency agility

technique in radars based on which he develops the rationale for the SSP technique. Bilgutay also provided an account of the SSP technique and method of processing parameter selection. He demonstrated that the frequency separation is related to the filter bandwidth for decorrelation of speckle. However, he did not provide any basis for selecting either a suitable frequency separation or the total number of filters necessary for the splitting process. However, he calculated the number of filters that could be used for processing by an arbitrary selection of the frequency separation between adjoining filters. He used equation (2.1) to calculate the number of filters, m , necessary for the processing.

$$m = B/\Delta f + 1 \quad (2.1)$$

where B is the half power bandwidth of the transducer and Δf is the frequency separation between adjoining filters. Bilgutay also stated, although with no rigorous theoretical proof, that the adjoining filters should overlap by as much as 50% to 75% because, otherwise, the spectral information would be lost. Further, with the help of computer simulated signals, he conducted performance tests for algorithms like linear averaging, nonlinear averaging and minimization. he also studied the SNR enhancement as a function of frequency separation between filters, filter bandwidth and input SNR. He repeated the performance analysis with Titanium and stainless steel samples also. In addition, he also studied the performance with respect to resolution, input flaw amplitude, dependence on incident angle and grain size. He concluded that minimization has superior results compared to the other conventional algorithms like linear and nonlinear averaging for SNR enhancement. He found that output SNR of minimization has nonlinear relationship to input SNR. Also, he showed that minimization is fairly insensitive to incident angle and is sensitive to the size of the scatterers present in the material.

Newhouse, Bilgutay, Saniie and Furgason, 1982 - [42], published the first journal article on SSP and discussed the technique, the processing parameter, performance and sensitivity of the SSP technique and minimization algorithm. Even though the paper discussed various aspects of processing, the parameter selection was still not formalized and hence remained an art. Thus, a state of ambiguity prevailed which is evident from the statement made by the authors [42] that even though correlation increased by decreasing the frequency separation between adjoining filters, the performance of minimization had had continued to improve with decrease in frequency separation!

Draheim and Furgason, 1983 - [43], extended the SSP technique developed earlier (for one dimensional A-scans) to two dimensional processing of ultrasonic B-scan images. They experimented with rectangular windows as well as circular Gaussian windows and concluded that Gaussian filters perform better in clutter suppression. They went on to show that minimization in two dimensional processing also outperforms conventional compounding techniques.

Bilgutay and Saniie, 1984 - [44], discussed the effect of grain size on the performance of SSP. They conducted experiments with large grained samples which had average grain dimensions of the same order of magnitude as wavelength. They found that, even though the performance of minimization algorithm progressively deteriorates with the increase in grain size, the algorithm is still effective in obtaining substantial grain noise suppression.

Brase, McKinnel, Blaedel, Oppenheimer, Wong and Simmons, 1984 - [45], utilized SSP in conjunction with minimization as a part of an automated ultrasonic test bed that they developed. They showed that SSP does indeed suppresses speckle in B-scan images.

Newhouse, Karpur, Rose and Amir, 1985 - [46], and Amir, 1986 - [47], introduced a new algorithm of SSP for speckle reduction in Ultrasonic Imaging. The new algorithm called 'Suboptimal Processing Algorithm', is used for improving the ROC of a A-mode signal so as to minimize the probability of false alarm for a given probability of detection. Amir and Newhouse et al constructed the receiver from the spectral decomposition components obtained by splitting the spectrum of the received signal. They theoretically modelled the splitting process by a K-L expansion and derived the optimum receiver which, with some simplifying assumptions, was shown to be the ratio of mean to standard deviation of the spectral decomposition components at a given time delay. The receiver operating characteristics (ROC) of the receiver was generated to study the performance of the technique. Newhouse et al [46] and Amir [47] also conducted experiments to support the theoretical analysis and also to evaluate the resolution and range bias. They concluded that the algorithm does not adversely affect the resolution, but does indeed have a bias in range delay when targets are separated by less than the resolution cell of the transducer. Newhouse et al [46] and Amir [47] suggested the use of the relationship $n = BT$ (B = available bandwidth and T = time range of the signal being processed) to calculate the number of filters necessary for splitting the spectrum. However, the rationale

behind such a relationship was to model the spectrum splitting process as the K-L expansion. Also, Amir stated that the adjoining filters should be nonoverlapping for the best performance of SSP, a contradiction to the earlier belief that there should be an overlap between adjoining filters. Newhouse, Karpur, Rose and Amir also introduced a new algorithm which later came to be known as 'Polarity Thresholding algorithm'.

Baligand, Grozellier and Romy, 1986 - [48], published their results of applying split spectrum processing to SNR enhancement in austenitic steels. They applied simple thresholding to the output signals of SSP, in conjunction with algorithms like minimization, linear averaging and nonlinear averaging. They indicated that such thresholding is an acceptable technique using probabilistic models. However, they could not predict the performance of the technique because of a lack of rigorous modeling and probability density functions.

Amir, 1986 -[47] and Amir, Bilgutay and Newhouse, 1986 - [49], conducted theoretical performance evaluation of some of the frequency compounding algorithms used in conjunction with SSP. They developed a stochastic model of the ultrasonic signal based on which they obtained expressions for SNR enhancement for minimization, linear averaging and nonlinear averaging and demonstrated the superior SNR enhancement obtained by the minimization algorithm. They also developed the probability density functions of the minimized signal as well as the averaged signal. They went on to calculate the ROC of the algorithms so that the probability of detection could be evaluated as a function of probability of false alarm. They concluded that, although linear averaging has the best ROC of the three algorithms for additive noise, the ROC of minimization is superior when noise in the target range cell is at least four times smaller than elsewhere in the signal.

Bencharit, Kaufman, Bilgutay and Saniie, 1986 - [50], summarized the theoretical analysis of Amir et al [47, 49] and provided experimental results to demonstrate the performance of some of the SSP algorithms. Their results showed the effectiveness of SSP and spatial compounding in speckle reduction of B-scan images.

Li, 1985 - [51], and Li and Ying, 1987 - [52], independently developed a variation of Polarity Thresholding algorithm at about the same time it was developed in the United States [46,47]. They utilized the algorithm in conjunction with spatial compounding as well as SSP. They also experimentally demonstrated the performance of the technique.

Karpur, Shankar, Rose and Newhouse, [61] - 1987, developed a theoretical model

based on the frequency sampling theorem and the theory of Fourier integrals to explain the frequency splitting process. They developed a theoretical expression to calculate the total number of filters and their bandwidth necessary for the splitting process. They also conducted experiments to corroborate the theory.

Shankar, Karpur, Newhouse and Rose, [54] - 1987, studied the performance of the Polarity Thresholding algorithm [46,47] by developing the probability density function (pdf) of the output of the algorithm. Using the pdf, they theoretically calculated the SNR enhancement obtainable with the algorithm. They also calculated the probability of detection and the probability of false alarm and hence the ROC of the algorithm. They further showed by experimentation that the algorithm yields excellent superior SNR enhancement and provides further improvement when used in conjunction with another algorithm such as minimization.

Rose, Karpur and Newhouse, [53] - 1987, experimentally demonstrated the utility of split spectrum processing. They showed the potential and the versatility of SSP for SNR enhancement in such materials as centrifugally cast stainless steel, composite materials, clad materials and welded joints. They also demonstrated the feasibility of utilizing the split spectrum processing in material characterization studies (for classifying and sizing the grains present in centrifugally cast stainless steel).

In summary, SSP has been in existence since 1979 when it was first proposed by Newhouse et al [15]. Since that time, many Ph. D. (as well as Master's) dissertations [2,47] and publications have followed. Extensive theoretical analysis [47, 49] and experimental corroborations [2, 47] have been performed by the original researchers who invented the technique and also by other groups around the world [45,48,51,52]. However, the process of parameter selection, which is vital to the success of the technique, remained an art until a short time ago. Contradicting and ambiguous statements existed in the literature regarding the number of filters necessary for the processing, their bandwidth, whether the adjoining filters should overlap or not etc. Also, the performance of the Polarity Thresholding algorithm [46, 47], had not been studied and understood thereby making it difficult to use the technique with confidence. These aspects of SSP that have been unanswered to date will be addressed in this dissertation.

3. PROBLEM STATEMENT, OBJECTIVES AND METHODOLOGY

Split Spectrum Processing (SSP) has been in existence since 1979 [15]. Many publications have appeared; a few Master's thesis and a couple of Ph. D. dissertations have been written. However, it is apparent from a review of the available literature that a need exists for further research in various aspects of SSP.

3.1 Problem Statement

There are three important processing parameters that affect the performance of the SSP technique. They are: 1. the total number (and the separation) of filters and to be used to split the spectrum, 2. the bandwidth of the filters and 3. the usable bandwidth of the received spectrum. Until the work conducted as a part of this dissertation, there were ambiguities and contradictory statements in the literature about a suitable selection of all the three parameters. It is apparent from literature that the total number of filters to be used for spectral splitting is being determined based on an arbitrary selection of the frequency separation between the adjoining filters. There have been equivocal and conflicting statements about the bandwidth and the degree of overlap between the adjoining filters. The prevailing ambiguity has led to uncertainties in the parameter selection process thereby rendering the process an 'art' possessed by the original research groups which invented the technique. As a result, the application and utilization of the technique has been mostly limited to the original inventors of the technique, even though a few other groups have reported [45,48,52] excellent results with the technique. The ambiguities in the parameter selection process stems from the fact that a rigorous theoretical modeling of the process of spectral splitting did not exist. Consequently, it was necessary to develop a theoretical basis to formalize the selection of the processing parameters.

The Polarity Thresholding algorithm (PT) was developed for ultrasonic applications in 1985 [46,47]. Polarity thresholding algorithm recognizes the noise amplitude by the frequency dependent variation of the amplitude and a 'target' by the frequency independent echo amplitude. However, when the signal-to-noise ratio (SNR) of the input signal is close to unity or less, the noise interference pattern completely masks the target amplitude so much so that the PT algorithm can no longer perform satisfactorily, especially when a large number of filters are used. Although the algorithm has been in existence for almost two

years, the performance limits of the algorithm has not been determined by rigorous theoretical modeling and analysis. Thus, if the PT algorithm is to be used with confidence, it is necessary to know the performance limits of the algorithm as a function of the SNR of the input signal and the processing parameters used for noise reduction. Since the performance limits of a processing techniques could be evaluated by factors like the SNR enhancement, probability of detection, probability of false alarm and the Receiver Operating Characteristics (ROC), it is necessary to calculate such performance evaluation factors of the algorithm so that it could be meaningfully used.

Another aspect of SSP that needed to be addressed was the necessity to demonstrate the utility of SSP in various engineering problems. The potential of SSP as a tool for SNR enhancement in materials with Raleigh scatterers (average grain diameter $\ll \lambda$) has been demonstrated in the past by other researchers [2,44,46,48,51]. However, the potential of the technique in highly reverberating and/or anisotropic materials like Centrifugally Cast Stainless Steel (CCSS - average grain diameter $\approx \lambda$), composite materials, welded joints, clad materials was yet to be proven. Also, the potential of SSP as a tool for material characterization needed to be explored. If the potential of SSP in material characterization is demonstrated, it would be a new application of the technique. Thus, there existed a need to explore and demonstrate the versatility and utility of SSP technique in various engineering problems of both noise suppression and 'noise' characterization.

3.2 Objectives and Contributions of this Dissertation

The achieved objectives of this dissertation were developed based on the need established from a literature review and are listed below:

1. Process modeling of SSP

- i. Develop a theoretical modeling of the frequency splitting process based on which the parameter selection can be formalized.
- ii. Conduct experimental parametric study to corroborate the theoretical model and to evaluate the performance of the technique as a function of
 - a. Total number of filters used for the splitting process, and
 - b. bandwidth and hence the overlap of the filters.
- iii. Conduct an experimental parametric study to understand the considerations

necessary to estimate the available bandwidth of the received signal.

2. Performance evaluation of the Polarity Thresholding algorithm

- i. Develop the probability density function of the output of the algorithm,
- ii. Define various SNR enhancement ratios (calculated using the pdf of the output) to evaluate different aspects of the performance of the algorithm and study the SNR enhancement as a function of the
 - a. input SNR
 - b. number of filters used to split the spectrum.
- iii. Using the pdf of the output of the algorithm, study the probability of detection and the probability of false alarm of the algorithm as a function of the
 - a. input SNR
 - b. number of filters used to split the spectrum,
- iv Using the pdf of the output of the algorithm, develop the ROC of the algorithm
 - a. when no threshold is set to the output of the algorithm,
 - b. when a threshold is set to the processed output based on the Neyman - Pearson criterion,

3. Demonstrate the utility of SSP in practical engineering problems

- i. Signal-to-noise ratio enhancement in
 - a. Centrifugally cast stainless steel (CCSS) - both equiaxed and columnar type,
 - b. Composite materials,
 - c. Cladded materials like Zircalloy/Zirconium interface.
- ii. Speckle suppression in B-scan images
 - a. Centrifugally cast stainless steel,
- iii. Material characterization: to establish the potential of SSP as a tool for material characterization in any future research work.

3.3 Methodology

This section presents the methodology that has been adapted in the following chapters of this dissertation to fulfill the objectives stated in the previous section of this chapter.

3.3.1 Process Modeling

A mathematical model of an ultrasonic signal is developed in order to perform a process modeling of the technique. An ultrasonic signal is modelled as a time limited, band unlimited process for which the frequency sampling theorem is invoked to find the minimum number of frequency samples (filters) necessary to completely represent the signal in the frequency domain. Further, based on the Fourier integral theorem, it is shown that the signals obtained from the minimum possible number of frequency samples are uncorrelated in spite of a large overlap between the adjoining samples.

Experimental correlation is provided to support the theoretical modeling. Three different kinds of test specimen - welded joint between two 1020 steel plates, CCSS and a Carbon-Epoxy composite material - are utilized for the experimental work. SSP is applied through minimization. The number of filters and their bandwidth are varied to determine the validity of the theoretical model.

3.3.2 Performance evaluation of the Polarity Thresholding algorithm

A stochastic model of an ultrasonic signal is presented using which the pdf of the output of the PT algorithm is developed. The pdf so developed yields theoretical SNR curves of various definitions including SNR of the output signal, SNR at a time delay of the output signal, etc.

The pdf is also used to calculate the probability of detection, probability of false alarm and hence the 'Receiver Operating Characteristics' (ROC) of the algorithm when every nonzero output of the algorithm is considered a detection (ie., no thresholding of the output of the algorithm).

Further, ROC of conventional definition (ie., thresholding of the output of the algorithm) are also developed. The 'conventional' ROC provide the variation of the

probability of detection as a function of the input SNR and varying probability of false alarm obtained by thresholding of the output signal.

3.3.3 Utility of Split Spectrum Processing in Ultrasonic NDE

The potential of SSP in various engineering applications is demonstrated by experimentation. Use of SSP for SNR enhancements, in materials like CCSS, Carbon-Epoxy composite materials, welded joints, Zircalloy tubes clad with Zirconium lining, is demonstrated. The potential of SSP as a tool to characterize the grain type in the CCSS material is demonstrated by experimentation.

It is a well known fact that the attenuation due to scattering varies as a fourth power of frequency if the average grain size is much smaller than the wavelength, varies as a second power of frequency if the average grain size is of the same order of magnitude as the wavelength and is independent of frequency if the average grain size is much larger than the wavelength. Thus, the material 'noise' (or the grain noise) level in an ultrasonic signal is an indication of the average grain size exposed to the direction of wave propagation and hence will indicate 'equiaxed' grain type under different angles of insonification and frequency. Similarly, if the grain type is 'columnar', the grains will act as either wave guides or as scatterers or a combination of both depending again on the angle of insonification and frequency. This phenomenon has been utilized to demonstrate the potential and utility of SSP in material characterization experiments.

4. PROCESS MODELING AND PARAMETER SELECTION*

This chapter provides a brief description of split spectrum processing, followed by a theoretical modeling of the frequency splitting process based on which the parameter selection process is formalized. Experimental results are also provided as a corroboration of the theory.

4.1 Split Spectrum Processing Methodology

Split spectrum processing (SSP) [15] was introduced for ultrasonic applications in the late seventies in an attempt to implement frequency agility techniques (used in radar) for signal-to-noise ratio (SNR) improvement in ultrasonic signals. The development of Split Spectrum Processing (SSP) is based on the physics of the interaction between ultrasonic waves and random scatterers like material grain structure. It is a well known fact that grain noise or clutter is an interference pattern produced by the interaction of the ultrasonic wavelets scattered by randomly packed, unresolvable scatterers that are present in the material being tested. Since it is an interference pattern, the clutter is not only dependent on the relative spatial position of the transducer and the test material but also on the frequency of the transmitted signal. The fact that the interference pattern changes when the transducer is moved with respect to the test material is utilized in the spatial compounding technique. Split spectrum processing makes use of the fact that the interference pattern changes with the change in frequency. However, SSP produces the frequency diverse signals by splitting the received spectrum instead of transmitting at different frequencies.

Split spectrum processing is pictorially represented in Figure 4.1 and shows the magnitude-frequency spectrum of the received signal and the filtering scheme. In practice many equally spaced Gaussian bandpass filters are used for 'splitting' the spectrum. The center frequencies of the first and the last filters are determined by the half-power bandwidth of the received signal. The bank of filters, when applied in frequency domain to the signal received from the test material, split the spectrum into 'N' narrow banded frequency spectra. Each one of the 'N' narrow banded spectra yields one time domain

* A version of this chapter has been published as a paper entitled "Split Spectrum Processing: Optimizing the Processing Parameter Using Minimization", P. Karpur, P.M. Shankar, J.L. Rose and V.L. Newhouse, Ultrasonics, Vol. 25, Issue 4, pp: 204-208, July, 1987.

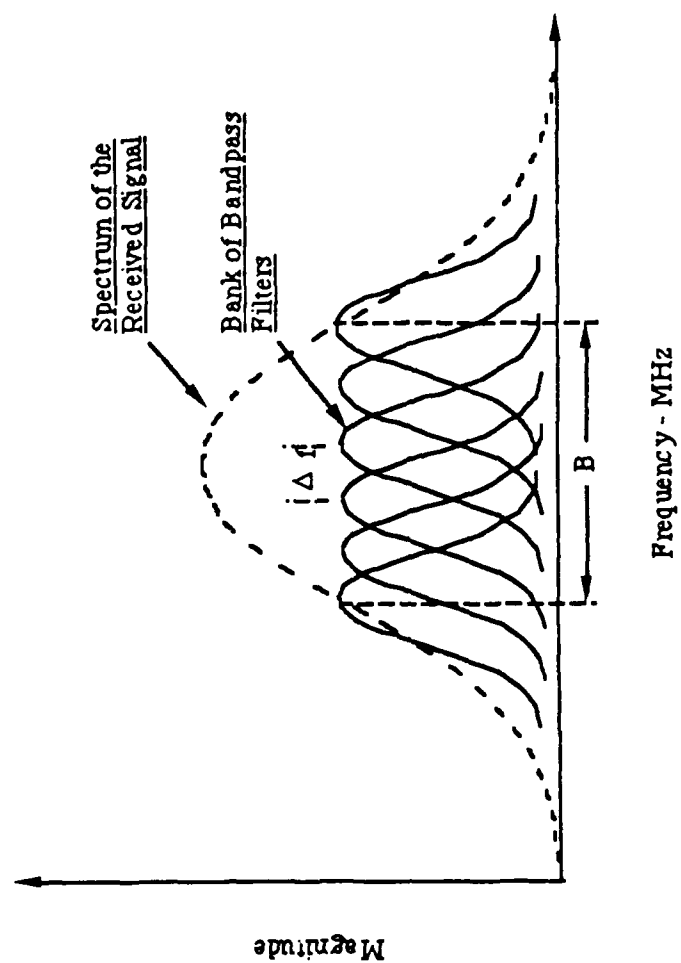


Figure 4.1 Filtering scheme for split spectrum processing

signal when the inverse FFT is taken. The resultant 'N' time domain signals (called split time domain signals or the spectral decomposition components) mark the completion of the initial step in SSP and sets the stage for further analysis.

There are many processing algorithms that could be applied to the split time domain signals: i) individual split time domain signal analysis [53] might yield information about the test material like the type of grain structure present in the material, attenuation as a function of frequency, dispersive property etc., ii) minimization [2,49] could be applied for enhancing the SNR, iii) polarity thresholding [46,47,54] could be used for improved detectability iv) decorrelation and clutter suppression algorithm could be used for speckle suppression [33] and so on. Each algorithm is best suited for a specific aspect of nondestructive testing. Hence, which of the algorithms is used for further analysis is dictated by the objective of the nondestructive test being conducted.

Even though the SSP technique has been in existence for over half-a-decade, even though its performance theoretically analyzed [46,47,48], and even though it has been successfully implemented all over the world [45,48,52,53], the utility of the technique has been somewhat limited because of a lack of theoretical modeling leading to the selection and optimization of the processing parameters critical to the success of the technique.

The processing parameters important for the success of the technique are the total number of filters to be used for spectral splitting, the frequency separation between adjacent filters, their half-power bandwidth (HPBW) and the spectral bandwidth over which the bank of filters are located. Until recently, it was the usual practice to optimize the processing parameters by 'trial and error' due to the lack of a formalized theoretical basis for the parameter selection. This chapter of the dissertation presents a theoretical model based on which the parameter selection is formalized. Further, the theory is corroborated by the experimental results presented in the body of the chapter.

4.2 Number of Filters and Their Bandwidth

This section deals with the theoretical modeling of the spectral splitting process based on which an expression is developed to calculate the total number of filters necessary for the spectral splitting process. Experimental corroboration is provided to validate the theoretical modeling.

4.2.1 Theory

A typical ultrasonic signal can be represented by a time limited signal in (4.1):

$$\begin{aligned} X(t) &= m(t) + n(t) \neq 0 & 0 \leq t \leq T \\ &= 0 & \text{otherwise.} \end{aligned} \quad (4.1)$$

where $m(t)$ is the signal from a target or a flaw and $n(t)$ is the noise signal from the grains. Since the signal $X(t)$ in (4.1) is time limited (T secs), the spectrum of $X(t)$ is of unlimited bandwidth. That is,

$$X(\omega) = \text{FFT} \{X(t)\} \neq 0$$

It should be pointed out that, in reality, the spectrum appears bandlimited due to the limitation of the FFT algorithm and the combined limited bandwidth of the transducer, digitizer and the pulser/receiver ensemble. Nevertheless, the assumption of unlimited bandwidth is still valid for the theoretical analysis.

The process of splitting the spectrum is equivalent to frequency sampling and hence is subject to the frequency sampling theorem [55,56] stated as: 'If a function is nonzero only in the time range of 0 to T secs., then its Fourier transform $X(\omega)$ can be uniquely determined from its values $X(2\pi n/T)$ at a sequence of equidistant points, distance $2\pi/T$ radians or $1/T$ Hz apart'. That is,

$$X(\omega) = \sum_{n=-\infty}^{n=+\infty} X_n(\omega) \quad (4.2)$$

where,

$$X_n(\omega) = X\left(\frac{2\pi n}{T}\right) \frac{\text{Sin}(\omega T/2 - \pi n)}{(\omega T/2 - \pi n)} \quad (4.3)$$

Thus, it is clear from (4.2) that the spectrum of $X(t)$ can be theoretically decomposed into

'infinite' samples, $X_n(\omega)$, called the 'spectral decomposition components', as defined by (4.3). However, because of the fact that the available bandwidth is usually governed by the limits imposed due to the transducer/instrumentation ensemble, the number of samples, 'N', of the spectrum is finite. Nevertheless, the frequency separation between the samples is still $1/T$ Hz.

Equation (4.3) establishes that it is possible to split the spectrum of an ultrasonic time limited signal into a number of frequency bins by using equidistantly spaced ($1/T$ Hz) SINC windows [$\text{SINC}(x) = \text{Sin}(x)/x$] having a main lobe bandwidth of $2/T$ Hz. The spectral samples obtained by the SINC windows so selected are uncorrelated with each other due to the orthogonality principle of the theory of Fourier series [55,57] which states as follows: 'If $g_m(x)$ and $g_n(x)$ are two real functions defined on an interval $a \leq x \leq b$ and are such that the integrand of the product $g_m(x)g_n(x)$ exists over the interval, then, the functions are said to be orthogonal on the interval $a \leq x \leq b$ if the integral in (4.4) is zero'. That is,

$$(g_m, g_n) = \int_a^b g_m(x) g_n(x) dx = 0 \quad m \neq n \quad (4.4)$$

It is immediately obvious from (4.3) and (4.4) that $X_n(\omega)$, $n = -\infty, \dots, 1, 2, \dots, +\infty$ form an orthogonal set. Further, because the (4.4) is zero, the crosscorrelation among the frequency samples, $X_n(\omega)$, $n = -\infty, \dots, 1, 2, \dots, +\infty$, is also zero. Therefore, the resulting uncorrelated split frequency bands will yield frequency diverse time domain signals as follows:

$$X_n(t) = \text{FFT}^{-1}[X_n(\omega)] \quad (4.5)$$

From (4.3), the sampling windows are separated by $1/T$ Hz and the signals $X_n(t)$ so created (Equation 4.5) are uncorrelated and hence could be compounded for an increased SNR. Therefore, the optimum frequency separation of the filters is,

$$\Delta f = 1/T \text{ Hz.} \quad (4.6)$$

Even though an infinite bandwidth theoretically exists because of the use of a time limited signal, the usable spectrum is limited to a frequency band of B Hz because of the frequency response of the transducer, instrumentation, type of scatterers in the material etc. Hence, for Δf obtained from (4.6), the effective number of uncorrelated frequency bands that could be obtained from the usable bandwidth B is,

$$\begin{aligned} N' &= B/\Delta f \\ &= BT \end{aligned} \quad (4.7).$$

However, since the actual filtering scheme is as per Figure 4.1, the actual number of filters that could be used is,

$$\begin{aligned} N &= N' + 1 \\ &= BT + 1 \end{aligned} \quad (4.8)$$

It is a well known fact that the SNR is enhanced when N frequency diverse signals are compounded. The factor by which the SNR is enhanced is given by [33],

$$\begin{aligned} \text{Enhancement} &= \sqrt{\frac{N_c}{1 + \frac{2(N_c-1)\rho^2}{N_c}}} \quad (4.9a) \\ &= \sqrt{N_u} \quad \text{when } \rho = 0 \quad (4.9b) \end{aligned}$$

where 'p' is the correlation between the signals from adjoining filters, N_c is the number of correlated filters and N_u is the number of uncorrelated filters. Thus it is obvious from (4.9a) and (4.9b) that large improvements in SNR are achieved when the signals are uncorrelated and relatively smaller improvements, when they are correlated. When the signals are correlated, the effective number of uncorrelated windows, N'_u , can be found out from (4.10) [N'_u calculated from (4.10) is not for the purpose of calculating the number of filters for signal processing but for use in (4.9b) to calculate the SNR enhancement factor when correlated windows are used]:

$$N'_u = \frac{N_c}{\left[1 + \frac{2(N_c - 1)\rho^2}{N_c} \right]} \quad (4.10)$$

Hence, the SNR improvement can be obtained by increasing N , the total number of windows used. However, by virtue of (4.6) to (4.9), the increase in N has to be achieved by increasing either B , T or both and not by simply increasing N for fixed values of B and T because this would reduce the SNR improvement due to increased correlation.

A SINC function has been used in the theoretical analysis to obtain uncorrelated samples. The bandwidth of the main lobe of the SINC function is $2/T$ Hz or $4\pi/T$ radians while the separation between the filters is $1/T$ Hz or $2\pi/T$ radians. Thus it is clear that the neighboring filters can overlap even though the resulting samples are uncorrelated. Because of this overlap, none of the frequency components of the original signal are lost in the processing. This explains the reason for the better performance reported below with overlapping windows than with nonoverlapping windows.

For the actual signal processing, the SINC window functions have been replaced by Gaussian window functions due to mathematical simplicity and ease of digital generation. Due to the limitations of the digital (discrete) FFT algorithm, it is not possible to have Δf less than $1/T$ Hz for a signal of time duration T . Hence, the technique of zero padding of the signal has been used whenever Δf of less than $1/T$ is necessary.

4.2.2 Experimental Results

In this section, the dependence of the performance of SSP on various processing parameters of SSP is studied experimentally. Three different transducers have been used, one each for the three types of test specimen examined: a welded joint between two 1020 steel plates, a centrifugally cast stainless steel block (CCSS) and a Carbon-Epoxy composite material. Minimization [2,15,49] algorithm has been used for the SNR enhancement.

Three sample signals used for the study are shown in Figures 4.2a, 4.3a and 4.4a. Figure 4.2a is a signal from a welded joint between two 1020 steel plates. A transducer of center frequency 2.07 MHz and a half-power bandwidth (HPBW) of 0.925 MHz was

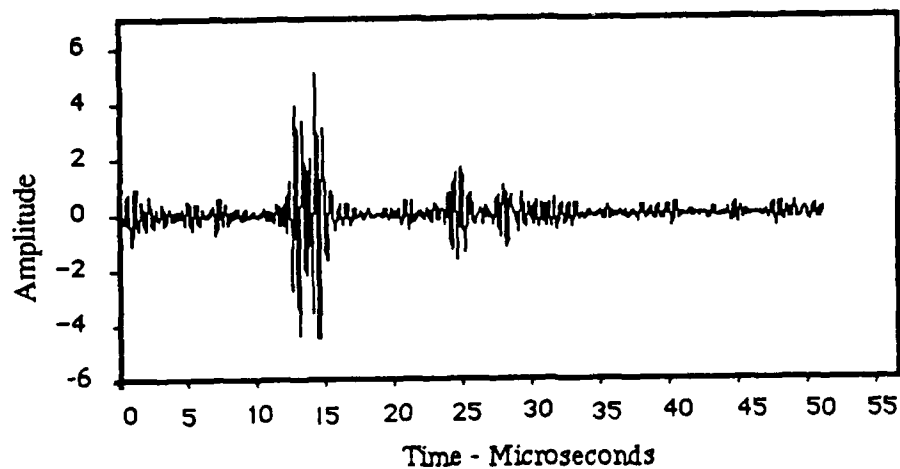


Figure 4.2 a Signal obtained from a welded joint between two 1020 steel plates

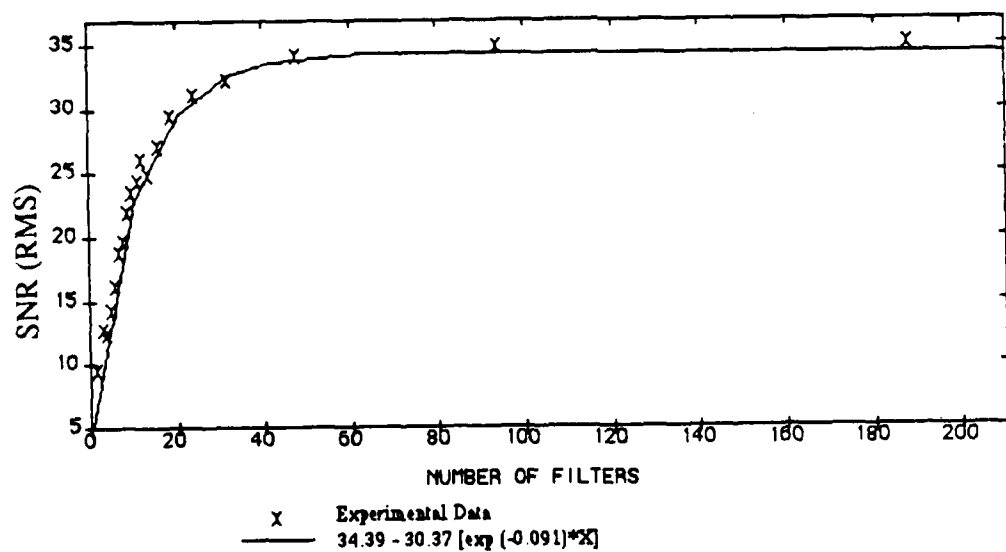


Figure 4.2b Graph of SNR (RMS) vs total number of filters used for the signal in Figure 4.2a

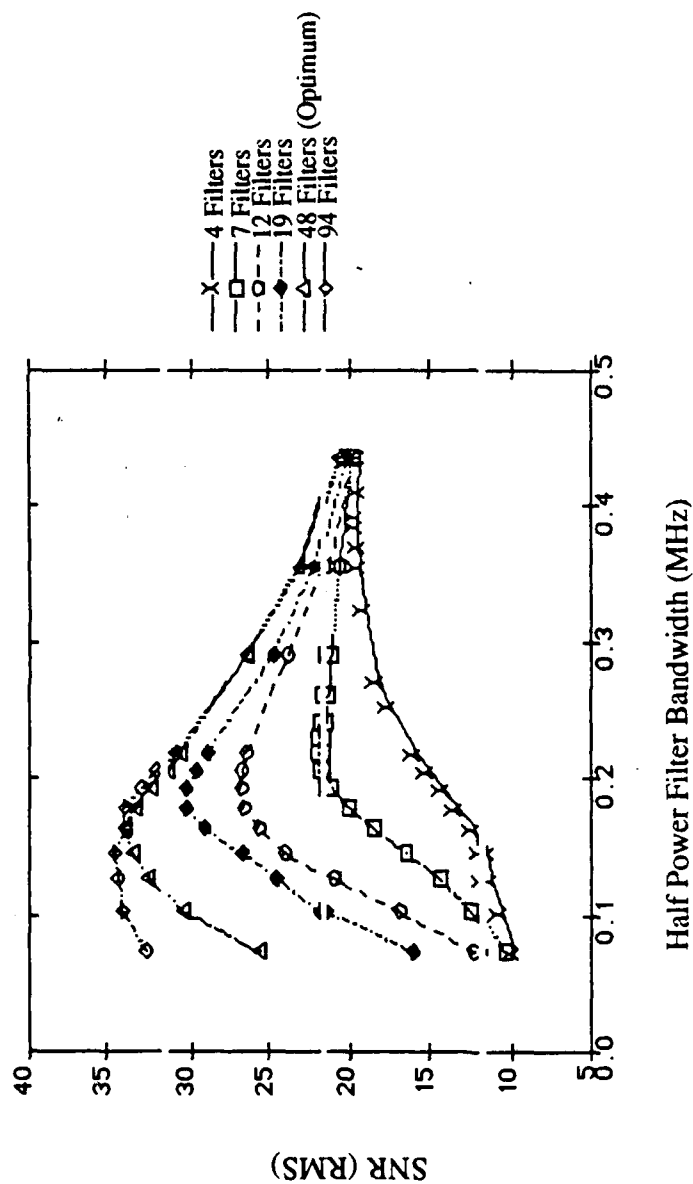


Figure 4.2c Performance curves showing the SNR as a function of the filter bandwidth for different number of filters

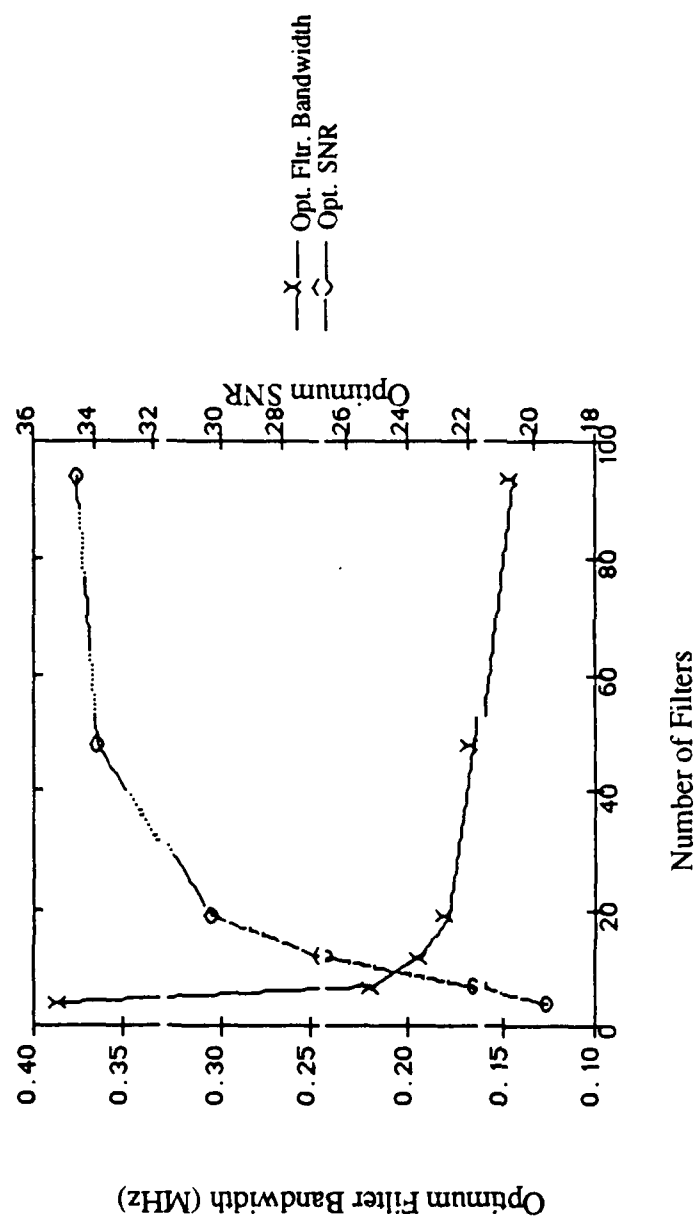


Figure 4.2d Graph showing the optimum filter bandwidth and the optimum SNR as a function of the total number of filters used

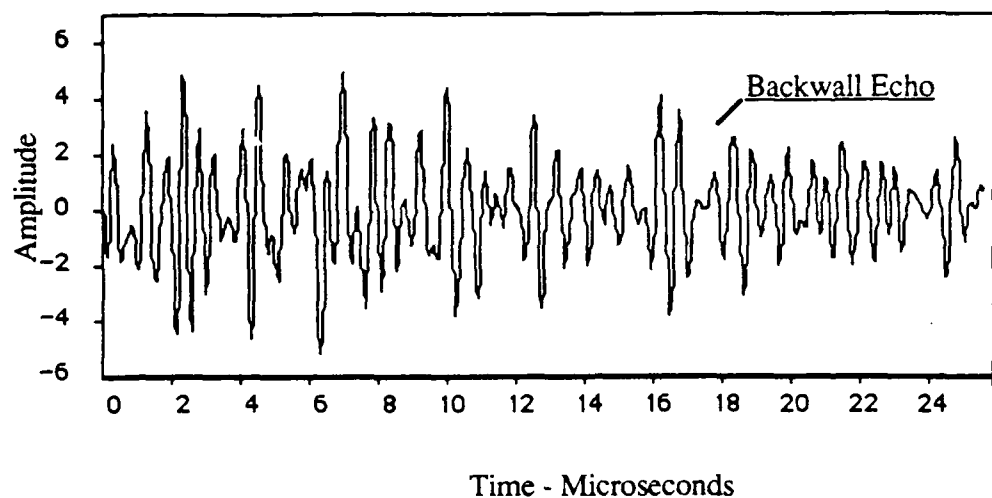


Figure 4.3a A signal obtained from an equiaxed CCSS test block showing the backwall echo. The signal from a cylindrical hole is completely obscured by grain noise.

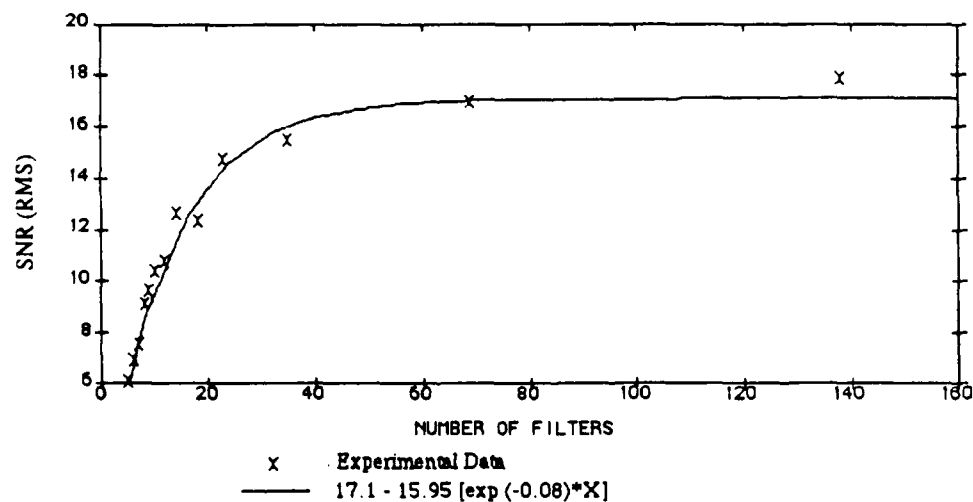


Figure 4.3b Graph of SNR (RMS) vs total number of filters used for the signal in Figure 4.3a

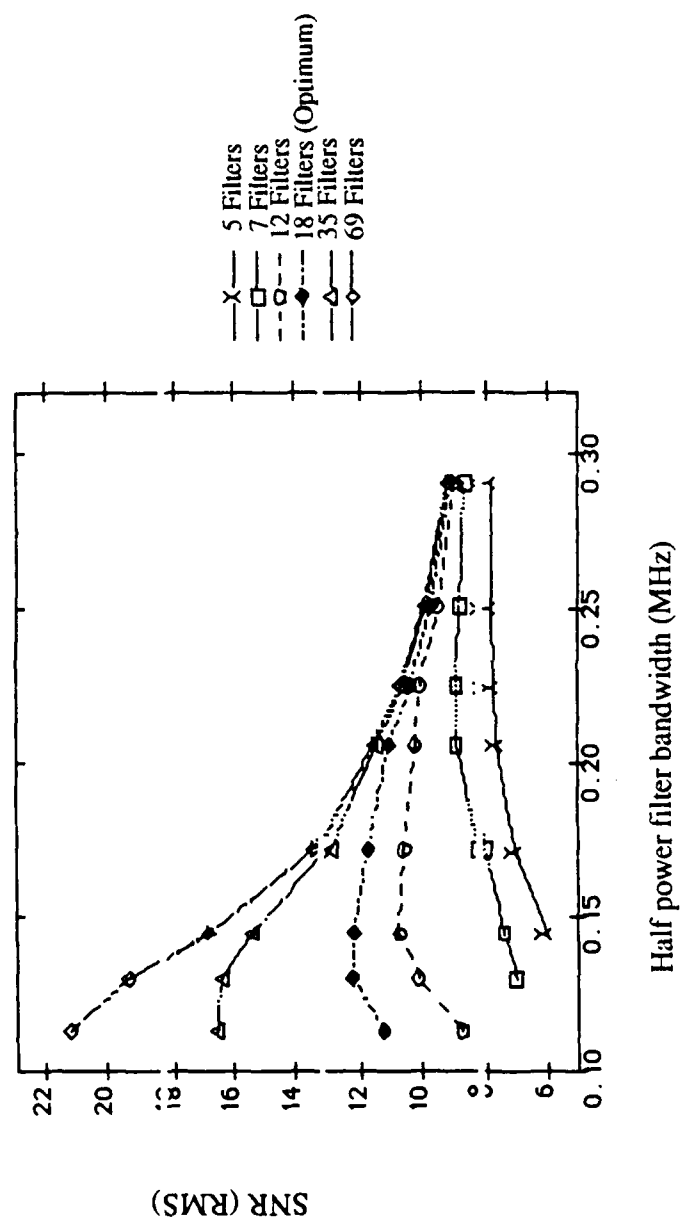


Figure 4.3c Performance curves showing the SNR as a function of the filter bandwidth for different number of filters

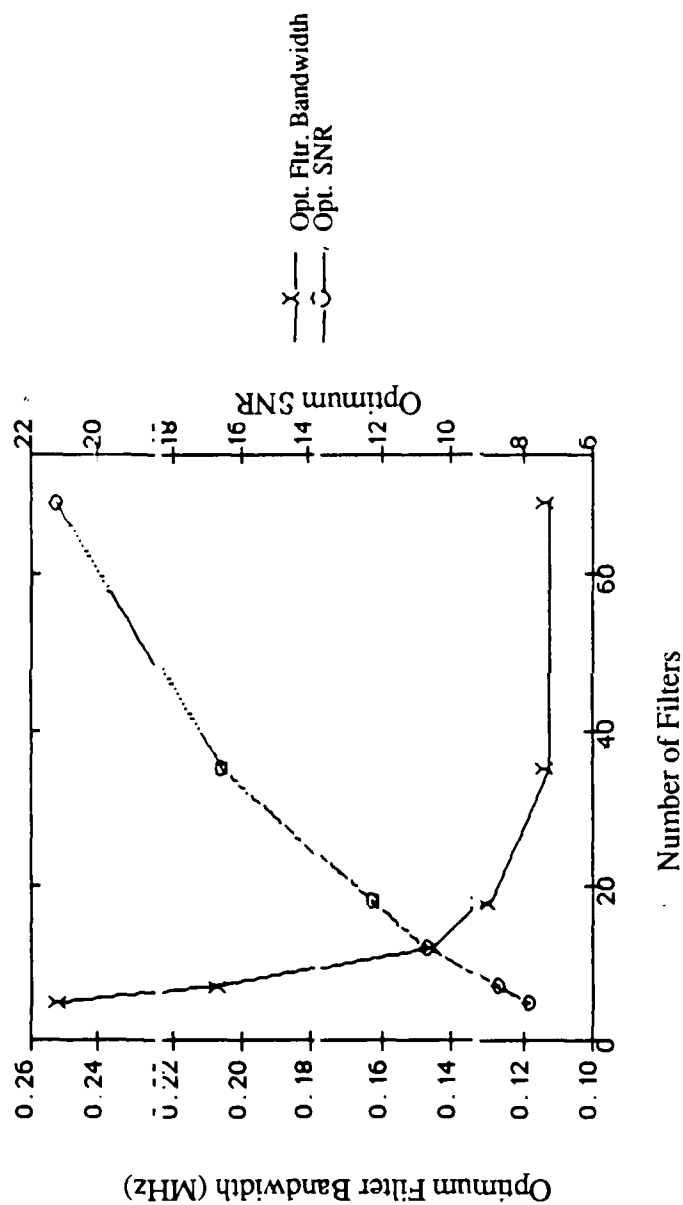


Figure 4.3d Graph showing the optimum filter badwidth and the optimum SNR as a function of the total number of filters

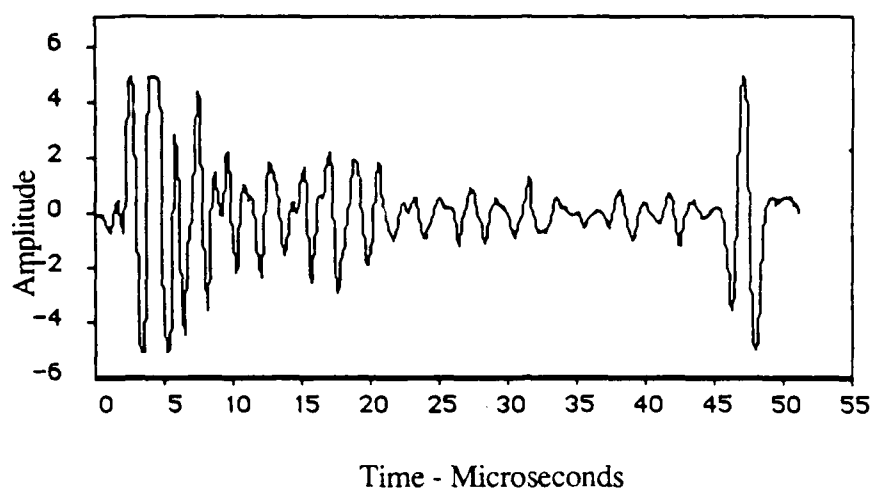


Figure 4.4a Signal obtained from a Carbon-Epoxy Composite Material

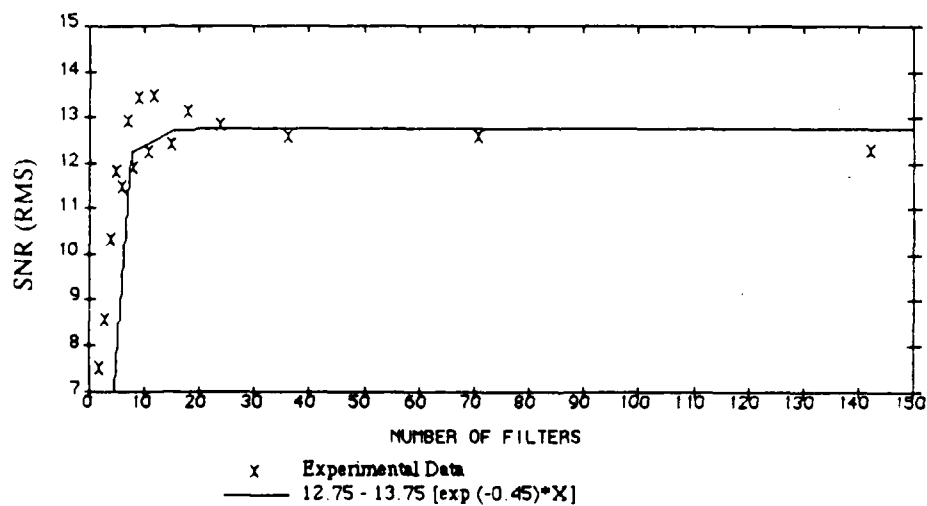


Figure 4.4b Graph of SNR (RMS) vs total number of filters used for the signal in Figure 4.4a

used. The time duration of the signal was 51.2 microseconds and hence, from (4.8), the optimum number of filters is 48. The signal shown in Fig. 4.3a is from a CCSS test block. It has been obtained using a transducer of center frequency 1.836 MHz and a HPBW of 0.673 MHz. The total time duration T of the signal is 25.6 microseconds. From (4.8), the optimum number of filters is 18. Figure 4.4a is a signal obtained from a Carbon-Epoxy composite material using a transducer of center frequency 5.66 MHz and a HPBW of 3.47 MHz. The total time duration of the signal is 5.12 microseconds. Hence, the optimum number of filters is 18. The performance of the technique has been evaluated using SNR calculated as per (4.11):

$$SNR_{rms} = \frac{\text{Maximum Peak to peak amplitude of the signal}}{\text{Root mean squared error of the signal}} \quad (4.11)$$

Figures 4.2b, 4.3b and 4.4b show the graphs of SNR vs. N , corresponding to Figs. 4.2a, 4.3a and 4.4a. The figures contain both the scatter diagram of the experimental data and the best fit exponential curve of the form ' $A - B\{EXP[(-C)X]\}$ '. It is clear from the graphs that the SNR saturates near the respective optimum number of windows calculated from (4.8). The SNR values plotted in Figs. 4.2b, 4.3b and 4.4b were obtained for a fixed 'optimum' filter bandwidth (determined experimentally) which yields a maximum SNR for the 'optimum' number of filters (This 'optimum' filter bandwidth corresponds to the bandwidth for which SNR is the maximum for the curve labelled 'optimum' in Figs. 4.2c and 4.3c).

The SNR defined by (4.11) is a good measure of performance only when a single target (flaw) is present. When multiple targets are present, as in the case of a composite material, the ratio in (4.11) fails to perform as a satisfactory evaluator because, the presence smaller targets contributes to an increased noise root-mean-squared value and hence reduces the calculated SNR value even though the detectability is increased. The effect is evidenced by the wide fluctuations of SNR in Fig. 4.4b. As a result, only CCSS and weld signals are considered for further detailed evaluation using SNR as a measure of performance.

Figures 4.2c and 4.3c are the performance curves plotted for various number of filters. The graphs are obtained by plotting SNR as a function of the filter bandwidth for each number of filters used for the study. It is clear from the figures that, the larger the

number of filters, the narrower the filter bandwidth must be to obtain the maximum SNR (hereafter referred to as the Optimum SNR and the corresponding filter bandwidth as the Optimum filter bandwidth).

Figures 4.2d and 4.3d are obtained from Figs. 4.2c and 4.3c respectively. The graphs show the optimum filter bandwidth and the corresponding optimum SNR for each number of filters used. That is, from each curve in Figs. 4.2c and 4.3c, maximum value of SNR and the corresponding filter bandwidth are selected and plotted in Figs. 4.2d and 4.3d. A discussion of these results is contained in the next section.

4.2.3 Discussion

The results presented in Figs. 4.2b, 4.3b and 4.4b clearly indicate that the SNR neither shows significant improvements nor deterioration when N is increased beyond that calculated from (4.8). This is because, even though the correlation of each filter with the immediately neighboring windows increases, there are more windows further away whose correlation is not significant. As a result, the effective number of uncorrelated windows, N'_u (Eqn. 4.10), is still close to the optimum N . Hence, the SNR remains asymptotic instead of deteriorating rapidly when the number of windows are increased beyond the 'optimum' level. Such a result can infact be readily predicted from (4.9a), (4.9b) and (4.10).

Figures 4.2c and 4.3c show results conforming to theory as defined by (4.1) through (4.8) and subject to (4.9a), (4.9b) and (4.10). That is, in both the figures, the curve for the optimum number of filters show better performance than when lesser number of filters are used. The higher SNR for the total number of filters larger than the optimum could be easily explained using Eqns. 4.9a, 4.9b and 4.10: as the total number of filters are increased, the effective number of uncorrelated filters (Eqn. 4.10) available increases, especially at smaller filter bandwidths (smaller filter bandwidth reduces the correlation between the neighboring windows and hence increases the effective number of uncorrelated windows). As a result, the SNR increases beyond that possible using the optimum number of filters. This might raise questions about using the word 'optimum' for the number of filters calculated using (4.8). However, the justification for the usage is immediately obvious from the Figs. 4.2d, and 4.3d. The improvement in SNR obtained in Fig. 4.2d is marginal even when N is almost doubled from 48 to 94, thereby proportionately increasing

the processing time. Similar results are evident from the performance curves in Fig. 4.3d also, wherein, the total number of filters has been more than tripled (from an optimum of 18 to a total of 69) while the SNR has increased only by about 1.7 times. Thus, the 'optimum' number of filters provide an excellent SNR enhancement for a relatively small processing time. It is also clear, referring to Figs. 4.2c and 4.3c, that the SNR from all the different number of filters converge to the SNR of the unprocessed signal with the progressive increase in the filter bandwidth.

This work uses Gaussian function rather than the theoretically optimum SINC windows for filtering. The energy contained in the main lobe of the SINC function is only about 54% while for a Gaussian window, the energy under HPBW is almost 70%. In other words, for a Gaussian function, lesser energy is contained outside its HPBW. Hence it is obvious that, in real practice, the bandwidth of the Gaussian filter used should be several times larger than that of the theoretically specified SINC function so that all the energy is not confined to a $2/T$ Hz frequency band for filters with 'optimum' frequency separation. The experimental results confirm that a larger HPBW overlap of the adjoining filters is necessary than that predicted for SINC filters. The results also show a strong dependence of the optimum filter bandwidth on the center frequency and bandwidth of the transducer and hence, the type of noise producing scatterers. This is shown by the data in Table 4.1 where the center frequencies and bandwidth of the transducers and the corresponding optimum bandwidth of the Gaussian filters determined experimentally have been tabulated.

4.3 Considerations for the Estimation of the Available Bandwidth of the Received Signal for the Spectral Splitting

The received bandwidth, 'B' [equations (4.7) and (4.8)], has been treated until now as a deterministically known value. However, in real practice, the received spectrum, and hence the available bandwidth 'B', is random to the extent of the presence of random material noise in the acquired signal. Consequently, it would be necessary to estimate the available bandwidth 'B' of the received signal for the use in (4.7) and (4.8).

The effect of material 'noise' on the spectrum of a received signal is evident from Figures 4.5 and 4.6. Figure 4.5a shows an impulse response of a transducer with negligible noise content. The corresponding spectrum is shown in Figure 4.5b. The spectrum in Figure 4.5b is close to a Gaussian shape due to the absence of material noise

Table 4.1 Table showing the relationship between the optimum filter bandwidth and the bandwidth of the transducer.

Transducer Designation	Center Frequency of the Transducer MHz	HPBW of the Transducer MHz	Optimum HPBW of the Gaussian Filter MHz
1	2.070	0.925	0.163
2	1.836	0.673	0.146
3	5.660	3.470	1.260

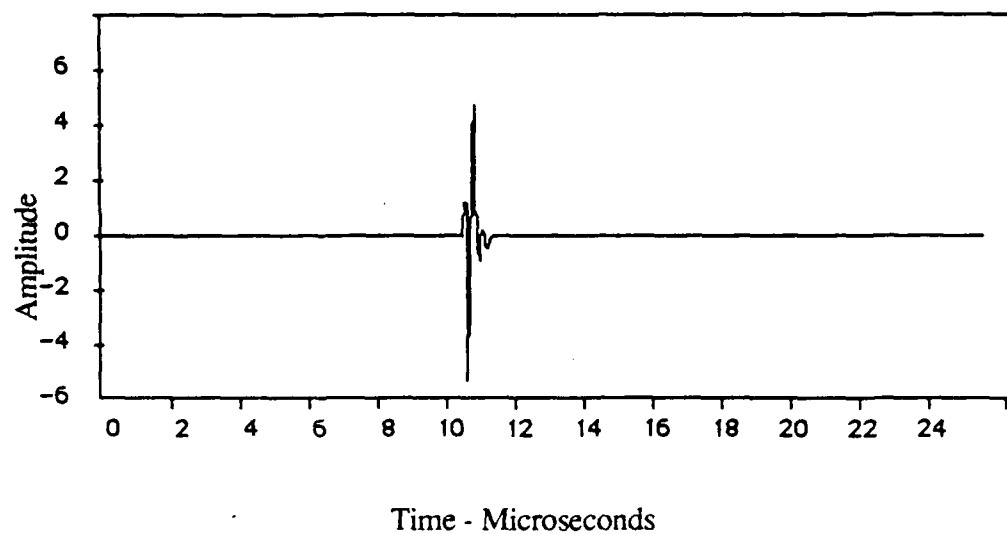


Figure 4.5a An impulse response of a 5 MHz nominal center frequency transducer in a standard reference stepped block

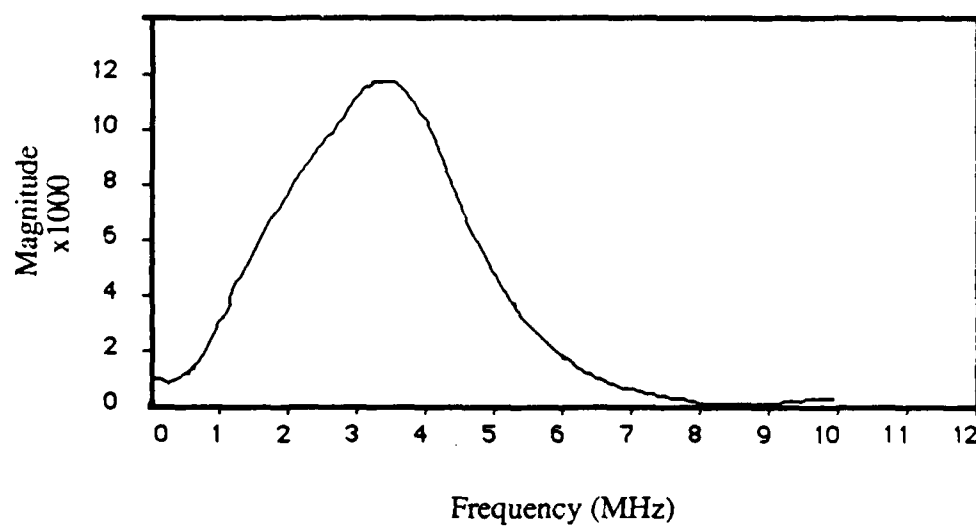


Figure 4.5b The magnitude-frequency spectrum of the impulse response shown in Figure 4.5a

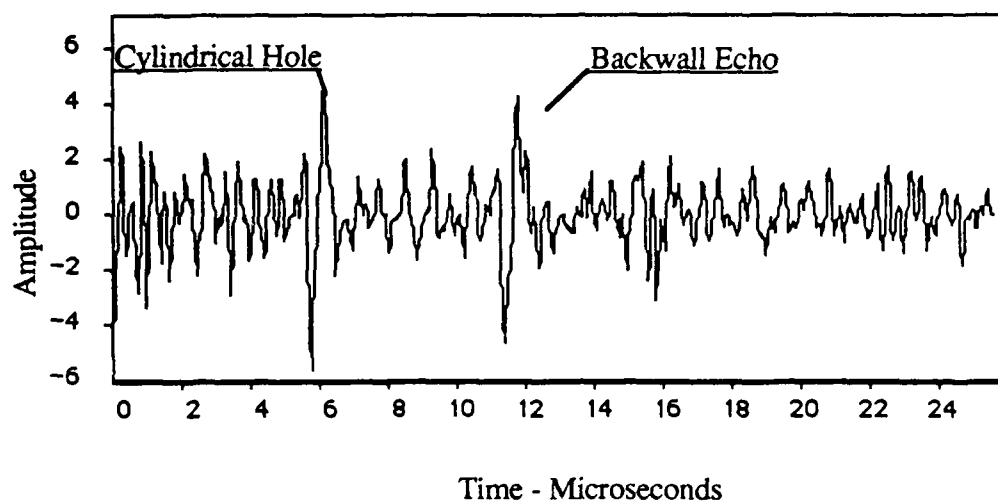


Figure 4.6a An ultrasonic signal obtained from an equiaxed CCSS test block using the transducer having an impulse response shown in Figure 4.5a

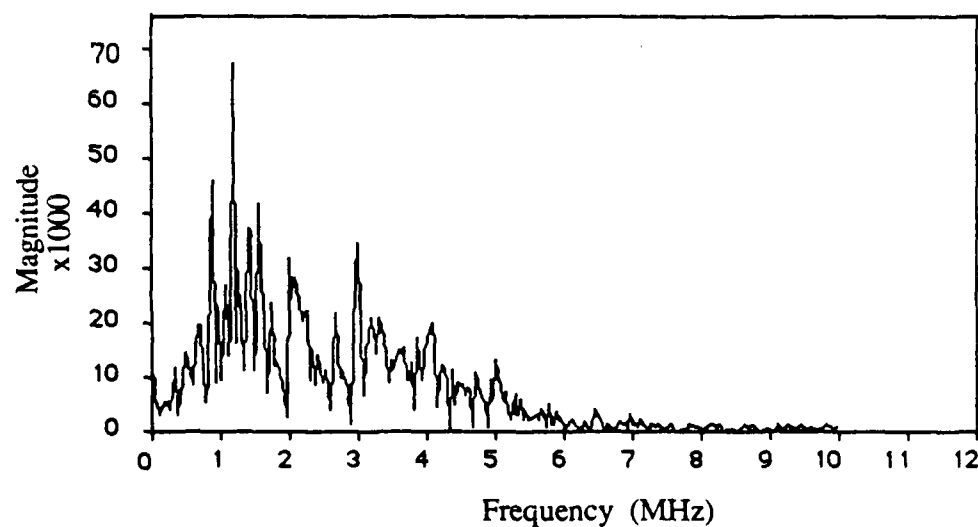


Figure 4.6b The magnitude-frequency spectrum of the signal shown in Figure 4.6a

content in the signal. However, in the presence of a high material noise content as in Figure 4.6a, the spectrum loses the smooth appearance as evidenced in Figure 4.6b. A comparison of Figure 4.5b and 4.6b shows that most of the energy content in the higher frequency band has been lost in Figure 4.6b. The fact that the spectrum becomes random and loses energy in the higher frequency range influences the bandwidth 'B' used for the spectral splitting process and has been studied experimentally in this section.

4.3.1 Experiments to Evaluate the Usable Bandwidth of the Spectrum of the Received Signal

A equiaxed CCSS test block with a side drilled hole is used for the experiments. A broad banded transducer of a nominal center frequency of 5 MHz has been used in conjunction with a Biomatron 8100 transient recorder and a 'PDP 11/23plus' computer to acquire the signals for the experiments.

The signal in Figure 4.5a is the transmitted impulse response with Figure 4.5b being the corresponding frequency spectrum. Figure 4.6a is a signal obtained from the CCSS test block and shows the echo signals from the cylindrical hole as well as the back surface of the test specimen. The spectrum of the received signal has been shown in Figure 4.6b and is the input to the spectral splitting process. The performance of the SSP technique is critically dependent on the extent and range of the spectrum (Figure 4.6b) over which the bank of bandpass filters are placed to split the spectrum.

The effect of using different bandwidths, B, on the performance of the SSP technique has been experimentally studied with the help of the signal in Figure 4.6a. The lower limit (ie., the location of the first, low frequency filter) of 'B' has been held constant while gradually increasing the upper limit of B (ie., the location of the last high frequency filter). The frequency separation, Δf , between the adjoining filters is a constant as determined by (4.6) which implies that an increase in the higher cut off limit of 'B' requires the use of more bandpass filters to split the spectrum. The first lowpass filter has been located at 0.98 MHz for these experiments ('A' in Figure 4.6b). Both minimization as well as minimization followed by polarity thresholding have been performed to study the effect of increasing B on the SNR enhancement. The SNR enhancement has been calculated by,

$$\text{SNR}_{\text{enhancement}} = \frac{\text{SNR}_{\text{output}}}{\text{SNR}_{\text{input}}} \quad (4.12)$$

where, the SNR values in the numerator and the denominator are defined by (4.11) and have been calculated with respect to the signal from the cylindrical hole (target echo).

The effect of increasing 'B' on the SNR enhancement has been presented in Figure 4.7 (minimization followed by polarity thresholding). The figure shows the SNR enhancement increasing gradually at first with increasing 'B' which allows a larger number of filters (N) at a fixed frequency separation, Δf . The SNR enhancement reaches a peak at about $B \approx 2.6$ MHz. However, if 'B' is increased further, the SNR enhancement begins to deteriorate rapidly. The deterioration is substantial even for small increases in 'B', although the values of 'B' are well within the transmitted bandwidth shown in Figure 4.5b. It is necessary to comparatively look at the spectra in Figures 4.5b and 4.6b to explain the deterioration in SNR enhancement which is discussed next.

4.3.2 Discussion

A comparison of the transmitted spectrum in Figure 4.5b with the received spectrum in Figure 4.6b reveals a large distortion in the received spectrum, especially in the higher frequency region resulting in the deterioration of SNR enhancement evidenced in Figure 4.7. It is essential to first understand the physical phenomenon which is responsible for the spectral distortion before arriving at some guidelines for the selection of an appropriate 'B'.

The spectral distortion observed in Figure 4.6b is primarily because of the attenuation due to scattering by the grain boundaries. It is a well known fact [65,71] that the scattering is proportional to the fourth power of frequency in the Raleigh region, is proportional to the second power of frequency in the stochastic region and is independent of frequency in the diffusion region of average grain size. The equiaxed CCSS sample used for the experiments has an average grain size of about 1.5 mm [68] and thus falls in the stochastic scattering region. As a result, for the given grain size, the attenuation due to scattering for increasing frequency can be represented by a curve as shown in Figure 4.8 which also shows a hypothetical transducer spectrum located on the same frequency axis.

Figure 4.8 demonstrates the effect of an overlap between the transducer spectrum

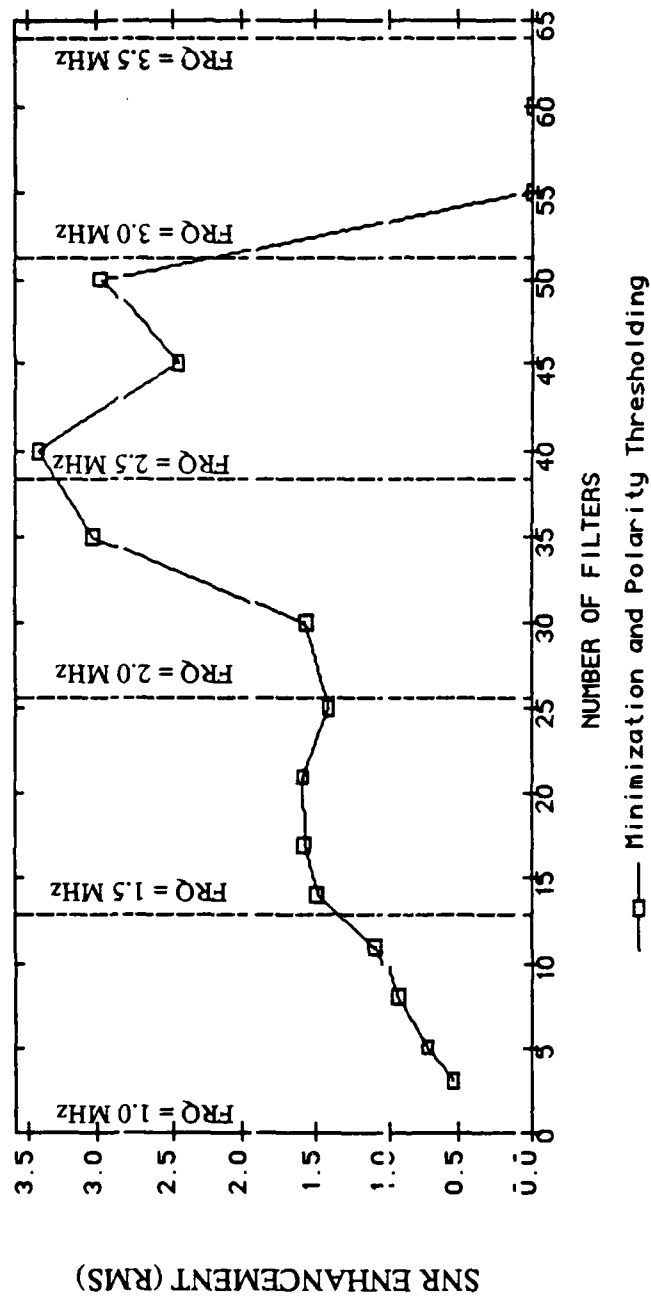


Figure 4.7 Signal-to-noise ratio enhancement curve due to split spectrum processing the signal in Figure 4.6a using minimization followed by polarity thresholding algorithms. The echo from the flat back surface of the sample has been used as a target.

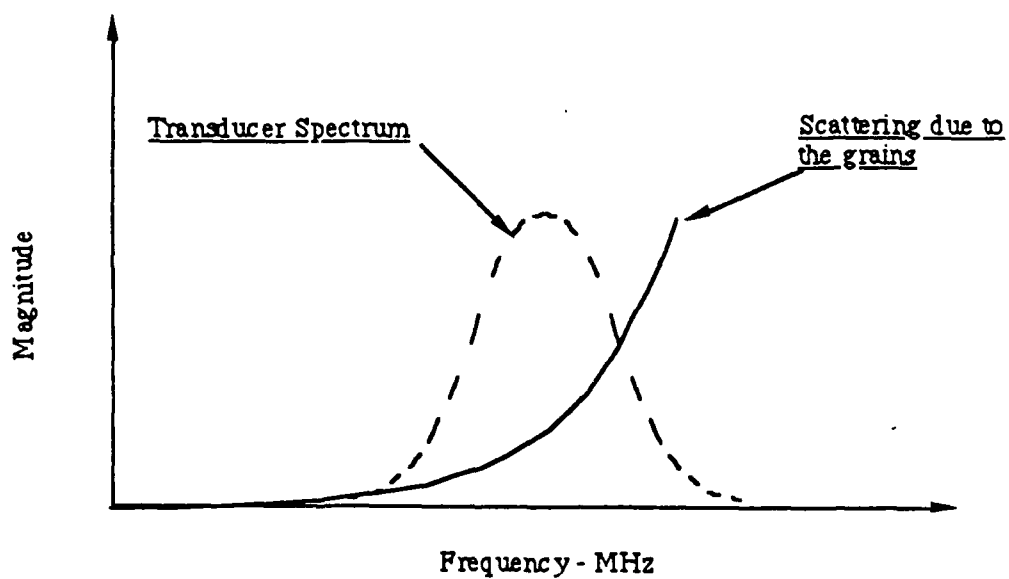


Figure 4.8 A hypothetical Transducer Spectrum and the grain scattering response shown on the same frequency axis to demonstrate the influence of grain scattering on the performance of a transducer.

and the scattering frequency response of the grains present in a material. As is evident from the figure, the effect of attenuation due to scattering is negligible at the lower end of the transducer spectrum while the scattering effect is quite pronounced towards the higher frequency range of the transducer. The consequence of using such a transducer to inspect a specimen of the scattering frequency response as shown in Figure 4.8 is the distortion of the spectrum of the received signal. The spectral distortion will be due to both the loss of energy in the higher frequency content and the randomness in the spectrum (Similar results, although in a slightly different context, have been reported by Shankar et al [72]). Although an immediate apparent solution to the problem is to use a transducer with the spectral contents located on the frequency axis where there is a low scattering response of the grains, such a solution is limited by the bandwidth and the center frequency requirements as determined by the axial and the lateral resolutions necessary for a given application. Also, on the other end of the limitation, the transducer spectrum should not be completely in the scattering region in which case hardly any energy reaches the target and returns to the receiver. Thus, it is a balance between the resolution requirements and the scattering limitations which determines the selection of a suitable transducer. A signal processing technique such as SSP helps in the selection of a transducer towards the higher frequency limits for a beneficial resolution while it would be necessary to select a transducer towards the lower frequency limits if a processing technique such as SSP is not used.

The preceding discussion leads to an important requirement for the success of SSP. Even a powerful technique such as SSP will be ineffective if the transducer spectrum overlaps the high scattering region because there is virtually no energy returning from a target of interest especially if the target is located deep in the material. Consequently, one of the most important criterion for the success of an ultrasonic NDE technique is that the transducer spectrum should be selected such that at least a portion of the transmitted spectrum reaches the target and returns to the transducer. It is this portion of the spectrum which should be used for the spectral splitting process.

The frequency range, 'B', over which the bandpass filters should be located to split the spectrum is dependent on grain scattering. If the objective of the experiments is to suppress grain 'noise' while retaining the target information, it is logical to conclude that the bank of bandpass filters used to split the spectrum should be located within the frequency range where the target information is present. If an improper range of frequencies is selected to locate the bank of bandpass filters, the filter/s towards the higher

frequency region might not contain any target information resulting in a drastic deterioration of the performance of the SSP technique. Such a deterioration can be easily explained by recalling the most important assumption of SSP: 'the target response is independent of frequency and hence is present in all the filters used for the splitting'. Consequently, if there is just a couple of bandpass filters at the high frequency range where very little target information exists, the assumption of frequency independence is violated resulting in a poor performance of the technique. Such a phenomenon of rapidly deteriorating performance with an increase in the value of 'B' is observed in Figure 4.7.

There is yet another important factor which dictates the location of the bank of bandpass filters and is again tied to the assumption of a frequency independent response of the target. The assumption of frequency independence implicitly assumes a planar target which is perpendicular to the direction of wave propagation. It has been shown by Bilgutay [2] that SSP in conjunction with minimization is fairly insensitive to the orientation of a planar target. However, his conclusion is valid only in the frequency range over which the wavelengths are relatively larger than the dimension by which the target is misoriented (ie., the same target might be detected by SSP using a transducer of lower frequency while being undetected using a transducer of higher frequency). Consequently, the requirement for the success of SSP is that the bank of bandpass filters should be located such that the wavelength due to the highest frequency bandpass filter is still relatively larger (at least 2 to 3 times) compared to the dimensions of the largest volumnar target (such as a side drilled cylindrical hole which offers the curved surface to the direction of insonification) or the largest dimension of misoriented target that has to be detected. This effect is demonstrated in Figure 9 wherein the SNR enhancement is calculated with respect to the echo from the cylindrical hole of 3 mm diameter (Figure 4.6a). From Figure 4.9, the SNR enhancement drops to zero when the center frequency of the highest frequency filter is about 2.6 MHz when the corresponding wavelength in CCSS is about 2.25 mm.

Based on the discussions on grain scattering and misoriented targets, an important conclusion can be drawn about the location of the bank of bandpass filters. Both scattering and orientation suggest the need for a conservative selection of the bandwidth 'B' over which the bank of bandpass filters can be located. In the absence of a pronounced scattering and for a small misorientation of a target, the entire bandwidth of the transducer can be used for the spectral splitting. On the other hand, if the scattering is pronounced and/or the orientation and the type of any target that might be present is difficult to estimate

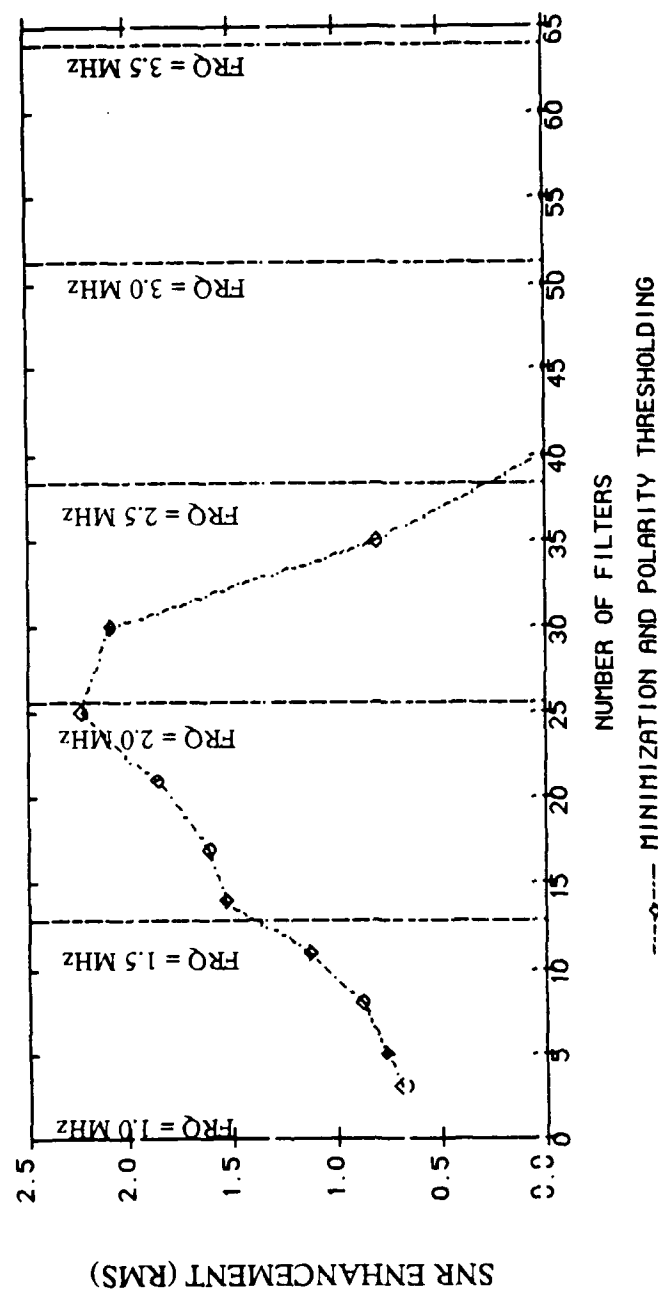


Figure 4.9 Signal to noise ratio enhancement plotted as a function of the number of filters used for spectral splitting. Minimization followed by polarity thresholding algorithms are used for the processing. The target echo is from a cylindrical hole of 3 mm diameter.

(which is usually true), then it is essential to place the filters over a conservatively selected bandwidth 'B' at the expense of a marginal reduction in SNR enhancement. Such a conclusion can be drawn from the Figures 4.7 and 4.9 wherein the maximum SNR enhancements are 3.5 and 2.3 respectively for a corresponding 'B' of 2.6 MHz and 2.25 MHz respectively. The selection of a larger 'B' drastically reduces the SNR enhancement while a conservative selection of 'B' will yield only a marginal reduction in the SNR enhancement while providing a reliable performance.

The fact that an apriori knowledge of the type and orientation of the target of interest is essential for a successful implementation of the SSP technique might appear to be a severe limitation of the usefulness of the SSP technique. However, the problem can be easily circumvented in a 'real life' implementation of SSP. Since the grain noise as well as the geometry and/or the orientation of the target might impose demanding limitations on the performance of the SSP technique, the parameter 'B' should be first determined by 'tuning' the processing algorithm using a reference block made of the same material to be tested and containing some programmed anomalies at appropriate depths closely representing the types that are expected to be found in the material. Once 'B' is selected, 'N' can be calculated from (4.6). Although an approximate bandwidth of the filters can be estimated from the theoretical considerations ($2/T$ Hz), the filter bandwidth is a function of the type of scatterers present as well as the type and size of the target to be detected and hence should be 'tuned' using the reference block approach. This process of 'tuning' is similar to the calibration process of the test equipment (such as the pulser/receiver, oscilloscope etc.) which is an essential part of any experimental work. Hence, the 'tuning' or the 'calibration' of the processing parameters with reference to the type of material being tested is a critical and an essential aspect of SSP which should be followed if the technique is to be successfully implemented with confidence. The calibration process has to be repeated and a new set of the processing parameters should be selected when any of the critical components (such as the transducer, test material etc.) of the test set up is altered. Further details of the determination of the available bandwidth for spectral splitting can be found in a paper by Karpur et al. [73]

4.4 Summary

A process model has been presented by considering an ultrasonic signal as a time limited, band unlimited process. The mathematical model so developed facilitates the use of the frequency sampling theorem and the principles of Fourier integral to arrive at the optimum number and the bandwidth of the filters used for the spectral splitting.

It has been experimentally corroborated that the SNR improvement is optimized by using the total number of filters calculated from the theory. There is no substantial improvement of SNR if N is increased beyond the optimum number. Even though SNR might show some increase beyond the optimum number of filters, increased processing time does not justify such an increased number of N . The optimum bandwidth of the filters show a strong dependence on the center frequency and the bandwidth of the transducer, and hence on the type of 'noise' producing scatterers present in the material.

It has also been experimentally shown that it is necessary to be conservative in the selection of the range of the bandwidth of the received spectrum over which the bank of bandpass filters is placed. The physical reasoning behind the need for a conservative estimate of the available bandwidth has been discussed using scattering theory and the relationship between the wavelength and the geometry of the target of interest. A method of circumventing the problem in a field application of the technique has been suggested.

5. POLARITY THRESHOLDING ALGORITHM; AN EVALUATION OF PERFORMANCE*,**

5.1 Introduction

Split spectrum processing is a frequency diversity technique which produces frequency diverse signals by splitting the broad band spectrum of the received echo instead of transmitting at different frequency bands as is done in classical frequency agility techniques in radar applications. Gaussian bandpass filters of different center frequencies but constant bandwidth are used to split the spectrum of the received signal into several overlapping frequency bands. The split frequency bands so obtained yield many time domain signals, one for each band, when inverse Fourier transformed. The several frequency diverse time domain signals (called spectral decomposition components) obtained by the splitting process makeup the input set of signals to the various SSP algorithms that have been developed for further processing. Many algorithms have been developed and theoretically analysed [47,49] in the past for processing the spectral decomposition components. These include the algorithms like minimization [2,15] optimal processor [46,47] square-of-the-mean and mean-of-the-square [47,49]. This chapter deals with the analysis of a newly developed [46,47] algorithm called 'Polarity Thresholding'.

Polarity thresholding algorithm is somewhat similar in operation to a 'sign detector' [69,70] and a Polarity Coincidence Correlator (PCC) [69,70] used in the past to detect signals in Gaussian and non-Gaussian noise. These algorithms were designed to detect 'nonreversal' of the sign of the amplitude in a channel when a sequence of independent samples was drawn from the channel. The similarity between the polarity thresholding algorithm on one hand and the PCC and the sign detector on the other, is limited to the fact that both classes of algorithms are sign detectors. However, in ultrasonic applications, the

* A version of this chapter is submitted to the IEEE transactions on Ultrasonics, Ferroelectrics and Frequency Control as a paper entitled "Split Spectrum Processing: Analysis of Polarity Thresholding Algorithm for Improvement of Signal-to-noise ratio and Detectability in Ultrasonic Signals", P. M. Shankar, P. Karpur, V. L. Newhouse and J. L. Rose

** A part of this chapter has been published as a paper entitled "Split Spectrum Processing: Performance of the Polarity Thresholding Algorithm in Signal-to-noise Ratio Enhancement in Ultrasonic Signals", V. L. Newhouse, J.L. Rose, P. Karpur and P. M. Shankar, proceedings of 'Progress in Quantitative NDE', June 1987.

signal of interest is not a constant d.c. offset but is a pulse of ultrasonic RF signal which is changing in sign as a function of time. As a result, a sequential sampling and sign test will not help in the detection of an ultrasonic signal of interest. Consequently the 'sign detection' by polarity thresholding is performed on several channels with identically distributed uncorrelated noise. The sign test is conducted at each time delay over a set of random variables obtained by sampling all the channels at that time delay. The process is repeated for each time delay until the complete time range of 0 to T sec is covered. Unlike a simple sign detector or a PCC, the polarity thresholding algorithm retains both the relative amplitude and relative phase of the signal of interest, especially when used in conjunction [53,58] with another split spectrum processing algorithm like minimization. Also, the polarity thresholding algorithm will indicate the presence or the absence of a target at a given time delay.

Polarity thresholding (PT) is based on the physics of wave-grain interaction. It is a well known fact that grain noise or clutter at a time delay τ_i is an interference pattern produced by the interaction of the ultrasonic wavelets scattered by the randomly packed, unresolvable scatterers that are present in the resolution cell at τ_i . Since it is an interference pattern, the clutter is not only dependent on the relative spatial position of the transducer and the test material but also on the frequency of the transmitted signal. The fact that the interference pattern changes when the transducer is moved with respect to the test material is utilized in the spatial compounding technique. Split spectrum processing, and hence PT, makes use of the fact that the interference pattern changes with the change in frequency. The details of the exact frequency splitting methodology can be found in the previous chapter of this dissertation. An analysis of the Polarity Thresholding algorithm follows.

5.2 Theory

This section contains a theoretical analysis of the Polarity Thresholding (PT) algorithm. A mathematical representation of an ultrasonic signal is defined. The PT algorithm, hereafter referred to also as 'the algorithm', is mathematically modeled based on which the probability density function of the processor is developed. Performance curves of the algorithm like the SNR curves and ROC curves are generated. Finally, experimental curves of SNR vs. filter bandwidth are also drawn.

5.2.1 Mathematical model of the signal

A typical ultrasonic signal of the type shown in Figure 5.1 can be mathematically represented by,

$$X(\tau_i) = m(\tau_i) + n(\tau_i) \quad \tau_0 < \tau_i < \tau_r \quad (5.1)$$

where $X(\tau_i)$ is the signal amplitude at time delay τ_i , $m(\tau_i)$ is the mean at time τ_i and $n(\tau_i)$ is the additive grain noise present at τ_i . Even though the signal of interest might exist beyond the range τ_0 to τ_r , it is considered only in the time range of $\tau_0 - \tau_r$ for the analysis.

The signal in Figure 5.1 is from a equiax grained, centrifugally cast stainless steel sample (CCSS). The signal shows two targets embedded in grain noise. It is a well known procedure to statistically model such grain noise by a Gaussian distribution of zero mean [49]. However, there is an additional assumption made in this analysis: for a signal with grain noise alone, it can be assumed that the process mean is zero and the variance is σ_n^2 along the time axis as well as across the ensemble at each time delay τ_i . However, such an assumption of zero mean in either direction will no longer be valid in the presence of a target signal, as in the case of Figure 5.1, the reason for which is discussed in the following paragraph.

Figure 5.1 shows two time delays τ_1 and τ_2 , selected respectively when there is no target signal and when there is a target signal. At time τ_1 , the signal is represented by $X(\tau_1) = n(\tau_1)$. Thus, at τ_1 , mean across the ensemble is zero and the variance is σ_n^2 . However, at τ_2 , the mean across the ensemble is no longer zero because of the presence of a target signal. The mean, 'm', can be either positive or negative depending on the time delay selected within the reflected pulse from the target which is present over the range $\tau_a - \tau_b$. Hence, within the range $\tau_a - \tau_b$, the signal is represented by $X(\tau_i) = m(\tau_i) + n(\tau_i)$ where $m(\tau_i)$ can be either positive or negative depending on τ_i . Nevertheless, because of the physical nature of the RF signal in Figure 5.1, the mean of the signal along the time axis still has to be zero. Hence, results of the ensuing theoretical analysis will be conducted at each time delay (across the ensemble) and will not be assumed applicable along the time axis also as was done in the earlier studies [47,49] conducted for the other algorithms. It should be noted that, the speckle or clutter noise is assumed to be the same both inside and outside of the target region. As a result, the variance σ_n^2 is the same in the presence or

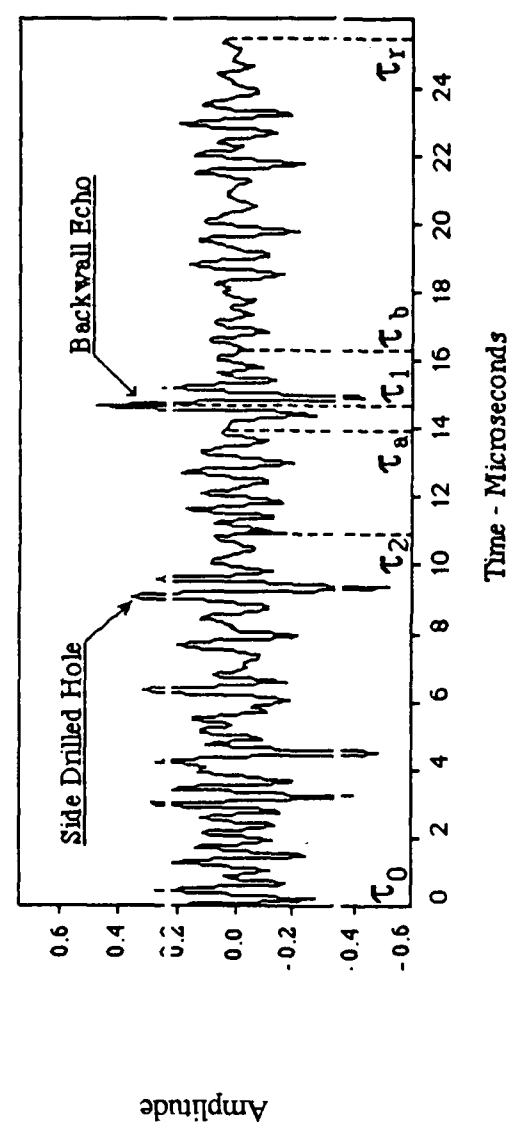


Figure 5.1 An ultrasonic signal obtained from a centrifugally cast stainless steel block with a side drilled hole. The figure illustrates the various time delays used in the theoretical analysis

absence of a target. Hence, the signal can be represented as,

$$X(\tau_i) = m(\tau_i) + n \quad \tau_a < \tau_i < \tau_b \quad (5.2) \text{ a}$$

$$X(\tau_i) = n \quad \text{elsewhere} \quad (5.2) \text{ b}$$

5.2.2 Polarity Thresholding algorithm

The theoretical analysis of PT presented in this chapter begins with the 'N' frequency diverse signals (also called spectral decomposition components) obtained by splitting the spectrum of the received signal. Let $W_j(\tau_i)$, $j = 1, 2, \dots, N$ be the spectral decomposition components at τ_i obtained by splitting the spectrum of the signal $X(t) = m(t) + n$; $m(t)$ is zero if there is no target at $t = \tau_i$ and nonzero if there is a target at $t = \tau_i$; n is the Gaussian distributed random noise of zero mean and σ_n^2 variance; N is the number of bandpass filters used to split the spectrum. The signals obtained by the process of spectral decomposition are given by,

$$W_j(\tau_i) = \mu(\tau_i) + n_j^* \quad j = 1, \dots, N \quad (5.3)$$

where $\mu(\tau_i) = m(\tau_i)/N$, n_j^* is the Gaussian distributed random noise of zero mean and a variance of $\sigma_j^{*2} = \sigma_n^2/N$. For mathematical simplicity, it has been assumed that the statistics of n_j^* , $j = 1, \dots, N$ is described by mutually independent Gaussian distribution of zero mean and σ^{*2} variance. Hence, $\sigma_1^{*2} = \sigma_2^{*2} = \sigma_3^{*2} = \dots = \sigma_N^{*2} = \sigma^{*2}$. Thus, (5.3) reduces to,

$$W_j(\tau_i) = \mu(\tau_i) + n^* \quad j = 1, \dots, N \quad (5.4) \text{ a}$$

$$W_j(\tau_i) = n^* \quad j = 1, \dots, N \quad (5.4) \text{ b}$$

The signals represented by (5.4a) and (5.4b) are frequency diverse because of the splitting process. As a result, the interference pattern produced by the grain boundaries is different in each $W_j(\tau_i)$. However, $\mu(\tau_i)$, which is the amplitude due to a target is frequency independent (in the range of frequencies transmitted by a suitably selected transducer). Since n^* in every $W_j(\tau_i)$ is independent of n^* in every other $W_j(\tau_i)$, the probability that $W_j(\tau_i)$, $j = 1, \dots, N$ defined in (5.4b) are all positive or all negative is very small and

decreases as a function of N . However, when in fact a target is present as in (5.4a), the probability that all $W_j(\tau_i)$, $j = 1, \dots, N$ are either positive or negative increases as a function of the ratios $(\mu(\tau_i)/\sigma^*)$ and $1/N$. This physical principle has been made use of in the development of the polarity thresholding algorithm which is mathematically defined as follows:

$$\begin{aligned} Z(\tau_i) &= X(\tau_i) && \text{if all } W_j(\tau_i) \text{ are positive, } j = 1, \dots, N \\ &= X(\tau_i) && \text{if all } W_j(\tau_i) \text{ are negative, } j = 1, \dots, N \\ &= 0 && \text{otherwise} \end{aligned} \quad (5.5)$$

where, $Z(\tau_i)$ is the processor output at each τ_i , $X(\tau_i)$ is the unprocessed signal amplitude at τ_i before spectral splitting and $W_j(\tau_i)$, $j = 1, \dots, N$ are the spectral decomposition components at the corresponding τ_i . Also, since it has already been stated that the following analysis is at each time delay, the term ' τ_i ' will be dropped from all the equations with the assumption that τ_i is implied whenever ' X ', ' m ', ' μ ', ' W ' or any functions of these variables are mentioned.

The algorithm defined by (5.5) is the most severe of the many possibilities. Lesser severe forms of the same algorithm can be easily implemented by allowing more than one polarity reversal before equating Z to zero. Depending on the severity of implementation and the number of bandpass filters used, a certain probability of losing a target altogether always exists, especially when $R = (m/\sigma_n)$ is very small. Consequently, it is imperative to understand the performance of the algorithm as a function of R and N ; hence the following theoretical analysis of the process.

5.2.3 Density function of Polarity Thresholding

According to the processor defined by (5.5), the output ' z ' can only take either of the two possible values: x , the input amplitude, or zero. Hence, the conditional probability density function of Z is given by,

$$f_Z(z|x) = P(Z = x) \delta(z - x) + P(Z = 0) \delta(z) \quad (5.6)$$

where, $P(Z = X)$ is the probability of $Z = x$, $P(Z = 0)$ is the probability of $Z = 0$, $\delta(z - x)$

and $\delta(z)$ are delta functions defined at $Z = x$ and $Z = 0$, respectively. Since 'X' and W_j are assumed to be represented by (5.2a), (5.2b) and (5.4 a), (5.4b) and have Gaussian statistics, the respective density functions are given by,

$$f_X(x) = \frac{1}{\sqrt{2\pi} \sigma_n} \exp\left(-\frac{(x-m)^2}{2 \sigma_n^2}\right) \quad (5.7a)$$

$$f_{W_j}(w_j) = \frac{1}{\sqrt{2\pi} \sigma^*} \exp\left(-\frac{(w_j-\mu)^2}{2 \sigma^{*2}}\right) \quad (5.7b)$$

where, $f_X(x)$ and $f_{W_j}(w_j)$ are the density functions of 'X' and spectral decomposition components W_j , respectively; $\mu = m/N$ and $\sigma^{*2} = \sigma_n^2/N$. It should be noted that m and hence μ can take the value of zero if there is no target signal at τ_i .

If there are N spectral decomposition components, then $P(Z = x)$ and $P(Z = 0)$ in (5.6) are defined by,

$$P(Z = x) = \left[1 - \frac{1}{\sqrt{2\pi} \sigma^*} \int_0^\infty \exp\left(-\frac{(w_i-\mu)^2}{2 \sigma^{*2}}\right) dw_i \right]^N \\ + \left[\frac{1}{\sqrt{2\pi} \sigma^*} \int_0^\infty \exp\left(-\frac{(x_i-\mu)^2}{2 \sigma^{*2}}\right) dw_i \right]^N$$

and, $P(Z = 0) = 1 - P(Z = x)$. Let,

$$C = \left[1 - \frac{1}{\sqrt{2\pi} \sigma^*} \int_0^\infty \exp\left(-\frac{(w_i-\mu)^2}{2 \sigma^{*2}}\right) dw_i \right]^N$$

and,

$$D = \left[\frac{1}{\sqrt{2\pi} \sigma^*} \int_0^\infty \exp\left(-\frac{(w_i-\mu)^2}{2 \sigma^{*2}}\right) dw_i \right]^N$$

Consider,

$$D^{1/N} = \left[\frac{1}{\sqrt{2\pi} \sigma^*} \int_0^\infty \exp \left(-\frac{(w_i - \mu)^2}{2 \sigma^{*2}} \right) dw_i \right] \quad (5.8)$$

Substituting $\frac{w_i - \mu}{\sqrt{2} \sigma^*} = t$, and differentiating with respect to t , we get, $\frac{dw_i}{\sqrt{2} \sigma^*} = dt$; hence, when $W_i = 0$, t becomes equal to $-\frac{\mu}{\sqrt{2} \sigma^*}$, and when $W_i = \infty$, t is also equal to ∞ .

Therefore, Equation (5.8) reduces to,

$$\begin{aligned} D^{1/N} &= \frac{1}{2} \left[\frac{2}{\sqrt{\pi}} \int_{-\frac{\mu}{\sqrt{2} \sigma^*}}^\infty \exp(-t^2) dt \right] \\ &= \frac{1}{2} \left[\frac{2}{\sqrt{\pi}} \int_{-\frac{\mu}{\sqrt{2} \sigma^*}}^0 \exp(-t^2) dt + \frac{2}{\sqrt{\pi}} \int_0^\infty \exp(-t^2) dt \right] \\ &= \frac{1}{2} \left[-\operatorname{erf} \left(-\frac{\mu}{\sqrt{2} \sigma^*} \right) + 1 \right] \end{aligned}$$

Since $\operatorname{erf}(-b) = -\operatorname{erf}(b)$, we have,

$$D = \frac{\left[1 + \operatorname{erf} \left(\frac{\mu}{\sqrt{2} \sigma^*} \right) \right]^N}{2^N} \quad (5.9a)$$

where,

$$\operatorname{erf}(b) = \frac{2}{\sqrt{\pi}} \int_0^b \exp(-t^2) dt \quad (5.9b)$$

Hence,

$$C = [1 - D^{1/N}]^N = \frac{\left[1 - \operatorname{erf} \left(\frac{\mu}{\sqrt{2} \sigma^*} \right) \right]^N}{2^N} \quad (5.10)$$

However, since W_i 's are obtained by splitting a gaussian distributed variable, X , and since it has already been assumed that W_i are mutually independent and that their amplitudes have identical Gaussian density functions of zero mean and a variance of σ^2 , we get,

$$\mu = \frac{m}{N} \text{ and } \sigma^2 = \frac{\sigma_n^2}{N} \quad (5.11)$$

Therefore, (5.9) and (5.10) become,

$$D = \frac{\left[1 + \operatorname{erf} \left(\frac{m}{\sqrt{2N} \sigma_n} \right) \right]^N}{2^N} \quad (5.12a)$$

and,

$$C = \frac{\left[1 - \operatorname{erf} \left(\frac{m}{\sqrt{2N} \sigma_n} \right) \right]^N}{2^N} \quad (5.12b)$$

Therefore, (5.6) becomes,

$$f(z|x) = (C + D) \delta(z - x) + [1 - (C+D)] \delta(z) \quad (5.13)$$

Let $A' = C + D$ and $B' = 1 - A'$. Then, the joint density function, $f(z,x)$, is given by,

$$\begin{aligned} f(z,x) &= f(z|x) f(x) \\ &= [A' \delta(z - x) + B' \delta(z)] \left\{ \frac{1}{\sqrt{2\pi} \sigma_n} \exp \left(-\frac{(x - m)^2}{2 \sigma_n^2} \right) \right\} \end{aligned} \quad (5.14)$$

The probability density function, $f(z)$, is given by integrating (5.14) with respect to x :

$$f(z) = \int_{-\infty}^{+\infty} f(z,x) dx$$

$$= \int_{-\infty}^{+\infty} [A' \delta(z-x) + B' \delta(z)] \left\{ \frac{1}{\sqrt{2\pi} \sigma_n} \exp\left(-\frac{(x-m)^2}{2\sigma_n^2}\right) \right\} dx$$

Therefore, the probability density function of the output of the algorithm is given by,

$$f(z) = \frac{A'}{\sqrt{2\pi} \sigma_n} \exp\left(-\frac{(z-m)^2}{2\sigma_n^2}\right) + B' \delta(z) \quad (5.15)$$

where,

$$A' = \frac{\left[1 - \operatorname{erf}\left(\frac{R}{\sqrt{2N}}\right)\right]^N + \left[1 + \operatorname{erf}\left(\frac{R}{\sqrt{2N}}\right)\right]^N}{2^N} \quad (5.16a)$$

$$R = \operatorname{SNR}_{\text{input}} = \frac{m}{\sigma_n} \quad (5.16b)$$

$$\text{and, } B' = 1 - A' \quad (5.17)$$

Expected value of the output, z

$$\begin{aligned} E[z] = \bar{z} &= \int_{-\infty}^{+\infty} z f(z) dz \\ &= \int_{-\infty}^{+\infty} z \left\{ \frac{A'}{\sqrt{2\pi} \sigma_n} \exp\left(-\frac{(z-m)^2}{2\sigma_n^2}\right) + B' \delta(z) \right\} dz \\ &= mA' \quad \text{if } m \neq 0 \end{aligned} \quad (5.18a)$$

$$= 0 \quad \text{if } m = 0 \text{ (ie., no target at the time delay)} \quad (5.18b)$$

Variance of the output, z

$$\sigma_z^2 = E[z^2] - (E[z])^2 \quad (5.19)$$

$$= \int_{-\infty}^{+\infty} z^2 f(z) dz - (mA')^2$$

$$\begin{aligned}
&= \int_{-\infty}^{+\infty} z^2 \left\{ \frac{A'}{\sqrt{2\pi} \sigma_n} \exp \left(-\frac{(z-m)^2}{2\sigma_n^2} \right) + B' \delta(z) \right\} dz - (mA')^2 \\
&= (\sigma_n^2 + m^2)A' - (mA')^2 \quad \text{if } m \neq 0 \quad (5.20a)
\end{aligned}$$

$$= \sigma_n^2 A' \quad \text{if } m = 0 \quad (5.20b)$$

5.3 Results of theoretical analysis

Theoretical performance curves have been generated under three categories:

1. SNR enhancement curves
 - a. for the signal in the range of 'T' sec,
 - b. at the time delay τ_i when there is no target at τ_i ,
 - c. at the time delay τ_i when there is a target at τ_i ,
2. probabilities of false alarm and detection and the ROC,
 - a. probability of false alarm vs. N,
 - b. probability of detection vs. N,
 - c. receiver operating characteristics (ROC),
 - i. ROC with no threshold set to the output signal,
 - ii. simple thresholding of the signal without any processing,
 - iii. ROC curves for 3 filters,
 - iv. ROC curves for 5 filters, and
 - v. ROC curves for 7 filters.

5.3.1 SNR enhancement curves

5.3.1.1 SNR enhancement for the signal in the total range of T sec

Several different definition of SNR are used for the evaluation of the various aspects of the performance of the algorithm. The conventional definition of SNR is given by,

$$\text{SNR} = (\text{mean}/\sigma) \quad (5.21)$$

For a signal of the type shown in Figure 5.1, it is usual that there are more time delays where no target exists than the number of time delays where a target exists. As a result, the variance of the output signal (variance of the output signal when all the time delays are considered together) can be approximated by the variance defined by (5.20b). Hence,

$$\text{SNR}_{\text{input signal}} = \frac{m}{\sigma_n} = R$$

$$\begin{aligned} \text{SNR}_{\text{output signal}} &= \frac{\text{Mean of the output when a target is present}}{(\text{Variance of the output without a target})^{1/2}} \\ &= \frac{m A'_{m \neq 0}}{\sigma_n (A'_{m=0})^{1/2}} = \frac{R A'_{m \neq 0}}{\left(\frac{1}{2}\right)^{(N-1)/2}} = A'_{m \neq 0} R 2^{(N-1)/2} \end{aligned}$$

where $A'_{m \neq 0}$ is given by (5.16a) and $A'_{m=0}$ is given by substituting $m = 0$ in (5.16a).

$$\begin{aligned} \text{SNR}_{\text{enhancement}} &= \frac{\text{SNR}_{\text{output signal}}}{\text{SNR}_{\text{input signal}}} = A' 2^{(N-1)/2} \\ &= \left(\frac{\left[1 - \text{erf} \left(\frac{R}{\sqrt{2N}} \right) \right]^N + \left[1 + \text{erf} \left(\frac{R}{\sqrt{2N}} \right) \right]^N}{2^{(N+1)/2}} \right) \end{aligned} \quad (5.22)$$

Figure 5.2 shows curves obtained by plotting the SNR enhancement (5.22) as a function of input SNR. From the figure, polarity thresholding algorithm has a beneficial SNR enhancement for $R > 1$. Also, if $R > 1$, SNR enhancement initially increases with increase in N and reaches a maximum. Upon further increase in N , the SNR enhancement starts to decline. Conceptually, the optimum number of filters, N' , for maximum SNR enhancement can be found by differentiating (5.22) with respect to N . However, since A' in (5.22) includes the error function (5.16a), the expression to be solved becomes too

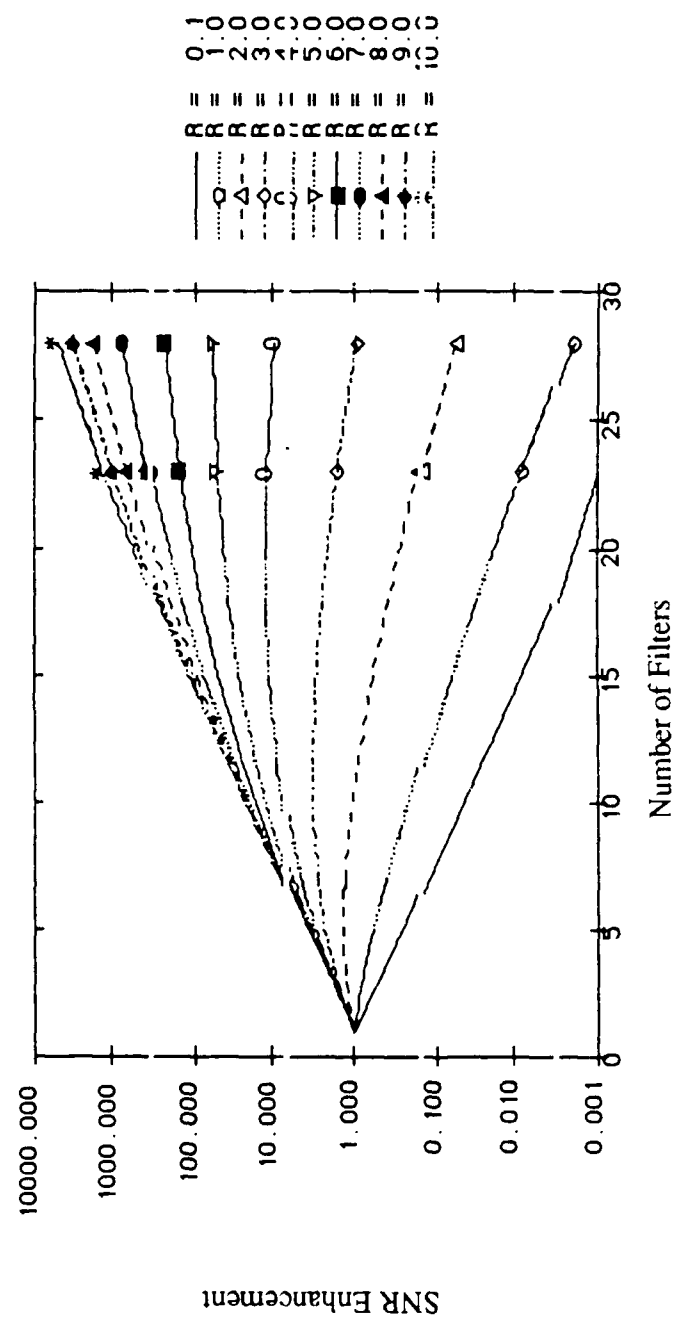


Figure 5.2 Theoretical signal-to-noise ratio curves showing the SNR enhancement of the whole signal when all the time delays are considered

complex thereby making a closed form of analytical expression for N impractical to derive. Nevertheless, the optimum number of windows can be obtained by numerical methods or directly from Figure 5.2. Thus, the optimum number of filters, N , is given by the smaller of the two N values calculated: i) from Figure 5.2 ii) from the equation $N = BT$ (4.8), where B is the halfpower bandwidth of the spectrum of the received signal and T is the total time duration of the received signal (for example, $T = \tau_r - \tau_0$ in Figure 5.1).

It should be remembered that for the sake of mathematical simplicity, the spectral decomposition components were assumed to be mutually independent and Gaussian distributed. However, in the actual implementation of the algorithm, the decomposition components will have a nonzero correlation coefficient because it has been shown in the previous chapter as well as [61], that for a good performance of the SSP technique, the bandpass filters should be substantially overlapping. The effect of such a correlation on the curves in Figure 5.2 would be to flatten the curves thereby producing a large plateau when $R > 1$ (and hence lower SNR enhancements). Thus, the output SNR and hence the SNR enhancement is also a function of the filter bandwidth (ie., the degree of overlap between the adjoining filters and hence their correlation). This effect has been studied by experimentation, the results of which are discussed next.

Equations (5.23a), (5.23b) and (5.23c) define a new SNR_{signal} to measure, experimentally, the SNR enhancement of the whole signal:

$$SNR_{\text{signal}} = \frac{\text{Maximum peak to peak amplitude of the target signal}}{\text{Standard deviation of the total signal}}$$

$$\therefore SNR_{\text{input signal}} = \frac{\text{Maximum peak to peak amplitude of the target signal}}{\sigma_n} \quad (5.23a)$$

$$SNR_{\text{output signal}} = \frac{\text{Maximum peak to peak output amplitude of the target}}{\sigma_z} \quad (5.23b)$$

$$SNR_{\text{enhancement}} = \frac{SNR_{\text{output signal}}}{SNR_{\text{input signal}}} \quad (5.23c)$$

Figure 5.3 shows the plots of experimental SNR enhancement (Eqn. 5.23c) vs. the half

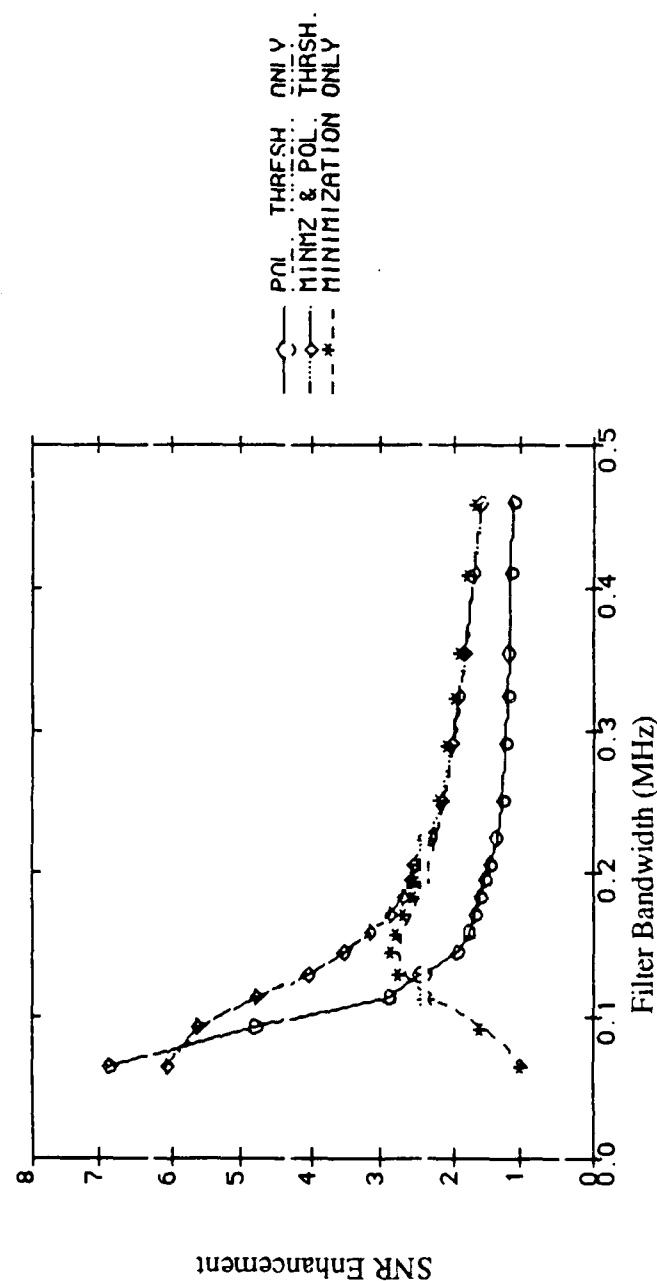


Figure 5.3 Experimental signal-to-noise ratio curves using i. polarity thresholding alone
 ii. minimization and polarity thresholding algorithms used in tandem and
 iii. minimization alone

power bandwidth (HPBW) of the Gaussian bandpass filters for $N = 18$. The SNR enhancement for these curves have been defined by Equation 5.23c. The curve (labelled 'Pol. Thresh. only') shows a large SNR enhancement for smaller filter bandwidths and gradually approaches the SNR of the unprocessed signal with the increase in the HPBW of the filters. The reason for this behavior is obvious from Figures 5.4a, 5.4b and 5.4c which show the processed outputs for HPBW of 0.092 MHz, 0.172 MHz and 0.46 MHz, respectively.

5.3.1.2 SNR enhancement at a time delay in the presence and in the absence of a target

When a processor like polarity thresholding is being applied to reduce the variance of the signals at time delays either with a target or without a target, it would be necessary to study the performance of the algorithm in reducing the variance of the output at a time delay. This is because, when the algorithm is applied for SNR enhancement, the objective is to reduce variance at each time delay, whether a target is present or not. It has already been shown that in the absence of a target, the mean of the input signal at the time delay is zero. As such, the ratio in Equation 5.21 is always zero and hence is not a good evaluator of performance for the reduction in the variance. However, if the measure of performance is defined by the ratio $(1/\sigma)$, the enhancement produced by a processor in the presence or the absence of a target can still be evaluated. In fact, the ratio $(1/\sigma)$ can be considered as the SNR enhancement per unit mean when a target is present at τ_i . As a result, the performance evaluator at a time delay has been defined by,

$$\text{SNR} = \frac{1}{\sigma} \quad (5.24)$$

The denominator in (5.24) will be the input σ for the signal before processing and the output σ for the signal after processing.

$$\text{SNR}_{\text{input}} = 1/\sigma_n = R_0 = R|_{m=1} \quad (5.25)$$

where, $R|_{m=1}$ is $R = m/\sigma_n$ evaluated at $m = 1$ implying the assumption of *unit mean* for

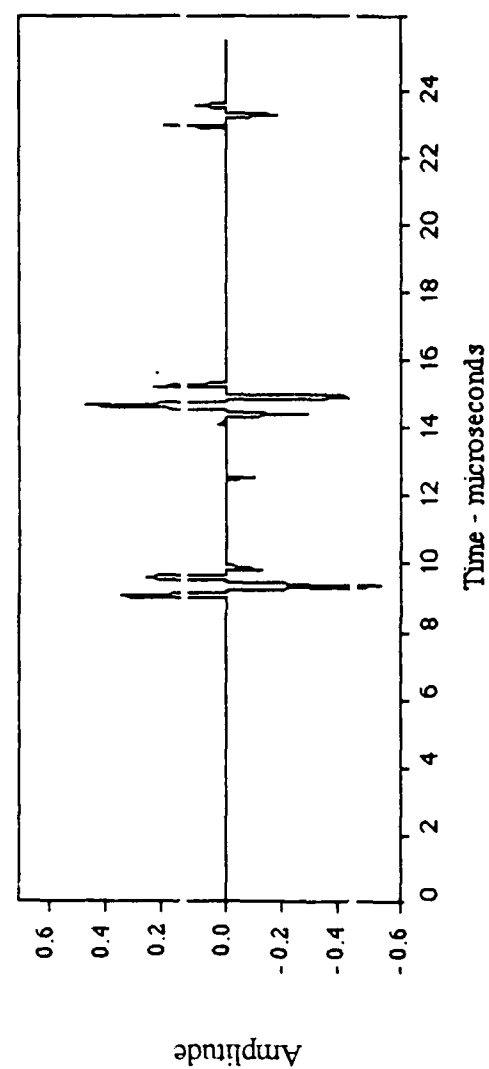


Figure 5.4a The processor output signal for an input signal as shown in Figure 5.1. Filters with a half power bandwidth of 0.092 MHz are used for the processing

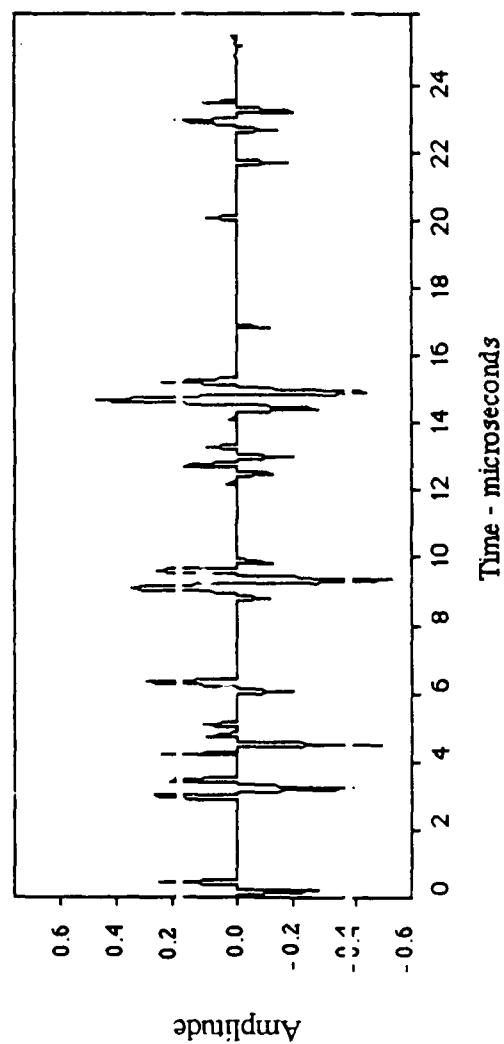


Figure 5.4b The processor output for filters of half power bandwidth of 0.172 MHz

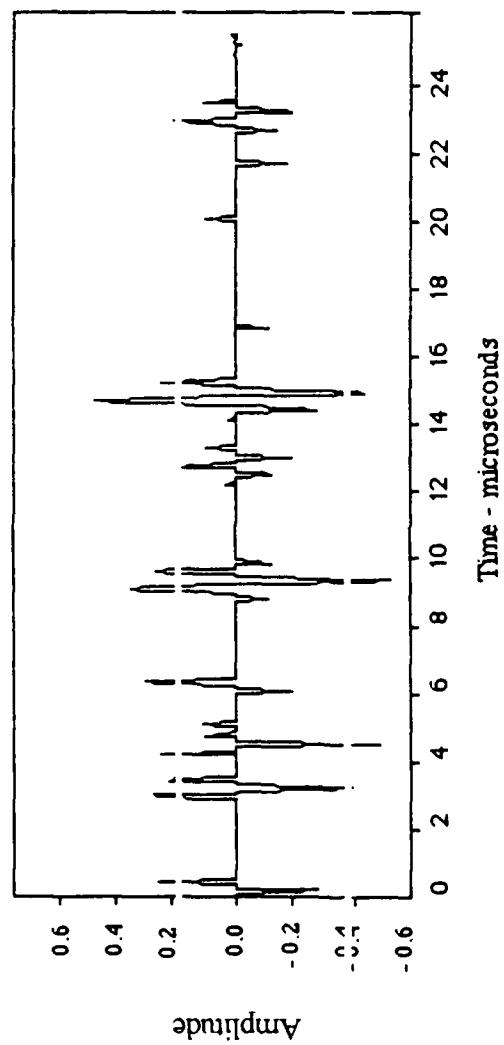


Figure 5.4b The processor output for filters of half power bandwidth of 0.172 MHz

the analysis. Also,

$$\text{SNR}_{\text{output}} = 1/\sigma_Z = R_m$$

From (5.20a),

$$\text{SNR}_{\text{output}} = R_m = \frac{R_o}{[A' (B' R^2 + 1)]^{1/2}} \quad (5.26)$$

where, $B' = 1 - A'$ and $R = R|_{m=1}$

$$\text{SNR}_{\text{enhancement}} = \frac{\text{SNR}_{\text{output}}}{\text{SNR}_{\text{input}}} = \frac{1/\sigma_Z}{1/\sigma_n}$$

$$\text{SNR}_{\text{enhancement}} = \frac{1}{[A' (B' R^2 + 1)]^{1/2}} \quad (5.27)$$

When $m = 0$ at τ_i , (5.25), (5.26) and (5.27) reduce to

$$\text{SNR}_{\text{input}} = 1/\sigma_n = R_o \quad (5.28)$$

$$\text{SNR}_{\text{output}} = \frac{R_o}{\sqrt{A'|_{m=0}}} \quad (5.29)$$

$$\text{SNR}_{\text{enhancement}} = \frac{1}{\sqrt{A'|_{m=0}}} \quad (5.30)$$

However, it should be noted that A' in (5.26) and (5.27) is different from that in (5.29) and (5.30) because $m \neq 0$ in the first set of equations (A' is a function of m - Equation 5.16a).

Figures 5.5a and 5.5b show the $\text{SNR}_{\text{enhancement}}$ curves at τ_i for the case of no target and the case of the presence of a target at τ_i . $\text{SNR}_{\text{enhancement}}$ has been plotted as a

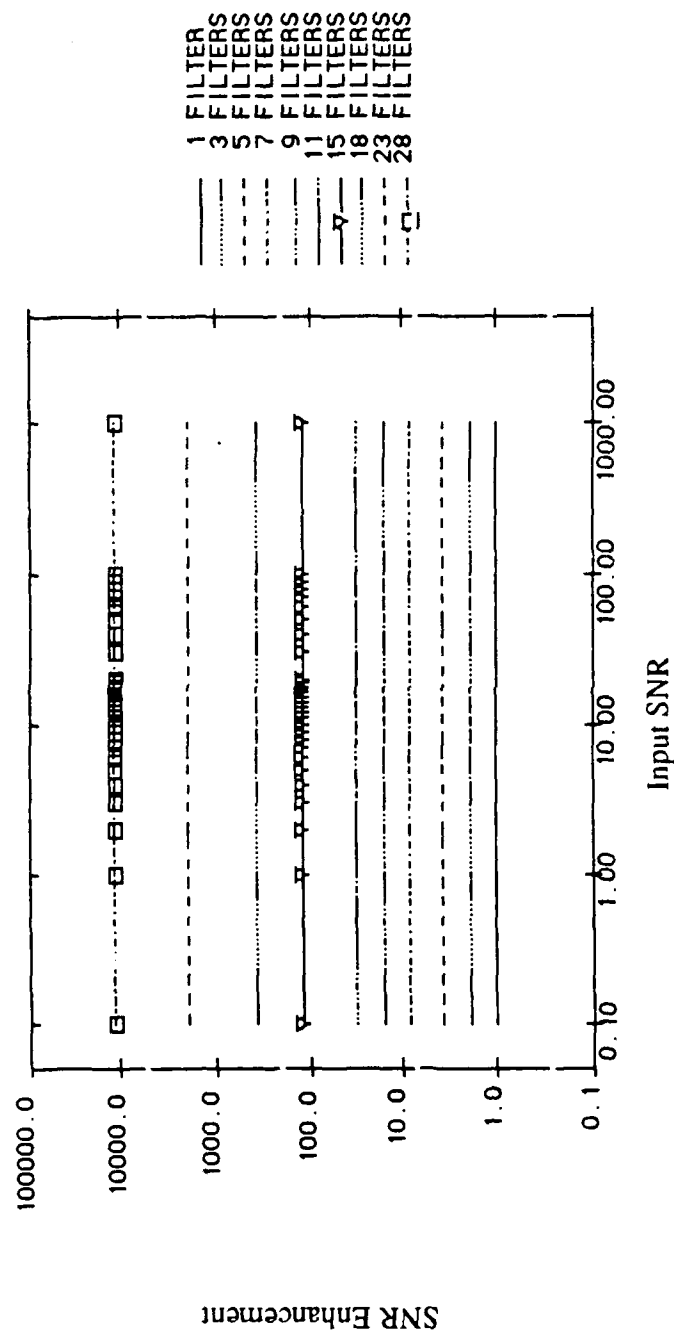


Figure 5.5a Theoretical signal-to-noise ratio (variance) curves of the processor at a time delay where only the grain noise and no target exists

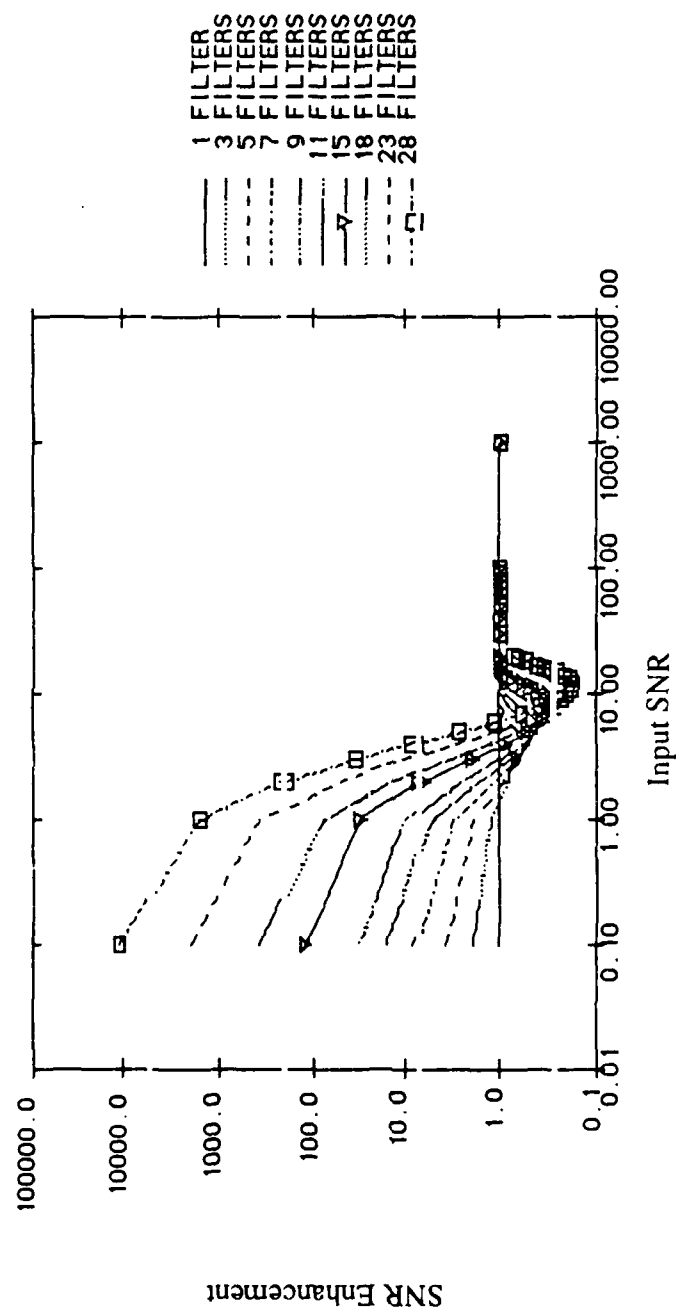


Figure 5.5b Theoretical signal-to-noise ratio (variance) curves of the processor at a time delay where both the grain noise and a target signal exists

function of $\text{SNR}_{\text{input}}$ for N ranging from 1 to 28 ($N = 1$ is for a case of no processing).

Figure 5.5a shows that, when $m = 0$, $\text{SNR}_{\text{enhancement}}$ is independent of R_0 and varies only as a function of N . This is because, the probability that the output, z , is equal to zero is given by B' in (5.16a) which is a function of N alone when $m = 0$. Thus, larger the value of N , higher the probability that $z = 0$ and hence smaller the variance σ_z^2 , thereby increasing the $\text{SNR}_{\text{enhancement}}$ at τ_i (Equation 5.30).

The pattern followed by the curves in Figure 5.5b shows that the $\text{SNR}_{\text{enhancement}}$ is very large [implying very small σ_z - Equation (5.27)] for very small values of $R = m/\sigma_n$; the enhancement drops below unity briefly and becomes unity for large values of R . In the range when the enhancement is very large, ($m \ll \sigma_n$), the behavior is close to that when $m = 0$, thus increasing the probability that $z = 0$ and decreasing detectability. In the range when $m \approx \sigma_n$, the probability that $z = 0$ decreases but still is not negligible. As a result, the variance, σ_z^2 , increases thereby decreasing SNR enhancement (Equation 5.27) below unity. When m increases further (and hence R), the probability that $z = x$ increases. Hence σ_z^2 approaches σ_n^2 at the time delay τ_i . From the discussion so far, it is clear that there is a larger reduction of variance at a time delay when $m \ll \sigma_n$. However, the probability of detection of a target is also reduced when $m \ll \sigma_n$, thereby reducing the output mean. Such an effect can be seen in Figure 5.6 wherein the output SNR enhancement defined by (5.33) is plotted as a function of input SNR as defined by (5.31).

$$\text{SNR}_{\text{input}} = R = \frac{m}{\sigma_n} \quad (5.31)$$

$$\begin{aligned} \text{SNR}_{\text{output}} &= \frac{\text{Mean of } z}{(\text{Variance of } z)^{1/2}} = \frac{mA'}{[A'(m^2 + \sigma_n^2) - (A'm)^2]^{1/2}} \\ &= R \left[\frac{A'}{(B' R^2 + 1)} \right]^{1/2} \end{aligned} \quad (5.32)$$

$$\text{SNR}_{\text{enhancement}} = \frac{\text{SNR}_{\text{output}}}{\text{SNR}_{\text{input}}} = \left[\frac{A'}{(B' R^2 + 1)} \right]^{1/2} \quad (5.33)$$

From Figure 5.6, it is obvious that when $m \ll \sigma_n$ the output variance is reduced and the

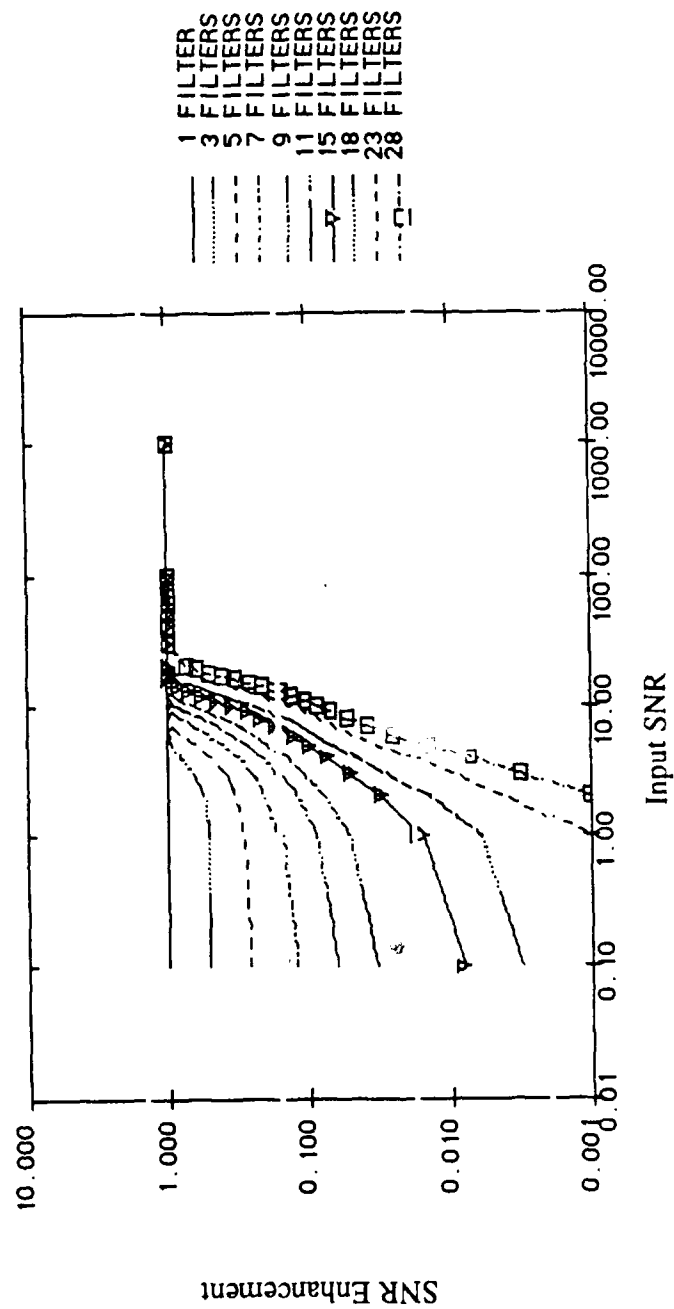


Figure 5.6 Theoretical signal-to-noise ratio curves showing the effect of processing on the mean of the output signal

expected value of the output is reduced by even a larger factor. It is also apparent from Figure 5.6 that when m is $\approx \sigma_n$ or $m \gg \sigma_n$, the best SNR enhancement at a time delay is achieved and is equal to unity! This is the situation when the detectability is the largest for the corresponding N . The fact that the SNR at a time delay before and after the processing should be equal for a good detectability might raise questions about the usefulness of the algorithm as a tool for SNR enhancement. However, the clarification is obvious from Figures 5.1 and 5.4a and is discussed next.

Figure 5.4a is the processor output for an input signal as shown in Figure 5.1. The result is without any thresholding (thresholding was discussed only for the generation of the ROC curves and has not been implemented in any of the experimental results presented herein). It is obvious that at time delays like τ_1 in Figure 5.1, when there was no target signal present, the output amplitude has been mostly rejected thereby substantially reducing σ_z^2 (across the ensemble) at that time delay. Further, at time delays in the range $\tau_a - \tau_b$, when in fact there was a reflected pulse from a target, the edges of the pulse (when m is very small) have been lost. However, the central part of the pulse (when m is large as at τ_2) is retained by the processor and hence at such time delays the variance across the ensemble approaches the input variance and mean. Thus, when the whole signal is viewed as in Figure 5.4a (instead of at a specific time delay), it is clear that the suppression of the coherent grain noise has been dramatic. This aspect of SNR enhancement has already been shown in (5.22) and Figure 5.2.

It should be pointed out here that PT algorithm can be either used by itself for SNR improvements or in concert with another algorithm like minimization [2,49] (that is the output of the minimization algorithm will be the input to the PT algorithm). Such a cascaded processing has been found to yield better SNR enhancement than either of the two algorithms by themselves. The curve labelled 'Minmz. and Pol.Thresh' in Figure 5.3 shows the SNR enhancement curve of a cascaded processor comprising of minimization and PT. Signal-to-noise ratio curve for minimization alone has also been shown in the same figure for the sake of comparison.

5.3.2 Probabilities of false alarm and detection

The processor, in its present form, is quite severe in performance. As a result, it would be necessary to find the probabilities of false alarm and detection for the output of

the processor. If it is assumed that every $z \neq 0$ is a detection of a possible target (thus setting no threshold to the output of the algorithm), the probability of false alarm is obtained by substituting $m = 0$ in Equation (5.15) and integrating the term containing A' in it from $-\infty$ to $+\infty$. If $P_{m=0}(Z \neq 0)$ is the probability of false alarm (that is, the probability that the processor output is not zero even when no target signal exists at τ_i),

$$P_{m=0}(Z \neq 0) = \int_{-\infty}^{+\infty} f_Z(z)|_{m=0} dz - P_{m=0}(Z = 0) = A'|_{m=0} = \frac{1}{2^{N-1}} \quad (5.34)$$

Similarly, the probability of detection is given by integrating the term containing A' in Equation (5.15) from $-\infty$ to $+\infty$ ($m \neq 0$). Thus, if $P_{m \neq 0}(Z \neq 0)$ is the probability of detection (that is, the probability that the output of the processor is not zero when a target signal is present at τ_i),

$$P_{m \neq 0}(Z \neq 0) = \int_{-\infty}^{+\infty} f_Z(z) dz - P_{m \neq 0}(Z = 0) = A'|_{m \neq 0} \quad (5.35)$$

where, $A'|_{m \neq 0}$ is given by (5.16a).

The output of the processor at each time delay will be either a zero or a non zero amplitude depending on which of the conditions in (5.5) is satisfied. If every non zero amplitude is considered a detection (that is, the indication of the presence of a target signal at that time delay), the probability of false alarm is the probability that the output at a time delay is nonzero even when there is no target at that time delay. Similarly, the probability of detection is the probability that the output at a time delay is nonzero when a target signal is indeed present at that time delay.

The probability of false alarm, P_F given by (5.34) is plotted in Figure 5.7 as a function of the the number of frequency windows N . Note that this expression is independent of m/σ_n . The probability of detection P_D , is plotted in Figure 5.8, as a function of the parameter $R = m/\sigma_n$ which may be considered as the input voltage signal-to-noise ratio. Figures 5.7 and 5.8 are the probabilities of false alarm and detection when the output is not thresholded. The probability of detection curve when $R = 0.1$ (Figure 5.8) approaches the curve in Figure 5.7 while that for $R = 20$ is close to unity for all N . However, when R is in the range of 0.1 to 20, the probability of detection decreases with

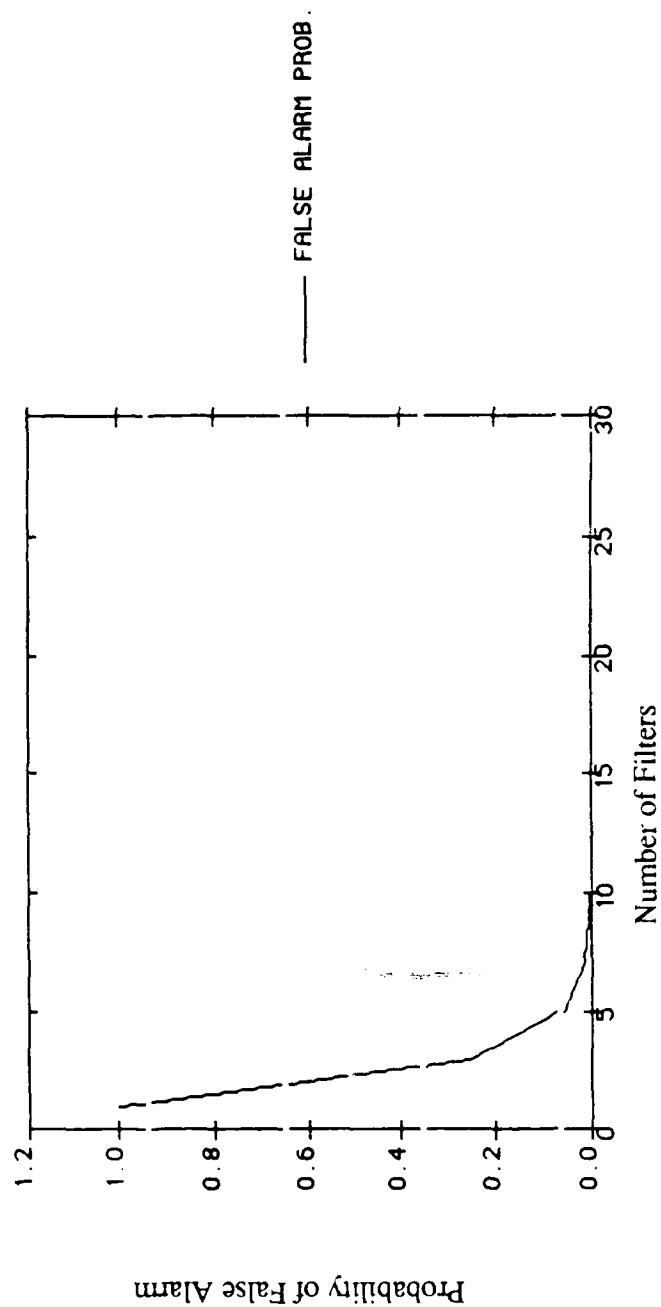


Figure 5.7 Probability of False Alarm as a function of the number of windows used for the processing

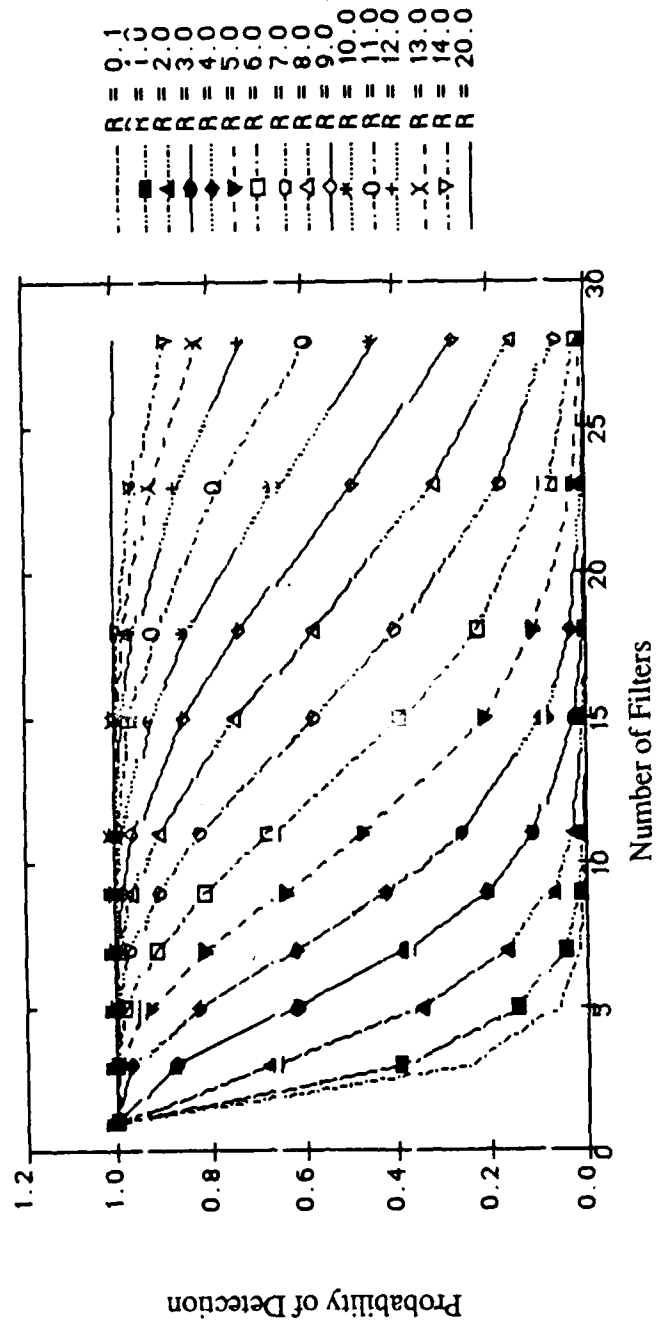


Figure 5.8 Probability of Detection curves plotted as a function of the number of filters used and the input signal-to-noise ratio

N because, the probability that at least one of the spectral decomposition components changes polarity increase with the increase of N.

5.3.3 Receiver Operating Characteristics (ROC)

5.3.3.1 Receiver Operating Characteristics when no threshold is set to the processed output

Receiver operating characteristics is the curves obtained by plotting the probability of detection vs. the probability of false alarm and as a function of the input SNR. Such ROC for the PT algorithm can be obtained by eliminating N between (5.34) and (5.35). The curves so obtained are shown in Figures 5.9 and 5.10. These curves are the ROC of the PT algorithm if every nonzero output of the algorithm is considered as a detection of a possible target. It can be seen from the figures that for $N = 1$, both P_F and P_D equal 100%. As N is increased (the abscissa in Figure 5.9 is an inverse function of N - Equation 5.34), P_F falls more rapidly than P_D until $N \approx 6$. Hence the number of windows used in polarity thresholding has an optimum number which varies with input signal-to-noise ratio.

5.3.3.2 ROC of the algorithm by Neyman-Pearson Criterion

Equations (5.34) and (5.35) are the probabilities of false alarm and detection with no threshold set to the output of the processor. However, if a threshold based on the Neyman - Pearson [59,60] criterion is set to the output, the probabilities of false alarm and detection are modified. *Since a threshold is set to the processed (PT) signal, it would be necessary to square the processed signal before the ROC can be calculated.* A plot of the probability of detection as a function of the probability of false alarm, $R = m/\sigma_n$ and N for the squared processed (PT) signal yields a set of curves. The curves so obtained constitute the Receiver Operating Characteristics (ROC) of the polarity thresholding algorithm.

Theory [59,60]

Consider an ultrasonic signal of time duration T sec which might either contain a signal from a target or no target signal at all. The ultrasonic signal also contains coherent

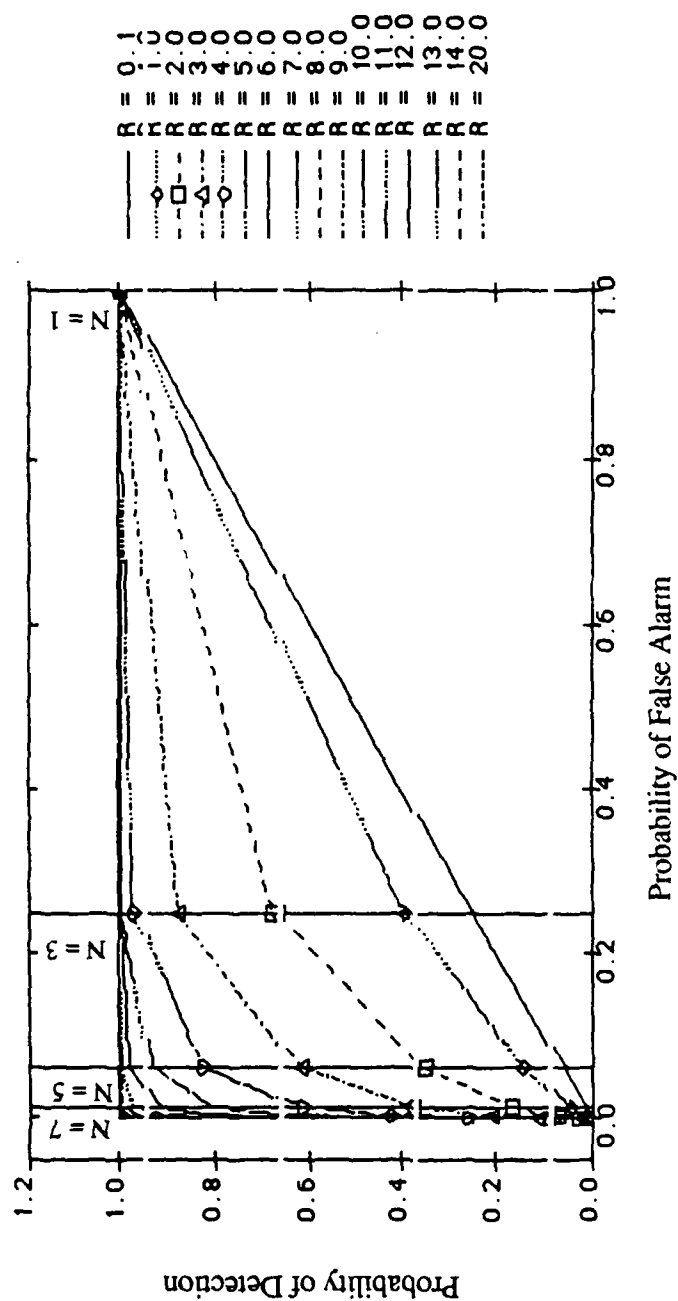


Figure 5.9 Receiver operating characteristics of the algorithm obtained for a case when no threshold is set to the output of the algorithm

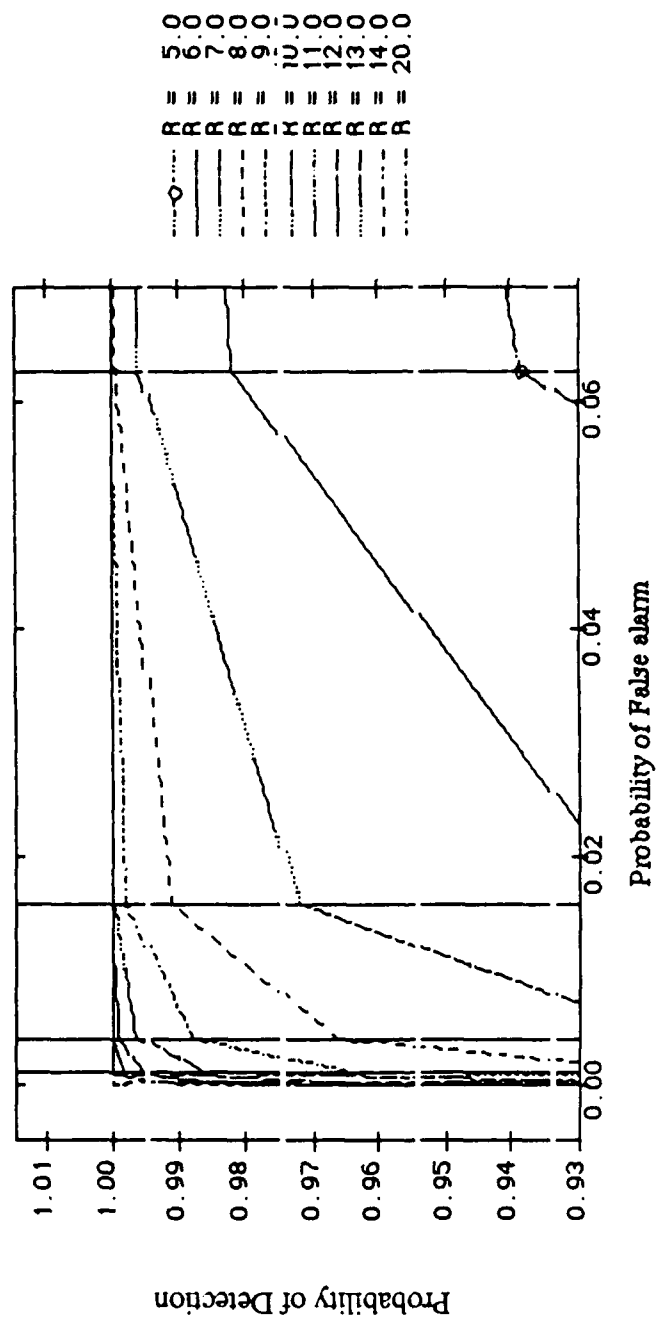


Figure 5.10 An enlarged version of the curves in Figure 5.9

noise amplitude, $n(t)$, due to the scatterers being present in the material. The objective now is, given the ultrasonic signal which might or might not contain a target, to decide whether a target signal is present or not. Thus, two hypotheses, H_0 and H_1 , are possible which can be defined as follows:

H_0 : No target present in the range of zero to T sec - $Z(t) = n(t)$

H_1 : Target present in the signal - $Z(t) = m_z(t) + n(t)$

Given a sample value, 'z', a decision has to be reached about which of the two hypothesis is true. Hence, a reasonable criterion should be selected to choose between the two hypotheses.

Let D_0 and D_1 be the decision of selecting the hypotheses H_0 and H_1 , respectively. Let C_{ij} be the cost associated with choosing hypothesis H_i when in reality H_j is true. Hence, the average cost for the decision procedure is given by,

$$\begin{aligned} \bar{C} = & P(H_0)[P(D_0|H_0) C_{00} + P(D_1|H_0) C_{10}] \\ & + [1-P(H_0)][P(D_0|H_1) C_{01} + P(D_1|H_1) C_{11}] \end{aligned} \quad (5.36)$$

Although Equation (5.36) gives the average cost or risk of making a decision, it is frequent that the a priori probabilities and the cost of each kind of error is difficult to estimate. Under such circumstances, the Neyman-Pearson criterion is used, the objective being to maximize the probability of detection for a given probability of false alarm. The objective of maximizing the probability of detection (POD) can be accomplished by using a likelihood ratio test as shown below.

The objective of the analysis is to maximize $P(D_1|H_1)$ - or equivalently, minimize $[1-P(D_0|H_1)]$ - subject to a given $P(D_1|H_0) = 'a'$. Since $P(D_1|H_0)$ is equal to 'a', a constant, maximizing $P(D_1|H_1)$ is equivalent to minimizing the following expression:

$$\bar{C} = P(D_0|H_1) + \mu P(D_1|H_0) \quad (5.37)$$

where, μ is an arbitrary constant. It can now be shown that by substituting $C_{00} = C_{11} = 0$, $[1 - P(H_0)] C_{01} = 1$ and $P(H_0) C_{10} = \mu$ in (5.36), (5.37) is obtained. Thus, (5.37) is the

cost function to be minimized and, consequently, Neyman-Pearson criterion is a special case of Baye's Criterion. Hence, (5.37) can be minimized by choosing H_1 (presence of a target) when the following condition is satisfied:

$$\frac{f_1(z)}{f_0(z)} \geq \frac{P(H_0) (C_{10} - C_{00})}{[1 - P(H_0)] (C_{01} - C_{11})} \quad (5.38)$$

Substituting the assumed values, $C_{00} = C_{11} = 0$, $[1 - P(H_0)] C_{01} = 1$ and $P(H_0) C_{10} = \mu$, equation (5.38) reduces to: choose H_1 if,

$$\frac{f_1(z)}{f_0(z)} \geq \mu \quad (5.39)$$

It has already been shown that $f_1(z)$ and $f_0(z)$, the pdf of the output of the polarity thresholding algorithm when a target is present and when no target is present respectively, are given by

$$f_1(z) = \frac{A'_{m \neq 0}}{\sqrt{2\pi} \sigma_n} \exp\left(-\frac{(z-m)^2}{2\sigma_n^2}\right) + B'_{m \neq 0} \delta(z-0) \quad (5.40) a$$

where, $A'_{m \neq 0}$ is given by (5.16a), and

$$f_0(z) = \frac{A'_{m=0}}{\sqrt{2\pi} \sigma_n} \exp\left(-\frac{z^2}{2\sigma_n^2}\right) + B'_{m=0} \delta(z-0) \quad (5.41) a$$

where, $A'_{m=0}$ is given by (5.34). However, since it would be necessary to square the processed signal before an ROC analysis can be conducted, a new random variable 'Y' is defined such that,

$$Y = Z^2$$

where, 'Z' is the output of the PT algorithm at a time delay τ_i . Hence,

$$f_Y(y) = \frac{U(y)}{2\sqrt{y}} [f_Z(\sqrt{y}) + f_Z(-\sqrt{y})]$$

where, $U(y) = 1$ if $y > 0$ and $U(y) = 0$ if $y \leq 0$.

$$\therefore f_Y(y) = \frac{A' U(y)}{2\sqrt{2\pi} \sigma_n} \left[\frac{\exp\left(-\frac{(\sqrt{y}-m)^2}{2\sigma_n^2}\right) + \exp\left(-\frac{(\sqrt{y}+m)^2}{2\sigma_n^2}\right)}{\sqrt{y}} \right] + B' \delta(y)$$

If $f_1(y)$ is the density function of Y when $m \neq 0$ and $f_0(y)$ is that when $m = 0$, then

$$f_1(y) = \frac{A'_{m \neq 0} U(y)}{2\sqrt{2\pi} \sigma_n} \left[\frac{\exp\left(-\frac{(\sqrt{y}-m)^2}{2\sigma_n^2}\right) + \exp\left(-\frac{(\sqrt{y}+m)^2}{2\sigma_n^2}\right)}{\sqrt{y}} \right] + B' \delta(y) \quad (5.40) b$$

and,

$$f_0(y) = \frac{A'_{m=0} U(y)}{\sqrt{2\pi} \sigma_n} \left[\frac{\exp\left(-\frac{y}{2\sigma_n^2}\right)}{\sqrt{y}} \right] + B' \delta(y) \quad (5.41) b$$

The next step in deriving the ROC is to select a threshold, λ_0 , to satisfy the probability of false alarm, 'a'. Thus,

$$a = \int_{\lambda_0}^{\infty} f_0(y) dy \quad (5.42)$$

From (5.42), the threshold, λ_0 , is calculated from which the POD is calculated by,

$$\text{POD} = \int_{\lambda_0}^{\infty} f_1(y) dy \quad (5.43)$$

Hence, the decision rule is to select H_1 if the amplitude $y \geq \lambda_0$. The same criterion can be stated in another way by substituting (5.40b) and (5.41b) into (5.39). That is,

$$\frac{f_1(y)}{f_0(y)} = \frac{\frac{1}{2} \left[A'_{l_{m=1}} \left\{ \exp \left(-\frac{(\sqrt{y}-1)^2}{2\sigma_n^2} \right) + \exp \left(-\frac{(\sqrt{y}+1)^2}{2\sigma_n^2} \right) \right\} + \sqrt{y} B'_{l_{m=1}} \delta(y) \right]}{A'_{l_{m=0}} \exp \left(-\frac{y}{2\sigma_n^2} \right) + \sqrt{y} B'_{l_{m=0}} \delta(y)} = \lambda(y) \quad (5.44)$$

where, an unit mean is assumed in (5.40) and $y \geq 0$. Then, choose H_1 if, $\lambda(y) \geq \lambda(\lambda_0)$ where $\lambda(\lambda_0)$ is defined by

$$\lambda(\lambda_0) = \frac{\frac{1}{2} \left[A'_{l_{m=1}} \left\{ \exp \left(-\frac{(\sqrt{\lambda_0}-1)^2}{2\sigma_n^2} \right) + \exp \left(-\frac{(\sqrt{\lambda_0}+1)^2}{2\sigma_n^2} \right) \right\} + \sqrt{\lambda_0} B'_{l_{m=1}} \delta(\lambda_0) \right]}{A'_{l_{m=0}} \exp \left(-\frac{\lambda_0}{2\sigma_n^2} \right) + \sqrt{\lambda_0} B'_{l_{m=0}} \delta(\lambda_0)}$$

and $\lambda_0 \geq 0$. Receiver operating characteristics of the polarity thresholding algorithm are generated by repeating the above described process of selecting different probabilities of false alarm, (5.42), followed by calculating the corresponding POD, (5.43), for the given input SNR and N (number of filters used for processing). The PODs so calculated are plotted as a function of the probability of false alarm, input SNR and N.

Figures 5.11a to 5.11d are the theoretical ROC curves for simple thresholding of the signal without any processing and processing with 3, 5 and 7 filters respectively. From the graphs presented, at low probabilities of false alarm, the probability of detection for PT is better than that for simple thresholding. At higher probabilities of false alarm, simple thresholding has a better probability of detection than PT. However, it should be remembered that for high probabilities of false alarm, simple thresholding yields almost no SNR enhancement!

The curves in Figures 5.11a to 5.11d display a plateau at higher probabilities of false alarm. The beginning point of the plateau is different for different values of R and N. The reason for such a plateau is that there is a finite nonzero probability that the output of

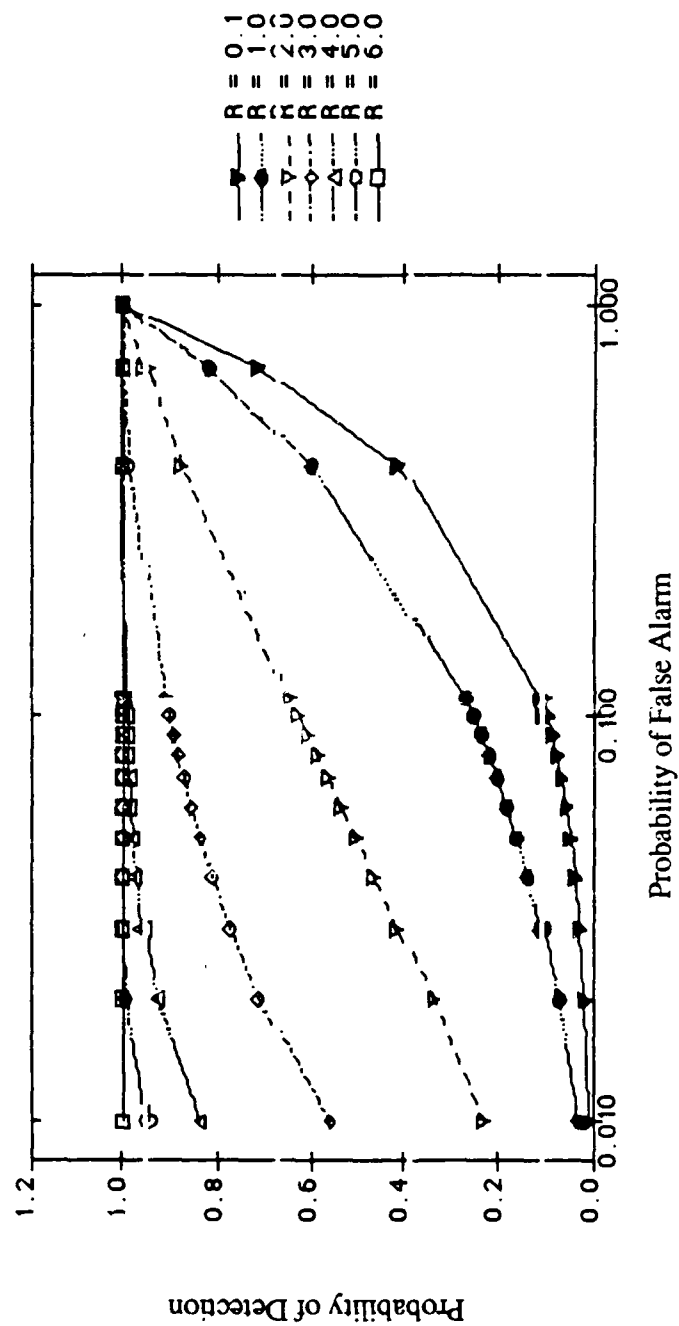


Figure 5.11a Receiver operating characteristics of the Neyman-Pearson criterion for a case of a simple thresholding of the input signal (without any processing)

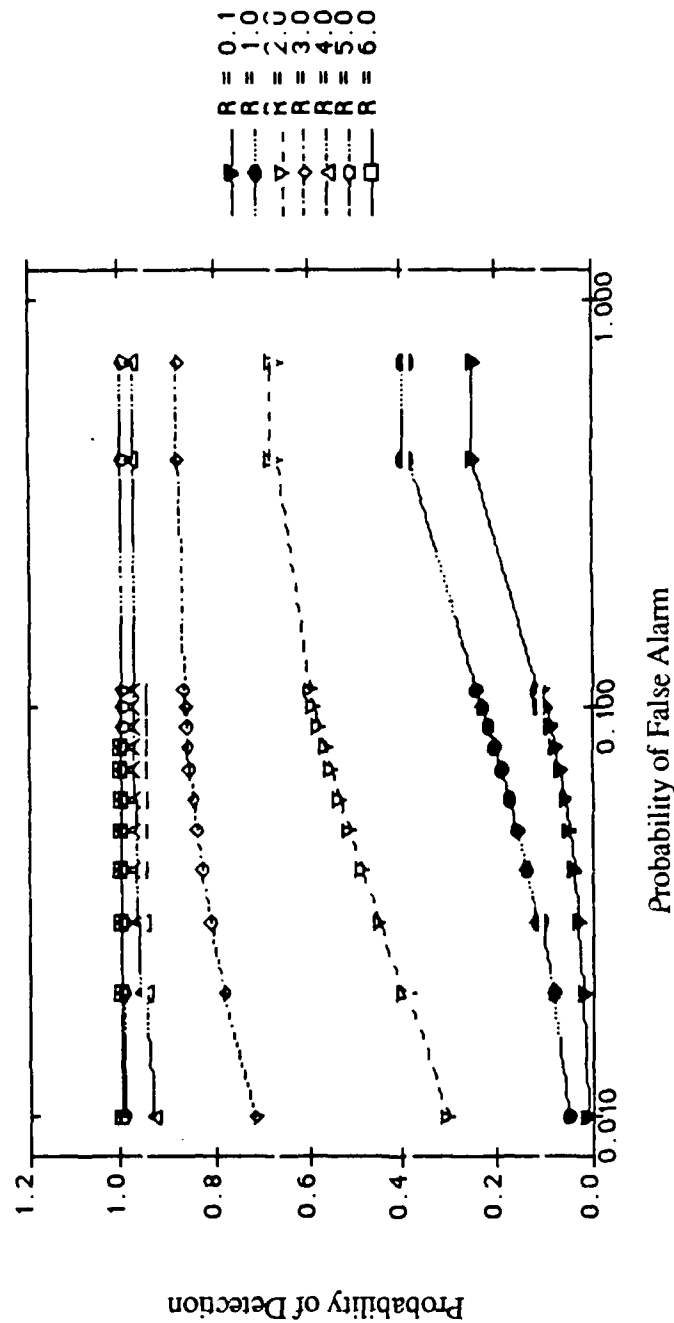


Figure 5.11b Receiver operating characteristics of the Neyman-Pearson criterion for the output of the Polarity Thresholding algorithm when three filters are used

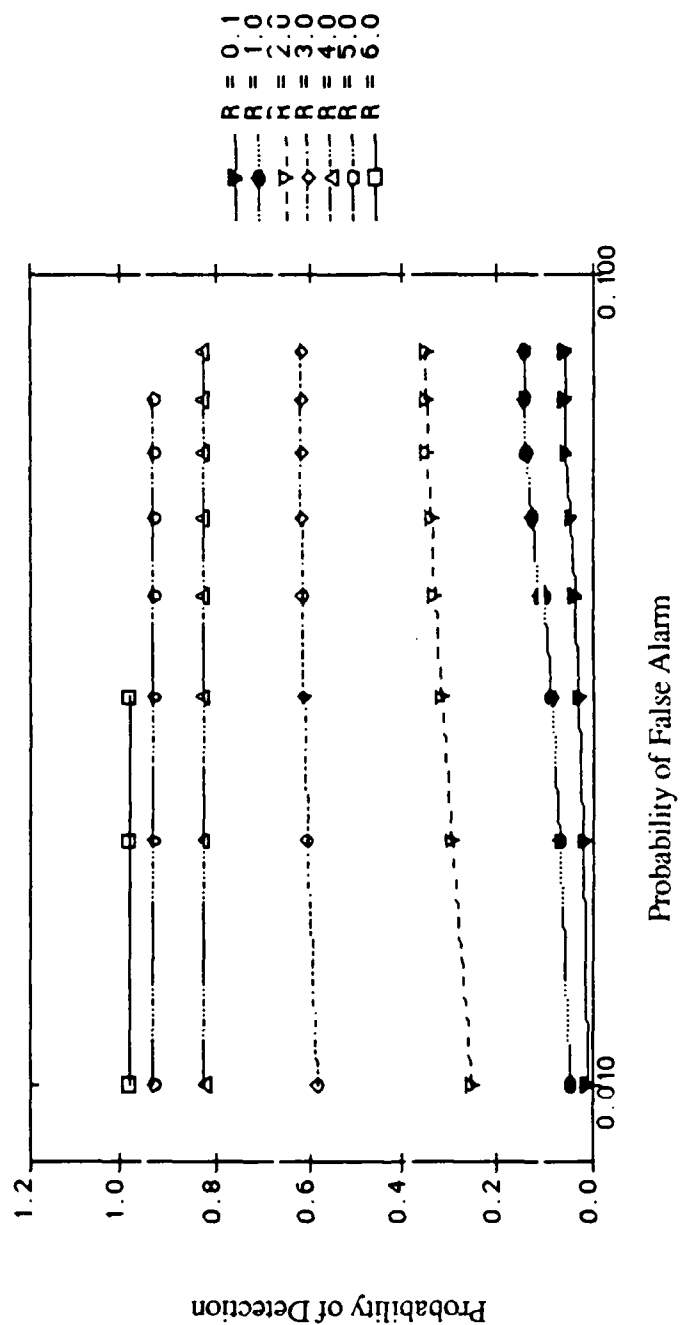


Figure 5.11c Receiver operating characteristics of the Neyman-Pearson Criterion for the output of the Polarity Thresholding algorithm when five filters are used

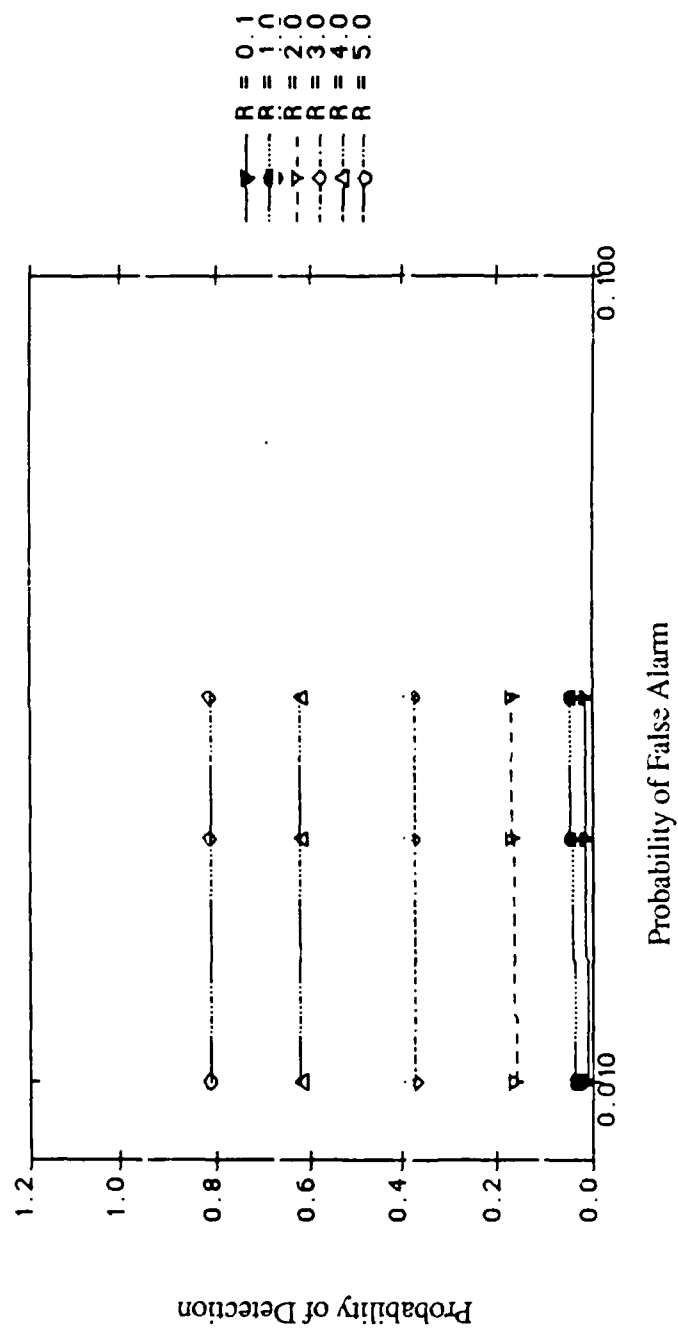


Figure 5.11d Receiver operating characteristics of the Neyman-Pearson criterion for the output of the Polarity Thresholding algorithm when seven filters are used.

the processor is zero (B' in Equation 5.15). Hence the probability of detection can not be equal to unity no matter how low the threshold is set (lower the threshold, higher the probability of false alarm), especially for small R and large N .

The processor defined by (5.5) is in its most severe form. Hence, it is necessary to exercise utmost caution because any further thresholding increases the probability of losing the target altogether (The processor can also be easily modified to be less severe by simply tolerating more than one polarity reversal before no detection is assumed in Equation 5.5).

5.4 Summary

Polarity thresholding algorithm is an SSP algorithm that could be used either alone or in conjunction with other SSP algorithms. Polarity thresholding algorithm is found to be very effective in SNR enhancement. It is possible to implement the PT algorithm in several different levels of severity by simply tolerating more than one polarity reversal.

Curves of the probability of false alarm and the probability of detection have been plotted in addition to the conventional ROC curves. Such curves are very useful in determining the applicability of the technique to materials of known grain characteristics. The effect of correlated spectral decomposition components on the results presented here, has to be kept in mind when implementing the algorithm.

Finally, subsequent to the development of the algorithm here [46,47] a variation of the algorithm has been independently developed [51,52] or experimentally validated [50] by other research groups.

6. UTILITY OF SPLIT SPECTRUM PROCESSING IN ULTRASONIC NDE*

6.1 Introduction

Ultrasonics plays an important role in the nondestructive evaluation of engineering materials. Anomalies in the test materials can be detected, located, sized and classified with the help of ultrasonic analysis, provided the signal obtained from the material has acceptable levels of signal-to-noise ratio (SNR). On many occasions, a meaningful ultrasonic NDE becomes improbable in 'noisy' materials like centrifugally cast stainless steel (CCSS), Carbon-Epoxy composites and welded joints because of the masking effect of the interfering noise or 'clutter', thereby necessitating pre-processing for SNR enhancement. If the noise is random and time dependent, a simple time averaging or temporal compounding is usually sufficient to improve the SNR. However, if the noise is coherent (time invariant), spatial compounding could be performed provided the orientation of the flaw and the geometry of the test specimen are suitable for the technique. Split Spectrum Processing (SSP) is a signal processing technique for the SNR improvement for signals cluttered by coherent noise. The technique overcomes, to a great extent, the above mentioned limitations of spatial compounding technique.

Another aspect of ultrasonic NDE is characterizing the 'noise' itself because the so called noise amplitude carries information about the material through which the sound is propagating. A successful NDE in metals like CCSS is critically dependent on characterizing the type of grains present in the material. Grain characterization is critical to NDE because, the type of grains present in the material has a strong influence on the acoustic properties of the material thereby rendering any NDE conclusions invalid when the influence of the grain type is ignored. The grain matrix present in a metal responds differently to insonifications of different frequencies. Such a frequency dependent response can in fact be utilized to characterize the grain matrix present in the material being tested. Split spectrum processing is a convenient method of introducing frequency diversity using which grain characterization studies could be performed.

* A part of this chapter has been accepted for publication in Materials Evaluation as a paper entitled 'Utility of Split Spectrum Processing for Ultrasonic NDE', J. L. Rose, P. Karpur and V. L. Newhouse.

There are many processing algorithms that could be applied to the frequency diverse signals obtained by the spectral splitting process of the SSP technique. They are, i) minimization [2,15] - for enhancing the SNR, ii) polarity thresholding [46,47] - for improved SNR and detectability iii) individual split time domain signal analysis - for information about the test material like the type of grain structure present in the material, attenuation as a function of frequency, dispersive property etc., iv) decorrelation and clutter suppression algorithm - for speckle suppression in 2-d images [33] and so on. Each algorithm is best suited for a specific aspect of nondestructive testing. Hence, which of the algorithms is used for further analysis is dictated by the objective of the nondestructive test being conducted. Thus, the utility of SSP is diverse in nature and are listed below:

1. Signal-to-noise ratio enhancement in materials like
 - a. Centrifugally cast stainless steel (CCSS),
 - b. Composite materials,
 - c. Cladded materials - example: Zircalloy pipes cladded with zirconium inner lining
2. Speckle suppression in B-scan images in materials like
 - a. Centrifugally Cast Stainless Steel,
3. Material characterization
 - a. Type and size of the grains present in the material being tested - example: equiaxed grain Vs. columnar grains in CCSS.

6.2 Algorithms of SSP

As already mentioned, each algorithm of SSP is best suited for a specific application. As such, three algorithms, minimization, polarity thresholding and individual split time domain signal analysis, have been used for the experimental results presented in this chapter. Hence, a brief description of minimization and polarity thresholding algorithm as implemented in conjunction with minimization, are provided next.

6.2.1 Minimization

Minimization is depicted in Figure 6.1. The 'N' split time domain signals are used to derive the 'minimized' signal. At each time delay ' τ ', the minimum absolute amplitude of the 'N' signals is selected. The algebraic sign of the selected amplitude is restored which now forms the amplitude of the processed signal at time delay ' τ '. The process can be mathematically represented as,

$$Z(\tau) = X_j(\tau) \quad (6.1)$$

where,

$$|X_j(\tau)| = \text{Minimum of } [|X_1(\tau)|, \dots, |X_j(\tau)|, \dots, |X_N(\tau)|]$$

$Z(\tau)$ = Minimized signal, and

$X_i(\tau)$ = Amplitude, at τ , of the i^{th} split time domain signal.

The algorithm provides superior SNR enhancement because, clutter, being an interference pattern produced by unresolved scatterers, is different at different frequencies. On the other hand, the response produced by a flaw is virtually invariant at different frequencies (over the range of frequencies contained in a transducer). As a result, the minimization process yields small amplitudes when only grain noise is present and large, relatively invariant amplitudes when a target is present. Superior results have been reported earlier on simulated data [2,47] as well as some limited experimental data [2,45,48].

6.2.2 Polarity Thresholding

When the polarity thresholding algorithm is used in conjunction with minimization, the spectral decomposition components (split time domain signals) obtained by splitting the spectrum of the signal and the minimized signal are the input of the polarity thresholding algorithm. The process is mathematically defined as follows:

$$\begin{aligned} Y(\tau) &= Z(\tau), & \text{if all } X_i(\tau) < 0, \text{ for } i = 1, \dots, N \\ &= Z(\tau), & \text{if all } X_i(\tau) > 0, \text{ for } i = 1, \dots, N \\ &= 0 & \text{otherwise} \end{aligned} \quad (6.2)$$

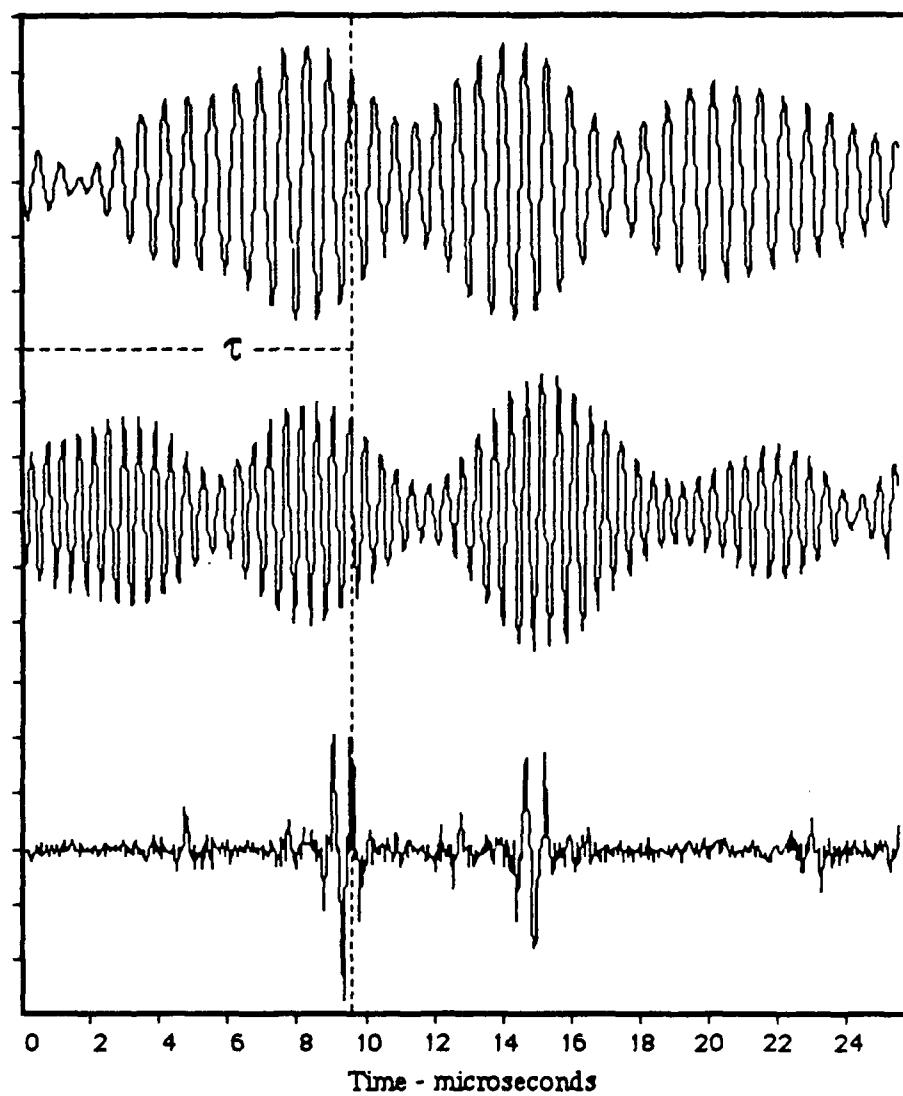


Figure 6.1 Minimization algorithm applied to the split time domain signals. Only the first and the 'N'th split time domain signals are shown along with the minimized signal.

where $Y(\tau)$ is the output of the polarity thresholding algorithm, $Z(\tau)$ is the minimized signal and $X_i(\tau)$, $i=1, \dots, N$ are the split time domain signals (refer to Fig. 6.1 which has been drawn for minimization but is applicable in concept to polarity thresholding also). Excellent results are reported [46,47,51,52] using this technique.

6.3 Experimental Results

Experiments have been conducted on CCSS, Carbon-Epoxy composites, and Zircalloy tubing clad with Zirconium. A KB-6000 pulser and a Biomation 8100 A/D converter have been used in conjunction with a microPDP-11/23plus computer for data acquisition and processing. The results are presented under three sections: i. SNR enhancement in one dimensional RF signals, ii. Speckle reduction in two dimensional B-scan images, and iii. Grain type characterization in CCSS samples.

6.3.1 Signal-to-noise Ratio Enhancement in 1-D RF signals

The experiments have been conducted on three types of specimen: 1) CCSS, 2) composite material and 3) a Zircalloy tube with a inner cladding of Zirconium.

6.3.1.1 Centrifugally Cast Stainless Steel

Equiaxial grained, rectangular CCSS block of dimensions (95 mm)x(59 mm)x(33 mm) as well as columnar grained samples have been used for the SNR enhancement experiments. Five different angles - 0° , 15° , 45° , 75° and 90° - have been machined on the columnar grained samples. The angles are with respect to the axis of the cylindrical grains. The blocks have a 3 mm side drilled hole which is used as a target embedded in noise producing grain scatterers. The side drilled cylindrical hole is at a depth of 42 mm from the surface of inspection. Immersion pulse echo technique was used for the equiaxed samples and contact pulse echo technique was used for the columnar grained samples. Further details of the samples could be found under section 6.3.3.2 of this chapter.

The results of processing a signal obtained from an equiaxed CCSS sample is shown in Figures 6.2a through 6.2h. The signal shown in Figure 6.2a is obtained from the region of the sample containing a side drilled cylindrical hole. The time duration of the

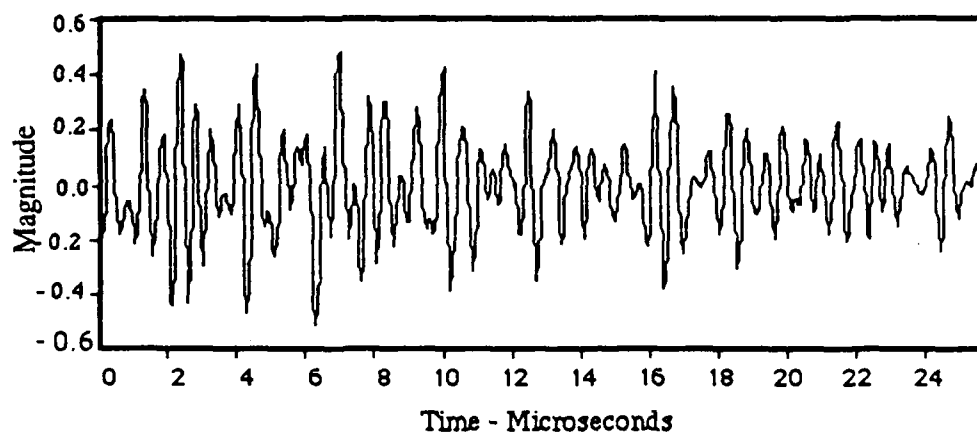


Figure 6.2 a An ultrasonic signal obtained from an equiax grained CCSS sample showing the backwall echo. The signal from a side drilled hole is completely obscured by grain noise.

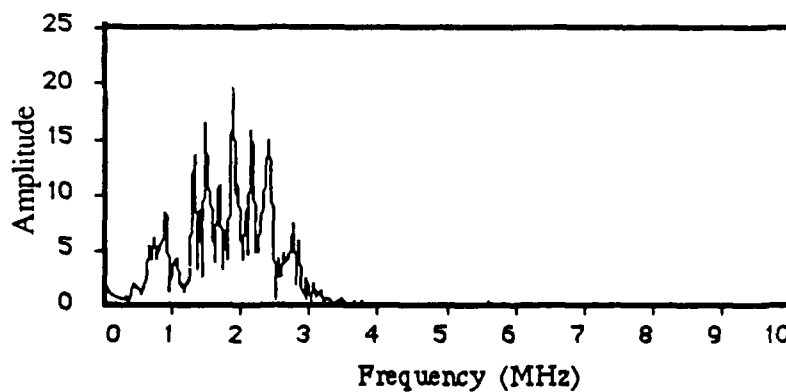


Figure 6.2 b The frequency-magnitude spectrum of the signal shown in Figure 6.2a.

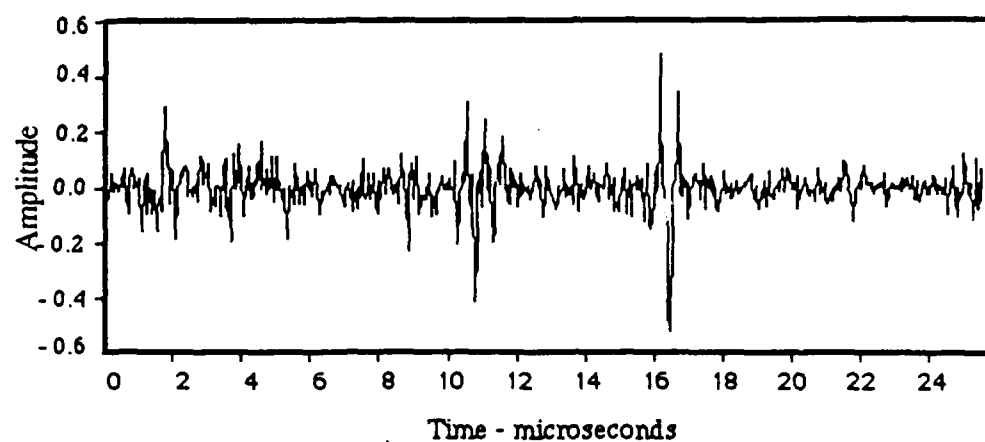


Figure 6.2 c The processed signal after applying minimization algorithm to the signal shown in Figure 6.2a.

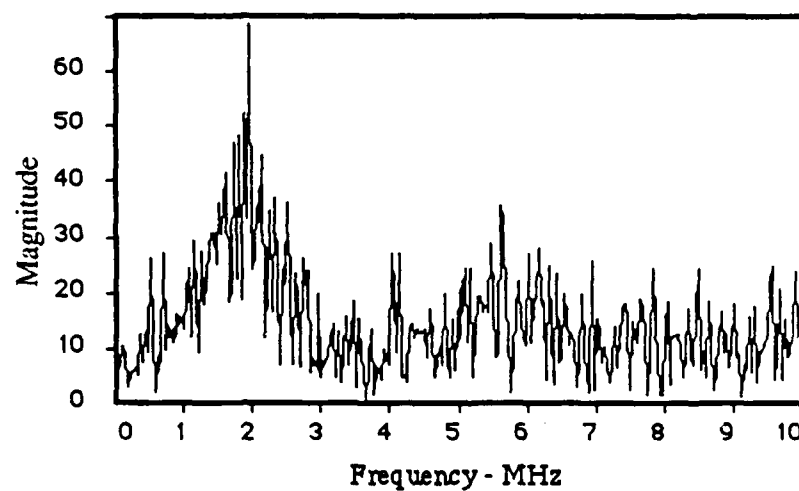


Figure 6.2 d The frequency-magnitude spectrum of the signal shown in Figure 6.2c.

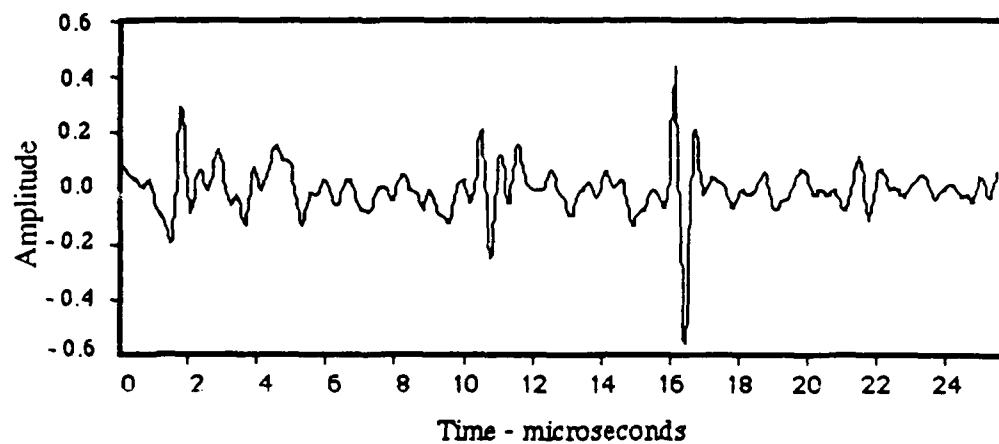


Figure 6.2 e The processed signal after a low frequency bandpass filtering of the spectrum shown in Figure 6.2 d. The backwall echo and the signal from the cylindrical hole are seen.

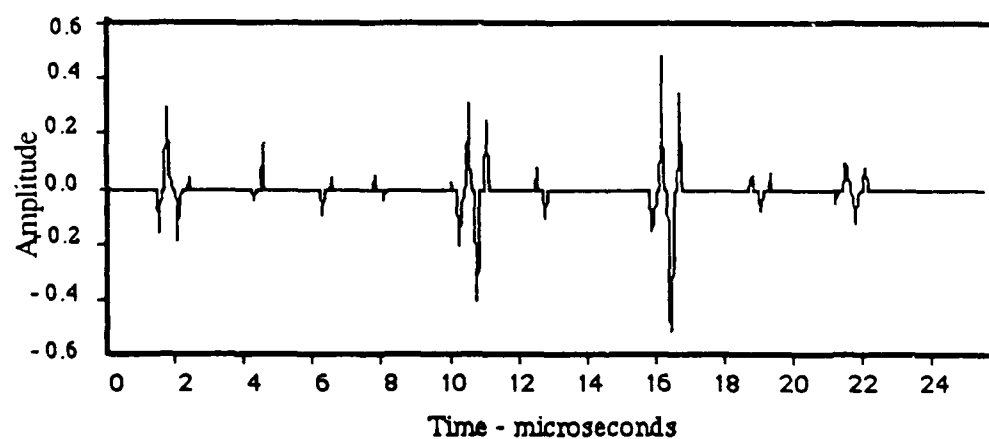


Figure 6.2 f The processed signal after applying minimization and polarity thresholding algorithms to the signal shown in Figure 6.2a.

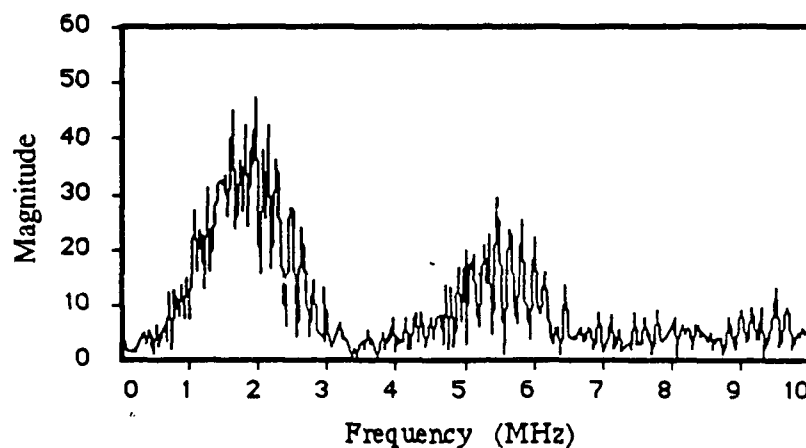


Figure 6.2 g The frequency - magnitude spectrum of the processed signal in Figure 6.2f.

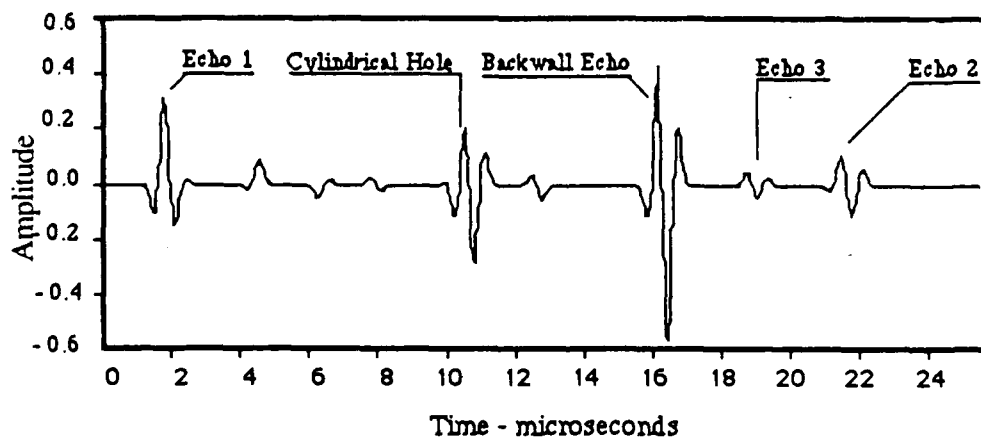


Figure 6.2 h The processed signal after a low frequency bandpass filtering of the spectrum shown in Figure 6.2g. The backwall echo, the signal from the cylindrical hole and the reverberating echoes are seen.

acquired signal is sufficient to include the backwall echo and some reverberating signals beyond the backwall echo. The noise level in Figure 6.2a is so high that the backwall echo is barely visible. The cylindrical hole is completely obscured by the coherent grain noise. The magnitude-frequency spectrum of the signal in Figure 6.2a is shown in Figure 6.2b from which it is clear that the spectral information of the targets and the grains overlap.

Figure 6.2c is the result of applying minimization algorithm to the signal in Figure 6.2a. The processed signal in Figure 6.2c clearly shows the backwall echo. The signal from the cylindrical hole is visible, but still has an unsatisfactory detectability. The grain noise shows high frequency contents which is imparted by the processing algorithm. Figure 6.2d is the magnitude-frequency spectrum of the processed signal in Figure 6.2c. It is immediately obvious from Figure 6.2c that the spectral information of the target is linearly treated by the processing algorithm and has been retained at the same frequency bandwidth as the input signal. At the same time, the spectral information of the grain noise has been shifted toward higher frequencies, thereby resulting in a spectral separation of the target information and the coherent noise. As a result, the high frequency content of the spectrum in Figure 6.2d can be easily rejected by using a low frequency bandpass filter (or a lowpass filter). The result of such a bandpass filtering of the spectrum in Figure 6.2d, is shown in Figure 6.2e. The improvement as a result of the filtering is enough to clearly show not only the backwall echo but also the cylindrical hole.

The results of processing the signal in Figure 6.2a using the polarity thresholding algorithm in conjunction with the minimization algorithm, are shown in Figures 6.2f through 6.2h. Figure 6.2f is the result of minimizing and then polarity thresholding the signal in Figure 6.2a. The high frequency noise which was evident in Figure 6.2c is completely eliminated in Figure 6.2f. The magnitude-frequency spectrum of the signal in Figure 6.2f is shown in Figure 6.2g which again shows some spurious high frequency contents. Figure 6.2h is the result of applying a low frequency bandpass filter to the spectrum in Figure 6.2g.

Figure 6.2h shows a dramatic improvement of SNR. The signal shows, in addition to the two known targets, a signal from a target (echo 1) yet to be identified by a destructive test of the sample on which other experiments are currently being conducted. The signal also shows two other echoes, echo 2 and echo 3, which are the reverberating echoes of the backwall and the cylindrical hole respectively. Echo 2 is the backwall echo reverberating from the cylindrical hole. Echo 3 is the cylindrical hole echo reverberating from the target

identified as echo 1. The presence of a target (echo 1) has not shadowed the other echoes because of using an unfocussed transducer; due to the beam spread phenomenon and because of the fact that the transducer has been slightly moved away from the axis of the cylindrical hole to simulate a weak target. The results shown in the sequence of Figures 6.2a to 6.2h, especially the reverberating echoes visible in Figure 6.2h, demonstrate that it is not necessary for the target echo amplitude to be larger than the surrounding noise level to achieve an effective and successful implementation of SSP provided the target signal is frequency independent in the bandwidth of the interrogating transducer.

Another signal from the equiaxed sample is shown in Figure 6.3a. Since the transducer is positioned aligned to the cylindrical hole, the signal from the cylindrical hole is clearly visible unlike Figure 6.2a where the transducer was slightly moved away from the axis of the hole. Figure 6.3b is the result of minimizing and lowpass filtering of the signal in Figure 6.3a. Figure 6.3c is the result of applying minimization and polarity thresholding algorithms followed by a lowpass filtering. The results demonstrate again that SSP is a viable method of signal processing for coherent noise reduction.

Most significant aspect of SSP evident from the series of experimental results presented so far is that SSP is effective even at the predicted limit of operation when the scatterers and the target are of the same order of magnitude as the wavelength. Such a conclusion is possible because the average grain size in the equiaxed sample used for the experiments is about 1.5 mm to 2 mm [68], the target (cylindrical hole) is 3 mm in size and the nominal wavelength is about 2 mm.

Experiments for SNR enhancement have been conducted also in columnar grained samples which are anisotropic in nature. The experiments have been conducted with four different angles - 0°, 15°, 45°, and 75° - of interrogation with respect to the axis of grain orientation. The results of the experiments are shown in Figure 6.4 through 6.7. Each figure has three parts: part 'a' is the original signal before processing, part 'b' is the signal after minimization and lowpass filtering and part 'c' is the processed signal after minimization, polarity thresholding and lowpass filtering. The results demonstrate the utility of SSP for SNR enhancement in anisotropic grain structure also.

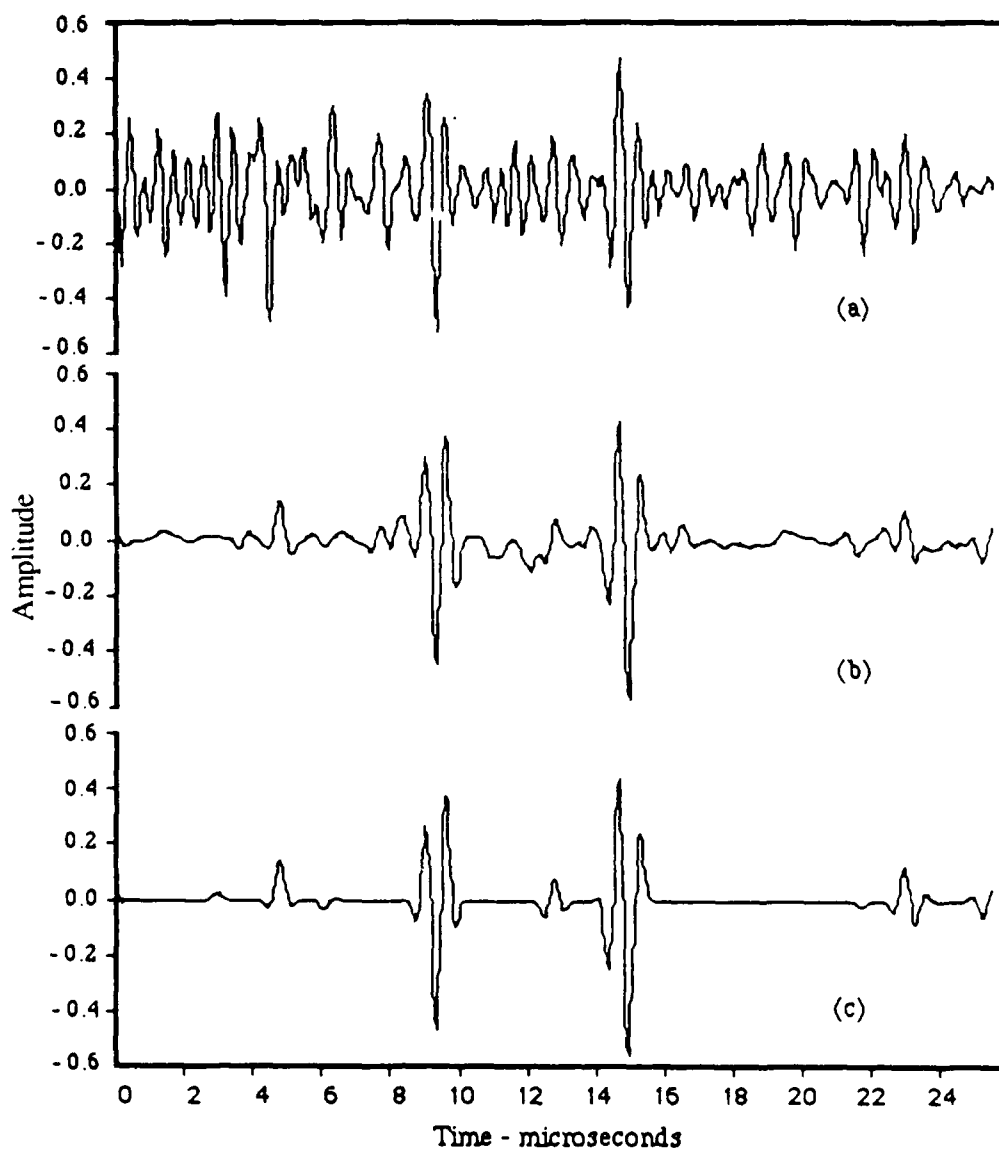


Figure 6.3 a An ultrasonic signal obtained from an equiax grained CCSS sample showing echo signals from the backwall and a cylindrical hole.

6.3 b Minimized and lowpass filtered signal.

6.3 c Minimized, polarity thresholded and lowpass filtered signal.

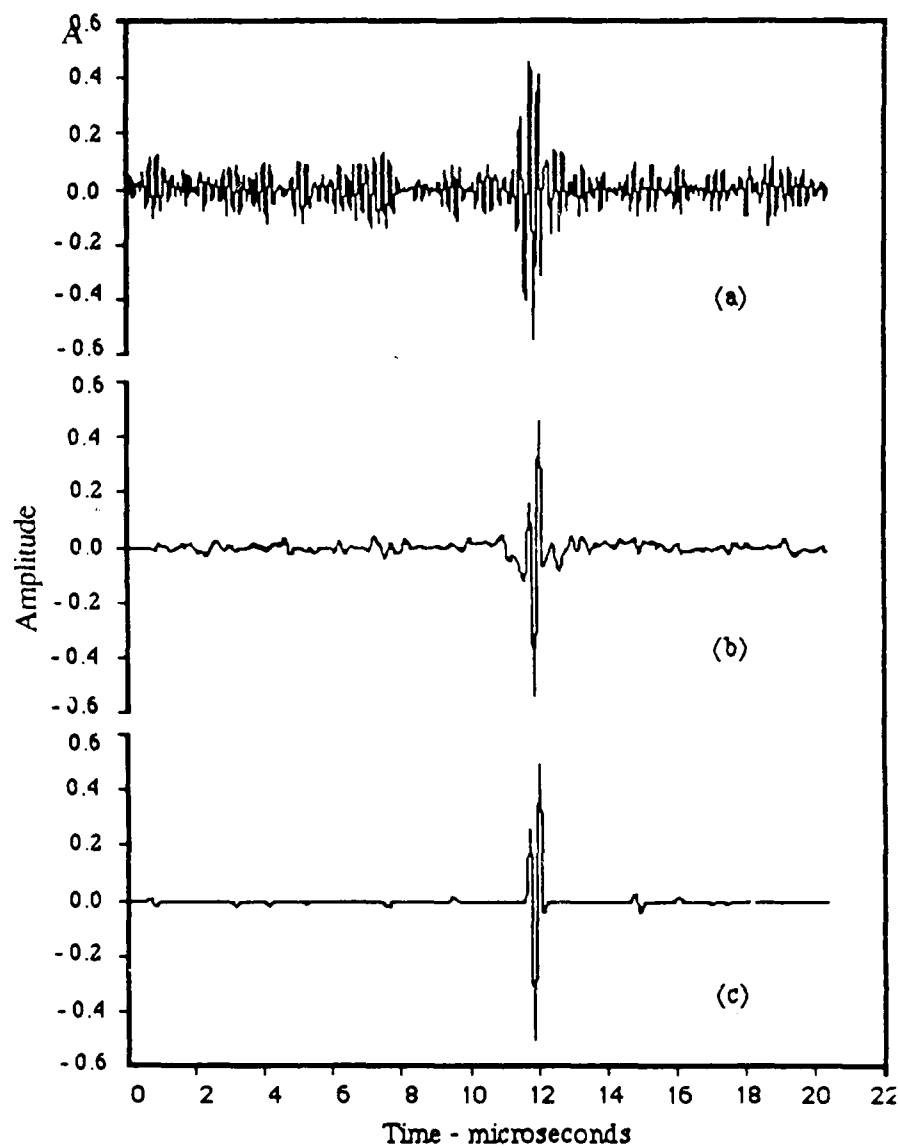


Figure 6.4 a An ultrasonic signal obtained from a columnar grained sample. The angle of interrogation is zero degree with respect to the axis of orientation of the grains.

6.4 b Minimized and lowpass filtered signal.

6.4 c Minimized, polarity thresholded and lowpass filtered signal.

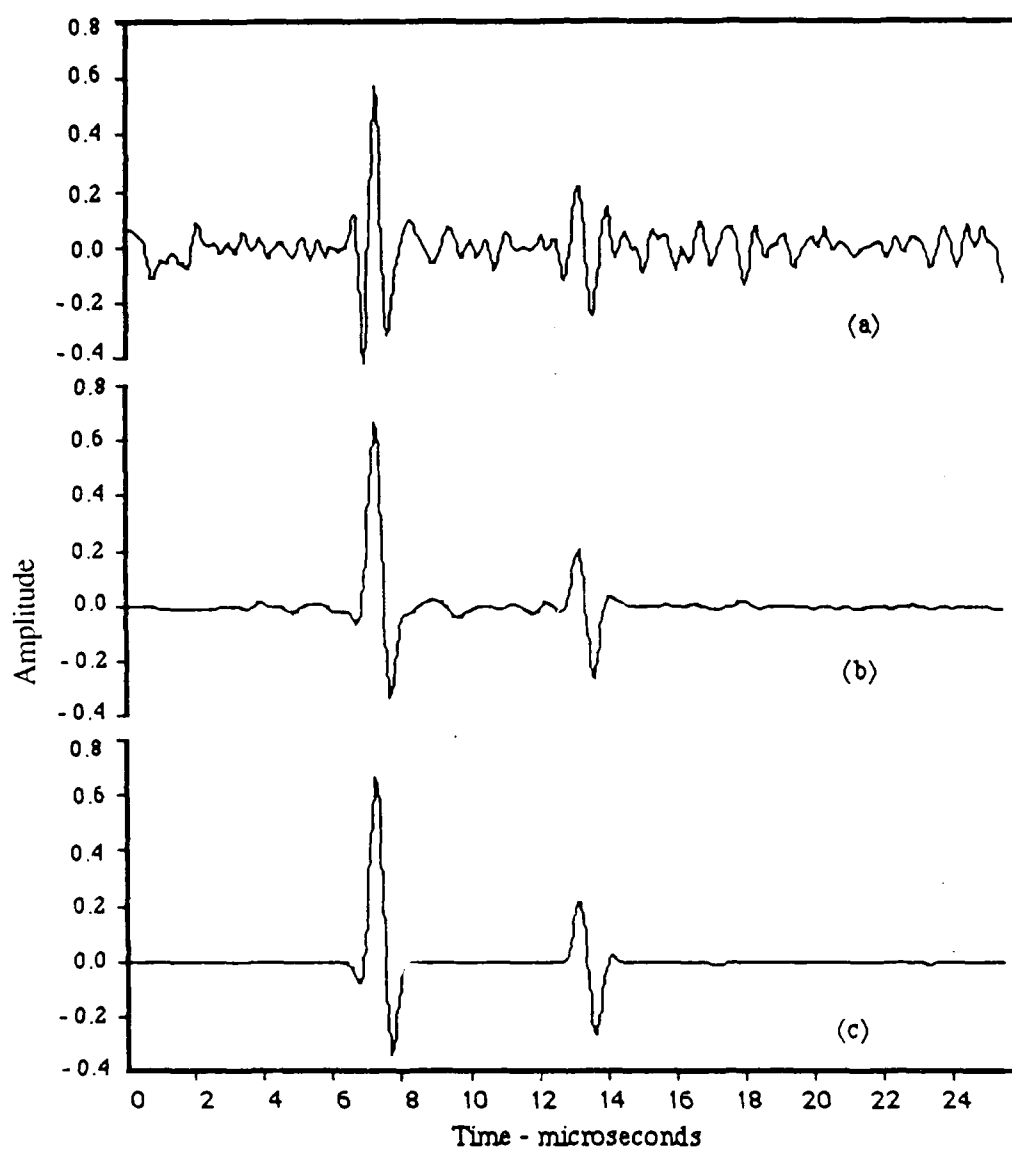


Figure 6.5 a An ultrasonic signal obtained from a columnar grained sample. The angle of interrogation is 15 degrees with respect to the axis of orientation of the grains.

6.5 b Minimized and lowpass filtered signal.

6.5 c Minimized, polarity thresholded and lowpass filtered signal.

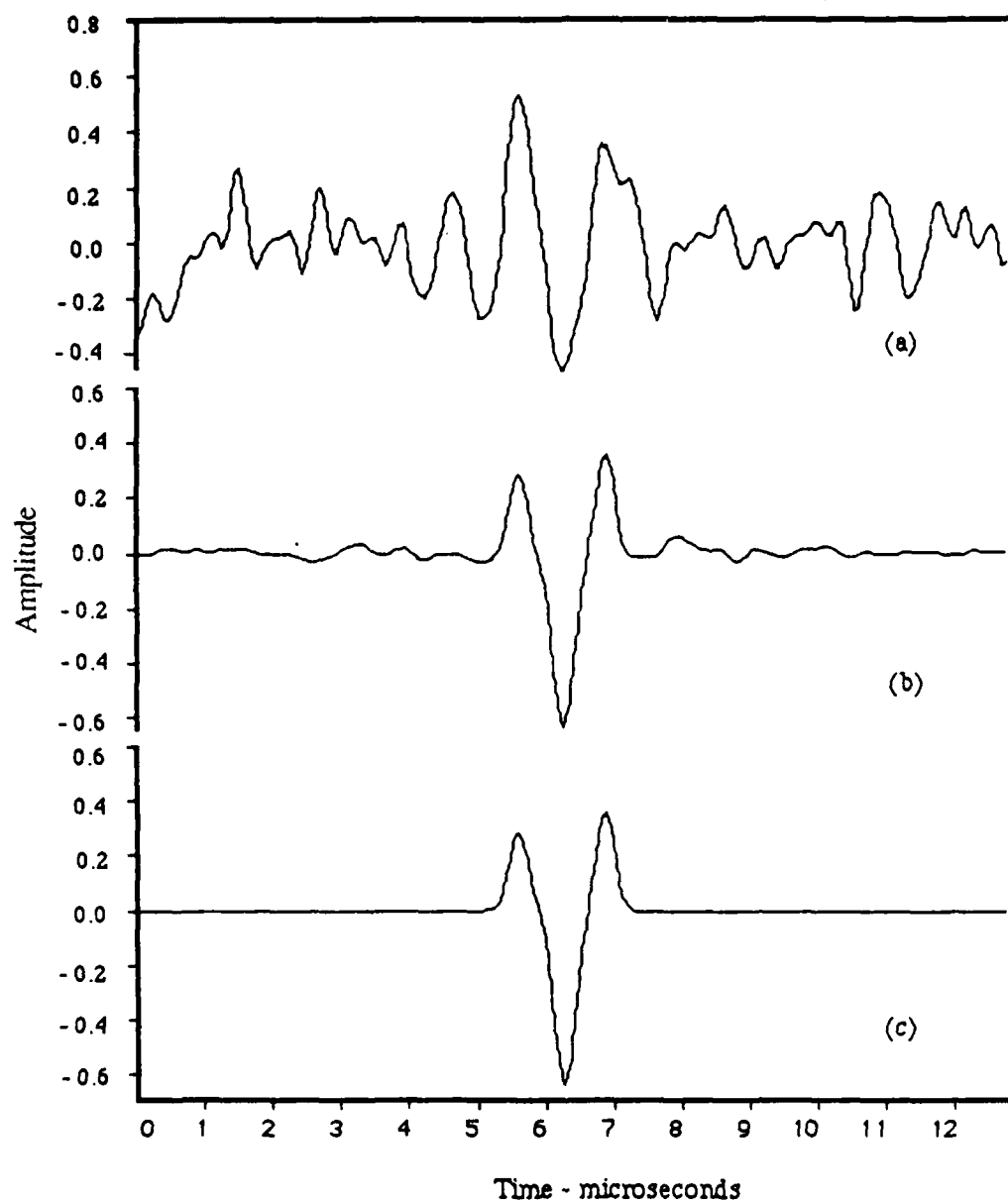


Figure 6.6 a An ultrasonic signal obtained from a columnar grained sample. The angle of interrogation is 45 degrees with respect to the axes of the grains.

6.6 b Minimized and lowpass filtered signal.

6.6 c Minimized, polarity thresholded and lowpass filtered signal.

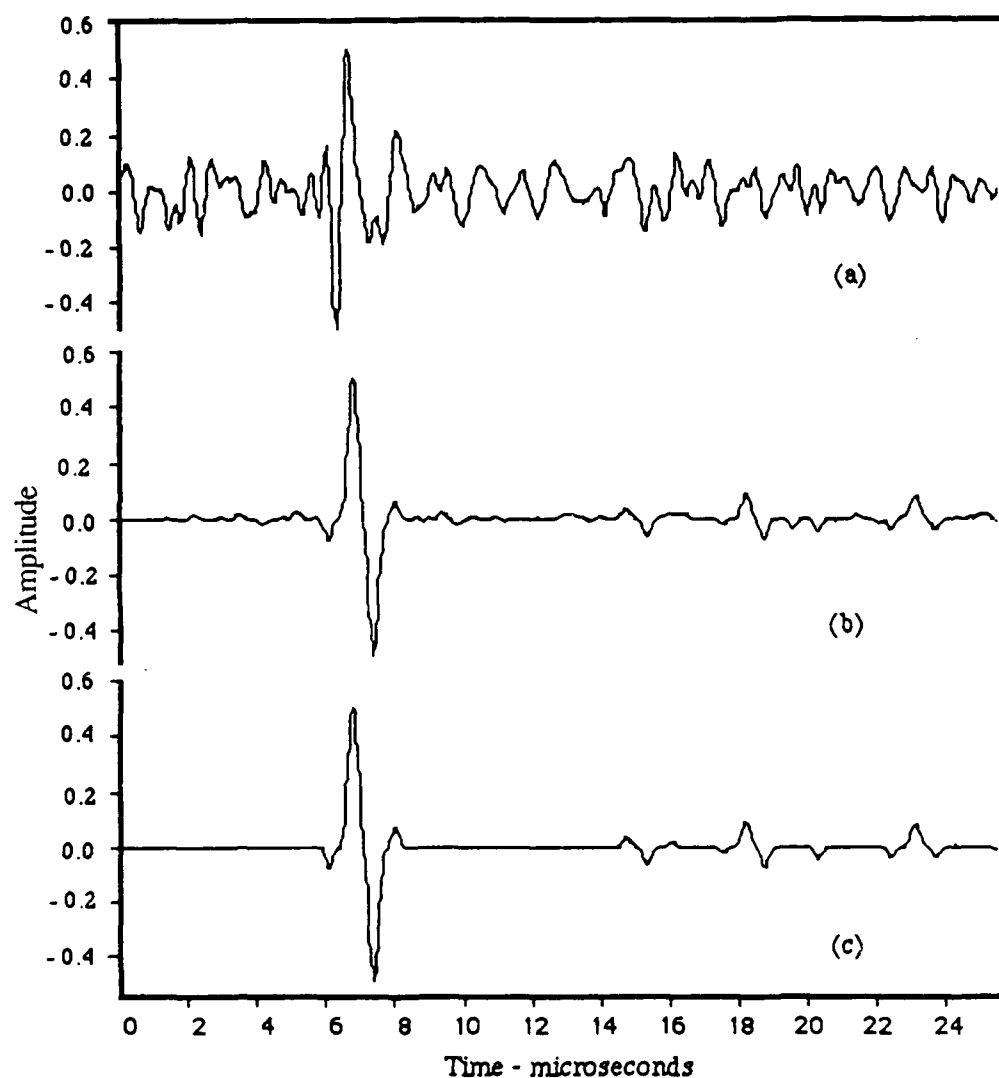


Figure 6.7 a An ultrasonic signal obtained from a columnar grained sample. The angle of interrogation is 75 degrees with respect to the axis of orientation of the grains.

6.7 b Minimized and lowpass filtered signal.

6.7 c Minimized, polarity thresholded and lowpass filtered signal.

6.3.1.2 Composite Material

The composite material used for the experiments is a Carbon-Epoxy composite material with a total thickness of 6.4 mm. A schematic diagram of the cross section of the composite test specimen is shown in Figure 6.8. The material has seven laminate layers. The two outermost laminates are 0.53 mm in thickness followed by two inner laminates of 0.75 mm thick. The innermost three laminates are 1.28 mm thick. Immersion pulse echo technique was used for the experiments.

Figure 6.9a shows the signal obtained from a Carbon-Epoxy composite material using a transducer of 5.66 MHz center frequency and 3.47 MHz bandwidth. The transducer impulse response has a pulse duration in water of 0.3138 microseconds. The corresponding pulse duration is 0.5650 microseconds in the composite material which represents 1.526 mm in the composite material (A measured velocity of 2700 m/sec in a direction perpendicular to the laminates has been used for these calculations with an assumption that the calculated velocity is constant across the cross section). As a result, the transducer will be unable to resolve any thicknesses less than about 0.75 mm. Referring to Figure 6.8, since the two outermost laminates are too thin to be resolved, the transducer can resolve only the inner five laminates. The result of the processing is shown in Figure 6.9b. The figure clearly shows the echoes from the inner laminates in addition to the reverberations produced by the sound energy caught between the laminates. The random noise due to the fibers and Epoxy is suppressed and the nonrandom signals from the laminates are retained. Eighteen overlapping windows of 1.26 MHz bandwidth each have been used for the processing.

6.3.1.3 Zircalloy - Zirconium Tubing

Signal-to-noise ratio enhancement experiments have also been conducted on a Zircalloy tubing with an inner cladding of Zirconium. The cladding has been diffusion bonded to the Zircalloy tubing. The thickness of the cladding ranges from 1.5 mm to 1.9 mm. The various dimensions of the tube are as shown in Figure 6.10. Immersion pulse echo technique was used for the experiments.

Zircalloy tubing is used in a nuclear reactor. The tube is made of Zircalloy and is clad with an inner lining of Zirconium. It is essential to maintain the Zirconium cladding

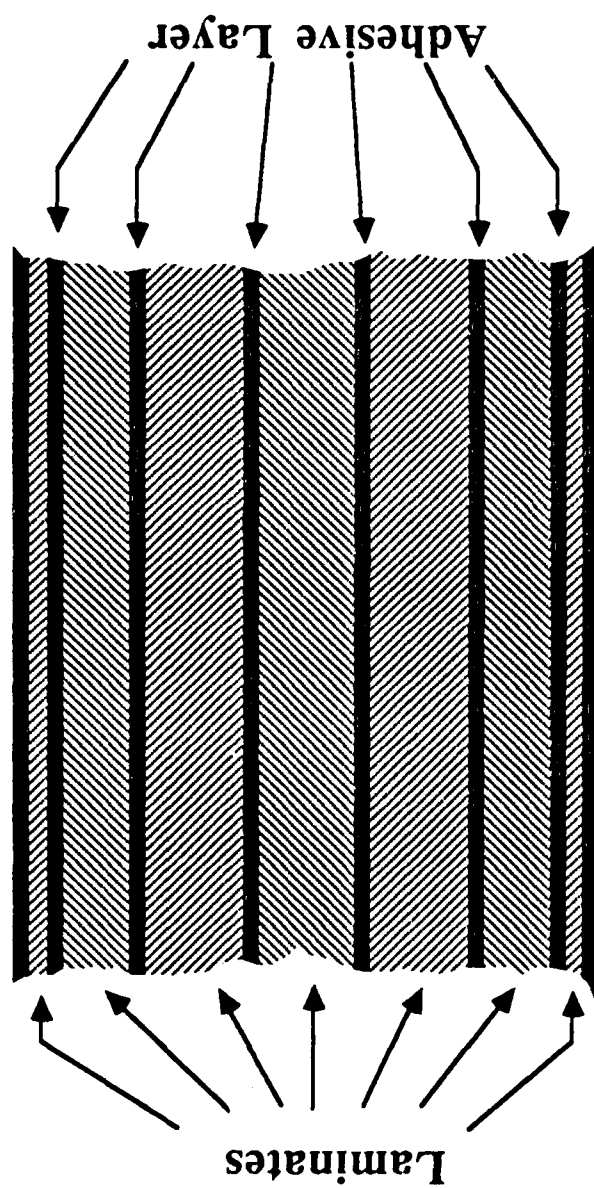


Figure 6.8 A pictorial cross section of the Carbon-Epoxy Composite material used for the experiment.

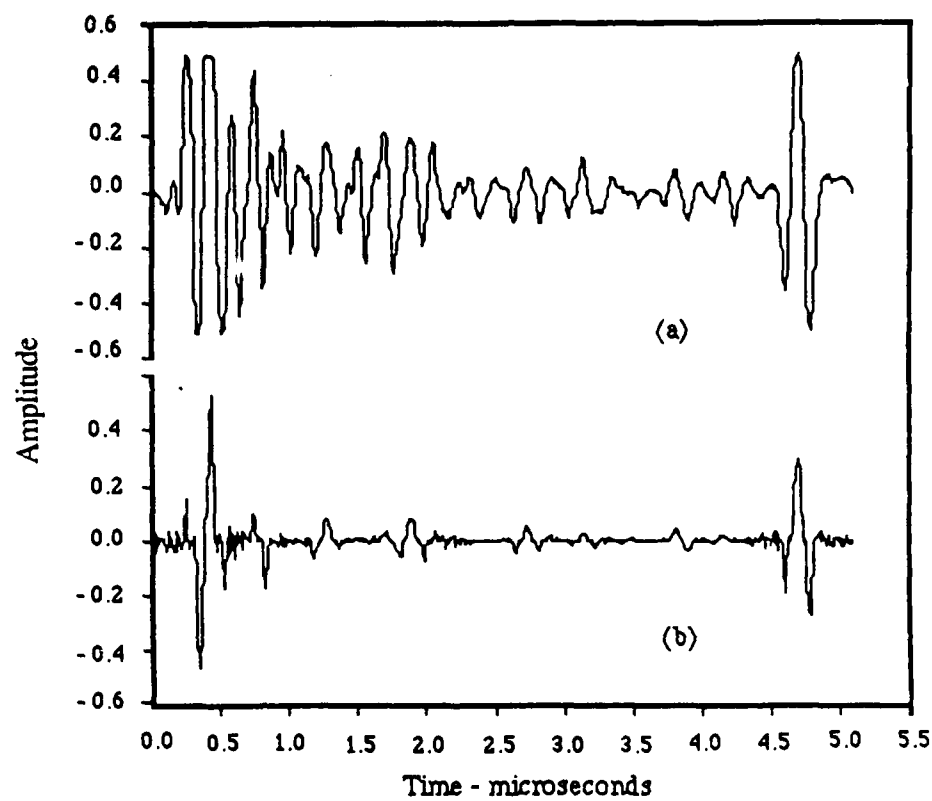


Figure 6.9 a Unprocessed signal obtained from the Carbon-Epoxy Composite material shown in Figure 6.8.

6.9 b Minimized signal showing the echoes from the composite layers.

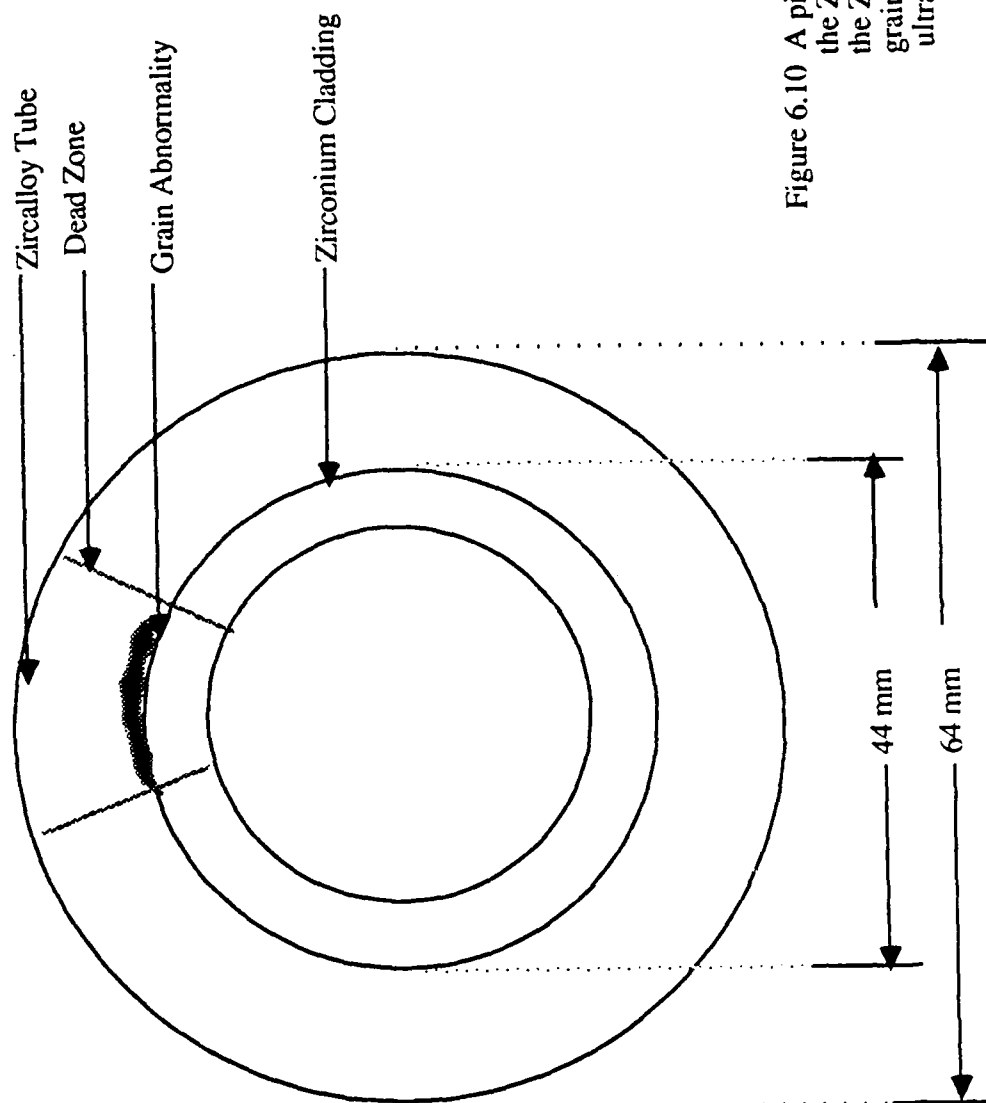


Figure 6.10 A pictorial cross section of the Zircaloy tube showing the Zirconium lining and a grain abnormality causing an ultrasonic 'dead zone'

thickness within a pre-defined range. Also, regulations require that it should be possible to nondestructively measure the cladding thickness at any given spot on the tubing. However, due to some grain abnormality near the Zircalloy - Zirconium interface, 'dead zones' are occasionally created wherein the interface echo will be hidden by grain noise making it difficult to ultrasonically measure the cladding thickness. Split spectrum processing technique has been used to effectively suppress the grain noise, thereby making it possible to measure the cladding thickness.

Zircalloy tubing poses a very difficult problem for ultrasonic nondestructive testing. Since Zircalloy is an alloy of Zirconium, they have similar physical properties. As a result, the acoustic impedances of the two layers will be very close to each other, thereby causing very little energy to be reflected from the interface, even when there is no grain abnormality masking the interface. Consequently, it would be necessary to have as much as 30 dB of amplification before the interface signal can be seen. This phenomenon is demonstrated in Figures 6.11a and 6.11b.

Figure 6.11a shows a signal obtained from a 'normal zone' (i.e. where the interface echo is not obscured by any grain abnormality). A 8.1 MHz cylindrical focus transducer of 3 inch focal length and a band width of 3.32 MHz has been used for the experiments. The amplification has been set such that the front wall echo of the signal in Fig. 6.11a is not saturated. It could be seen from the figure that the interface echo is practically nonexistent.

The signal in Figure 6.11b has an additional 29 dB of amplification. The interface echo is clearly visible because of the larger amplification. However, due to the high amplification, the backwall echo is spread over a long time range thereby introducing inaccuracies in the cladding thickness that might be measured from the signal in Figure 6.11b. Nevertheless, since Fig. 6.11a and 6.11b together give the undistorted arrival times of the backwall echo and the interface echo respectively, the cladding thickness can be found out by a combined use of Figs. 6.11a and 6.11b. From Figures 6.11a and 6.11b, the difference in arrival time between the two signals of interest is $0.353 \mu\text{s}$. Hence, the cladding thickness is 1.595 mm, using a measured velocity of 4520 m/s in Zirconium. Figure 6.11c is a schematic representation of the thickness measurement process wherein the gated portion of Fig. 6.11b has been superimposed on Fig. 6.11a.

The Zircalloy tubing occasionally exhibits 'dead zones' wherein the interface echo is masked by grain noise produced by some grain abnormalities appearing just above the interface (Figure 6.10). Figures 6.12a and 6.12b show signals obtained in a dead zone

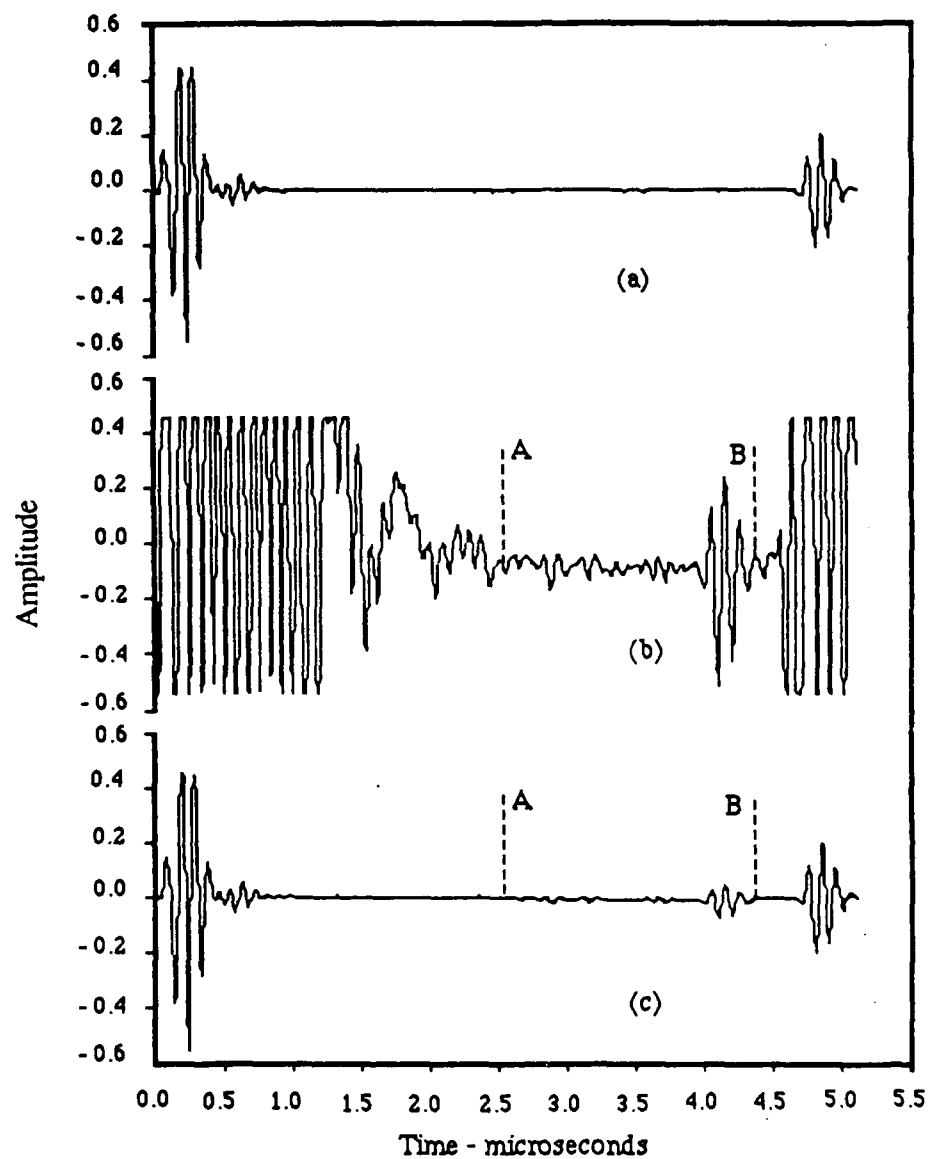


Figure 6.11 a Signal obtained from a 'normal zone' of a zircalloy tubing. The signal shows the front wall echo and the backwall echo. Interface echo is not seen due to insufficient gain.
 6.11 b Signal in Figure 6.11a after an additional 30 dB of amplification. The interface echo is seen. Front wall and the back-echoes are distorted.
 6.11 c A 'composite' signal obtained by superimposing the signal in gate A-B of Figure 6.11b on Figure 6.11a.

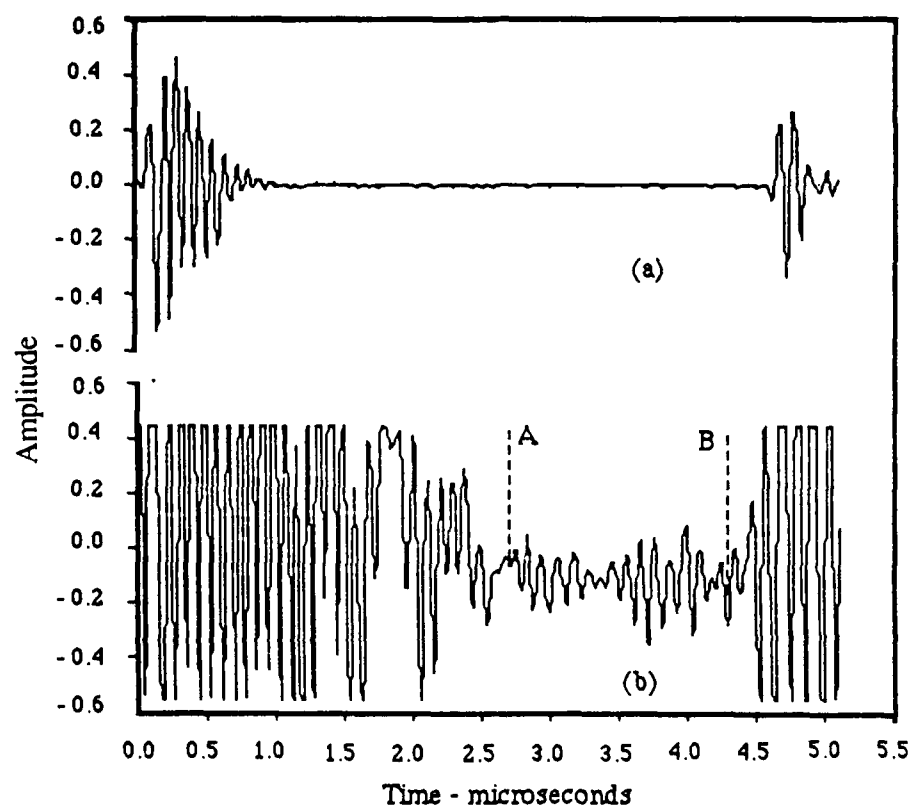


Figure 6.12 a Signal obtained from a 'dead zone' of a zircalloy tube. The signal shows the front wall and the backwall echoes. The interface echo is not seen due to insufficient gain.

6.12 b The signal in Figure 6.12a after an additional 30 dB of gain. The interface echo is obscured due to grain noise.

with low and high amplifications (an additional 29 dB) respectively. It could be seen from Figure 6.12b that the interface echo is not well defined due to the interfering grain noise around the interface area. The phenomenon makes it impossible to measure the cladding thickness at that spot which would cause the tubing to be rejected unless the problem could be solved by some form of signal processing like SSP.

Figure 6.12b shows the signal which should be processed for noise reduction. However, since the front wall and the back wall echoes are saturated, they will have a distorting effect on the frequency spectrum of the signal and hence will influence the performance of a frequency dependent technique like SSP. As a result, it would be necessary to eliminate the effect of the saturated portion of the signal by suitably gating the signal so that the gate is small enough to eliminate the saturated signals but not small enough to unduly bias the output of the processor. Gate A - B shown in Figure 6.12b has been used to select a portion of the signal for further processing using SSP. Minimization and polarity thresholding algorithms were applied. Figure 6.12c shows the processed signal from gate A-B and shows a complete suppression of grain clutter due to a combined use of minimization and polarity thresholding algorithms. The processing has indeed suppressed the grain clutter enough to find the arrival time of the interface echo. From Figures 6.12a and 6.12c, the difference in the arrival times is $0.345 \mu\text{s}$ and hence the thickness of the Zirconium lining is 1.59 mm. Figure 6.12d is a schematic representation of the thickness measurement process wherein the gated portion of Fig. 6.12c has been superimposed on Fig. 6.12a. Eighteen filters of 0.325 MHz bandwidth each have been used for the split spectrum processing of the signals from the Zirconium tube.

Split spectrum processing is a nonlinear method of signal processing. As such, the phase information of the input signal is nonlinearly altered by the processor in the presence of grain noise alone while the phase information of a target is linearly processed. Split spectrum processing has the effect of transforming the input signal to a new domain (just like, the signal is transformed into the frequency domain when FFT processor is used). Consequently, the output signal of the SSP technique can be meaningfully used in a feature extraction and classification technique [62,63] for anomaly classification provided the feature values are recalculated for the processed signal instead of linearly or nonlinearly extending the feature values obtained for the unprocessed signal.

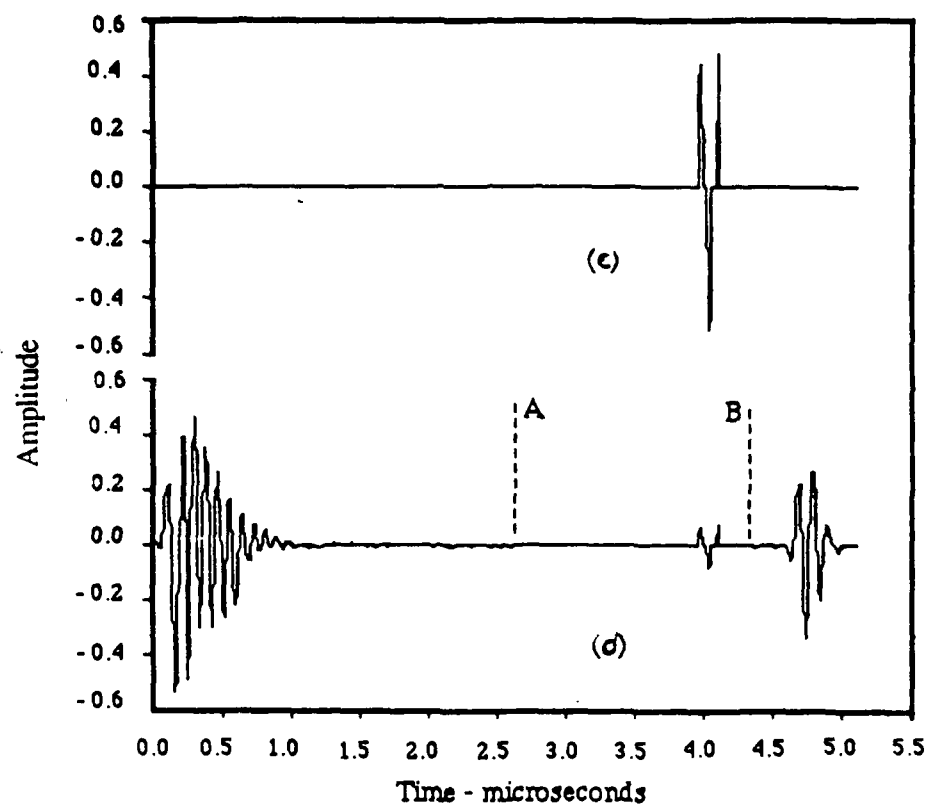


Figure 6.12 c Minimized and polarity thresholded output of the gated signal A-B in Figure 6.12b.

6.12 d A 'composite' signal obtained by superimposing the processed signal in Figure 6.12c on to Figure 6.12a.

6.3.2 Speckle Reduction in 2-D B-scan Images

The effectiveness of SSP in speckle suppression in ultrasonic B-scan images is demonstrated in this section of the chapter. An equiaxed CCSS sample with a side drilled hole is used for the experiment. Figure 6.13a shows an unprocessed B-scan image of the CCSS block. The image shows the backwall echo (toward the bottom of the image), and the side drilled hole in the middle of the image. The image is cluttered with ultrasonic speckle produced by the interference phenomenon due to the wavelets scattered by the granular structure of the sample.

Figure 6.13b is the result of processing the image in Figure 6.13a using polarity thresholding by itself. Each RF signal in the image is processed individually. The final processed image is formed from the processed RF signals. Fourteen filters of 184 KHz bandwidth each, placed in the range of 391 KHz to 1.406 MHz with an interfilter spacing of 78 KHz, are used for the processing. It should be noted that, even though a transducer of nominal center frequency of 2.25 MHz is used, the returned energy is concentrated in the range of 391 KHz to 1.406 MHz due to the scattering phenomenon. As such, only the available bandwidth is used for processing instead of the transmitted bandwidth.

Figure 6.13b shows a remarkable speckle suppression. The axial resolution is also sharper. However, the lateral resolution is unaffected and is still very poor. Nevertheless, there is an important conclusion that could be drawn from the result: due to a poor lateral resolution, the image of the hole extends laterally into a 'tail' which is an ultrasonic artifact. However, the significance of the result is that, even though the amplitude in the 'tail' section of the hole is weak and is comparable to the amplitude of the speckle in Figure 6.13a, the processing has retained the 'tail' portion of the image of the hole while the speckle amplitudes of similar magnitude are rejected. Such a discrimination is because the weak target amplitude is still frequency independent (within the bandwidth of the transducer) while that of the grain speckle is not. Thus, it is obvious from the result that the target amplitude does not have to be larger than the surrounding noise level for a successful implementation of the technique.

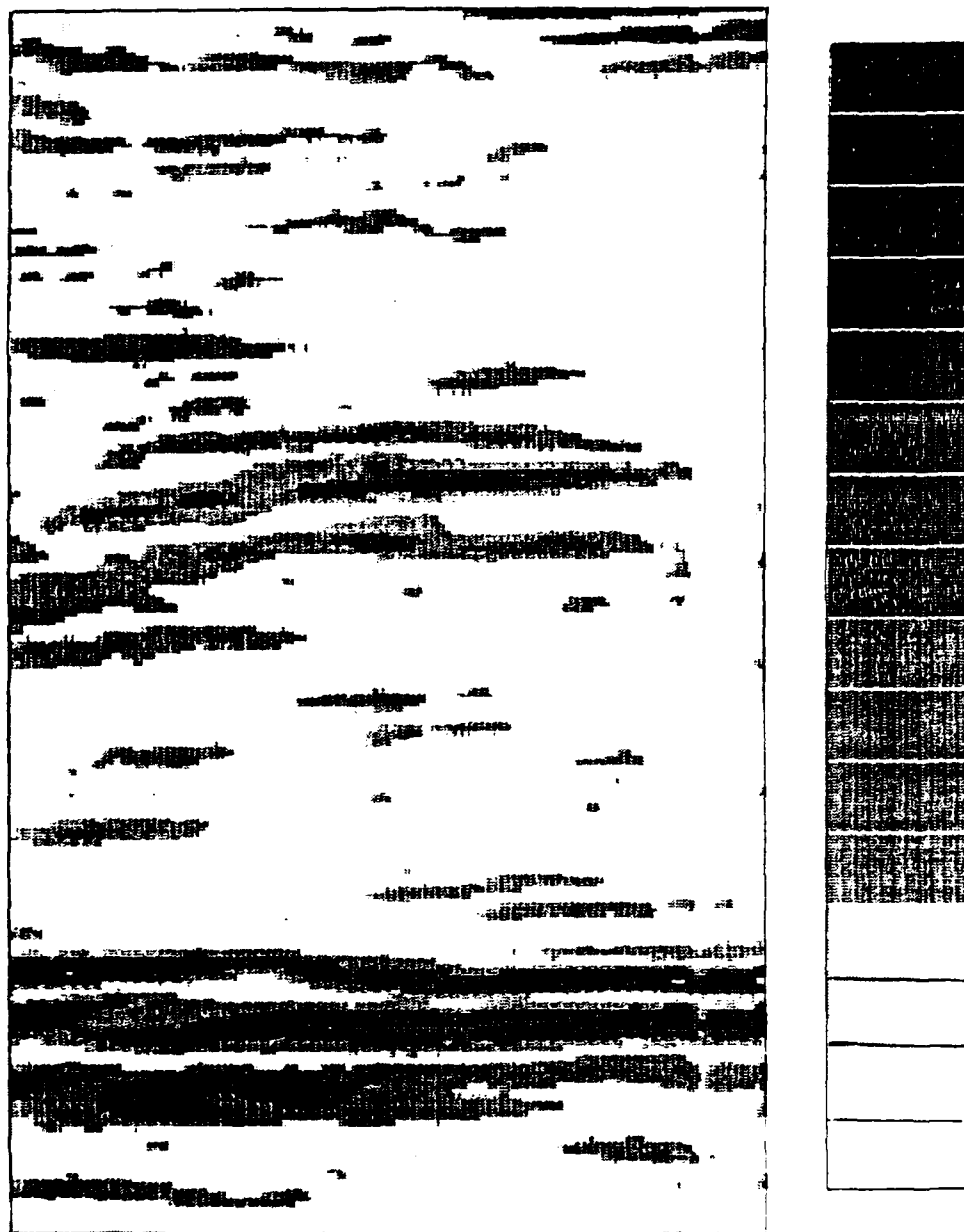


Figure 6.13 a An unprocessed B-scan image of an equiax grained CCSS block showing pronounced speckle pattern obscuring the signals from the backwall and the cylindrical hole.

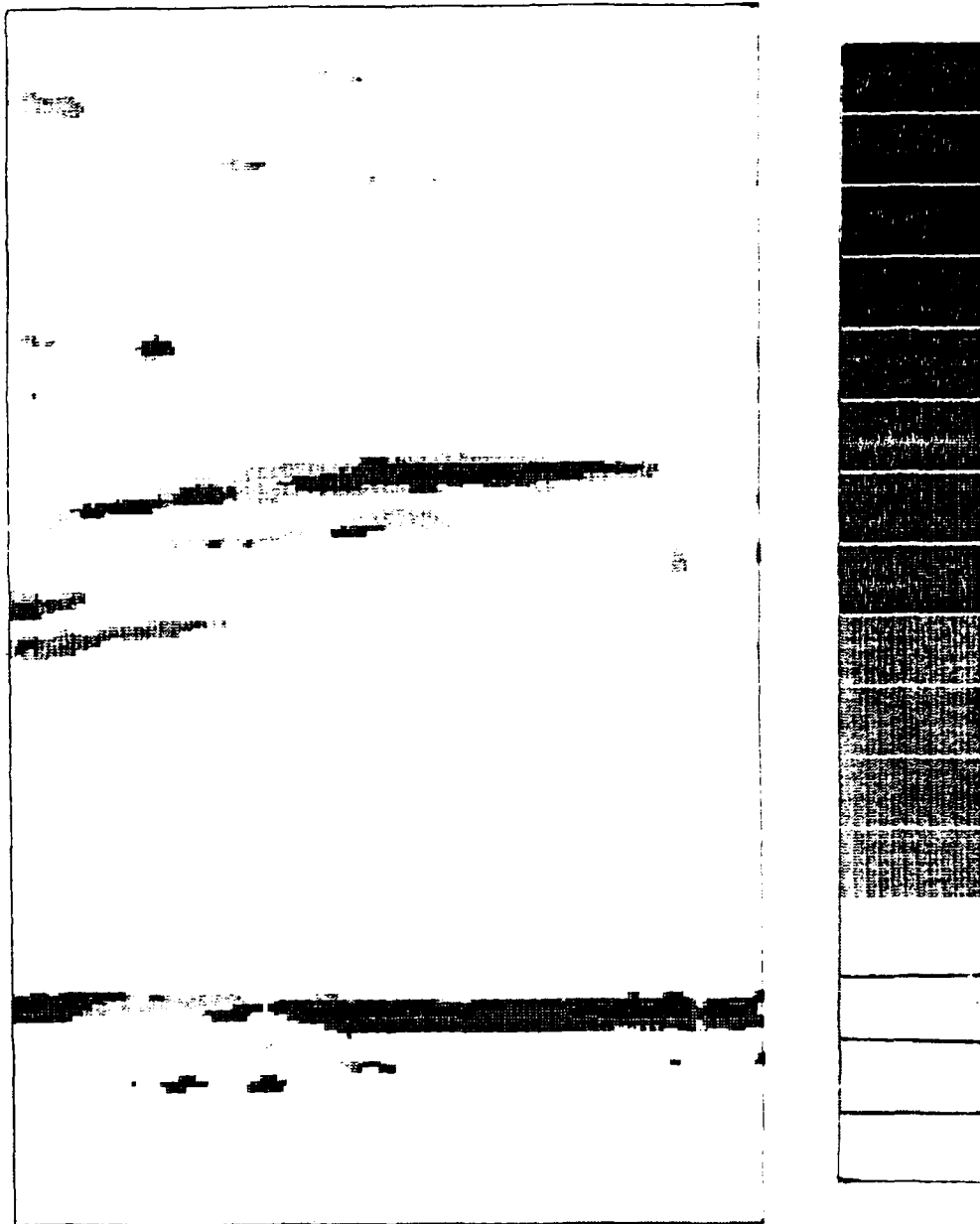


Figure 6.13 b Processed B-scan image after applying polarity thresholding to the image shown in Figure 6.13a.

6.3.3 Potential of SSP as a tool for material characterization

The process of splitting the spectrum of the received signal results in 'N' split time domain signals. It could be easily shown, using principles of Fourier analysis, that the process of splitting the spectrum is equivalent to using 'N' different narrow banded transducers of frequency contents identical to that of the bandpass filters used for the splitting process. Hence, it is possible to study certain frequency dependent properties of the test material by using just one broad banded transducer instead of many narrow banded transducers and the associated experimental complexities. For example, i) the test material might be dispersive i.e. it might have different wave velocity for different frequency contents of the incident wave, ii) the test material will attenuate different frequency contents by different factors depending on the relative size of the grains with respect to the wavelength. As a result, it should be possible to classify the material type by a careful analysis of the ultrasonic signals obtained by either SSP or many transducers of different frequencies. Theoretical aspects of frequency dependent attenuation is discussed next as a basis for some preliminary experimental results to be presented later.

6.3.3.1 Theory

Attenuation of ultrasonic waves travelling in a material is given by [1,71]

$$A = A_0 (-\alpha(f) x) \quad (6.3)$$

where A is the attenuated amplitude, A_0 is the initial amplitude, x is the distance over which the wave front has travelled, $\alpha(f)$ is the attenuation coefficient and 'f' is the frequency. The attenuation coefficient is defined by [64,65]

$$\alpha(f) = \alpha_a(f) + \alpha_s(f) \quad (6.4)$$

where α_a is the absorption coefficient and α_s is the scattering coefficient.

Three distinct cases of attenuation exist: i. Rayleigh zone when the wavelength λ is $> 2\pi D_g$, ii. stochastic zone when $\lambda \approx 2\pi D_g$ and iii. diffusion zone when $\lambda < 2\pi D_g$, where D_g is the average grain diameter with an approximation of spherical grains. These

attenuations are defined by,

$$\alpha(f) = a_1 f + a_2 D_g^3 f^4, \quad \text{when } \lambda > 2\pi D_g, \quad (6.5a)$$

$$\alpha(f) = b_1 f + b_2 D_g f^2, \quad \text{when } \lambda \approx 2\pi D_g, \quad (6.5b)$$

$$\alpha(f) = c_1 f + c_2 f^2 + c_3 / D_g, \quad \text{when } \lambda < 2\pi D_g, \quad (6.5c)$$

where, a_1, b_1, c_1, c_2 are absorption coefficients and a_2, b_2, c_3 are scattering coefficients.

Thus, from (6.5a), (6.4b) and (6.5c), it is clear that

$$\alpha_s(f) \text{ proportional to } D_g^3 f^4, \quad \text{when } \lambda > 2\pi D_g, \quad (6.6a)$$

$$\alpha_s(f) \text{ proportional to } D_g f^2, \quad \text{when } \lambda \approx 2\pi D_g, \quad (6.6b)$$

$$\alpha_s(f) \text{ proportional to } 1/D_g, \quad \text{when } \lambda < 2\pi D_g, \quad (6.6c)$$

Hence, the degree of scattering is a function of both the incident frequency and the average grain dimension. Since coherent noise level in an ultrasonic signal is due to the interference of the wavelets scattered by the grain boundaries, the signal-to-noise ratio of a signal should contain information about the relationship among noise level, grain size and scattering frequency (Eqns. 6.6a to 6.6c). It should be remembered that (6.6a) to (6.6c) are valid only if the grain shape could be approximated as spherical (as in equiaxial grained CCSS).

Columnar grains, quite frequently found in CCSS, do not conform to the model of spherical grains assumed for equiaxial grains. Equations (6.6a) to (6.6c) are no longer valid for columnar grains because the equations assume a mean spherical diameter D_g for the grains. Depending on the angle of wave incidence with respect to the grain axis, the columnar grains can be modeled as either acoustic wave guides (0° incidence) or scatterers (90° incidence). When the angle of incidence is between 0° and 90° , the situation becomes even more complex. Consequently, the noise level and hence SNR is substantially different for different angles of incidence as well as frequency. Changes in the angle of incidence drastically changes the ratio between λ and D (D is the grain dimension in the direction of wave propagation), thereby substantially altering the noise level in the signal. Thus, it is envisaged that SNR of split time domain signals can serve as a discriminator of both the grain type (equiaxial vs. columnar) and size when both the angle of insonification and frequency (induced by SSP or by different narrow banded transducers) are varied.

Columnar grains, because of the wave guide phenomenon, might cause different modes [56,66,67] of 'plate waves' to propagate in the test material, especially at 0° incidence. Propagation of higher modes is dependent on the frequency and the cross sectional dimension of the columnar grains. When the frequency is varied over a range, new modes of wave propagation are induced in the columnar material depending on the ratio of the cross sectional dimension and the wavelength. Mathematical relations are available [56,66,67] for circular and rectangular ducts from which the cross sectional dimension of the duct can be calculated as a function of the wavelength. However, since the columnar grains in CCSS have irregular cross sectional shape, further research would be essential before a sufficiently reliable approximation of the relationship between the wavelength and the average cross sectional dimension of the grains could be developed. Nevertheless, the feasibility of the concept can be demonstrated by some simple experiments in which the frequency diversity is introduced through SSP. The experimental results which demonstrate the utility of SSP as a tool for material characterization are presented next.

6.3.3.2 Experiments

The CCSS test specimens used for the grain characterization experiments have been made out of CCSS pipe sections as shown in Figure 6.14 (see Reference [68] for further details). The specimens are of two kinds: i. equiaxial grained and ii. columnar grained. Equiaxial grain samples are metallographically found [68] to contain randomly packed grains of an average size of about 1 to 1.5 mm while the columnar grained specimens have grains of about 1.5 to 2 cm length and about 2 to 3 mm width. Many test blocks have been made with different angled surfaces, ranging from 0° to 90° , machined on the blocks as shown in Figure 6.14. For example, Figure 6.14 c shows a block with 15° and 75° surfaces machined with respect to the radial direction (which is also the grain orientation direction for columnar grains) of the CCSS pipe section shown in Fig. 6.14 a. Five different angles - 0° , 15° , 45° , 75° and 90° - have been machined on both equiaxial and columnar grained samples. The blocks have a 3 mm side drilled hole as shown in Fig. 6.14 c and is used as a target embedded in noise producing grain scatterers. Contact pulse echo technique was used for the experiments.

Two sets of test blocks of equiaxial and columnar type, with 0° , 15° , 45° , 75° and

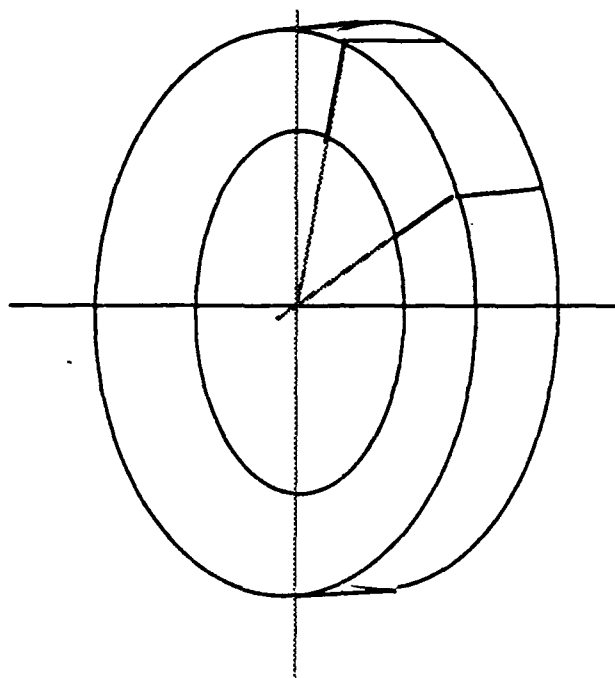


Figure 6.14 a A Centrifugally cast stainless steel pipe

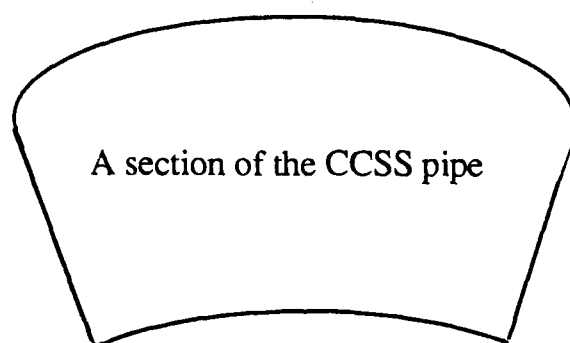


Figure 6.14 b A section of the CCSS pipe shown in Figure 6.14 a.

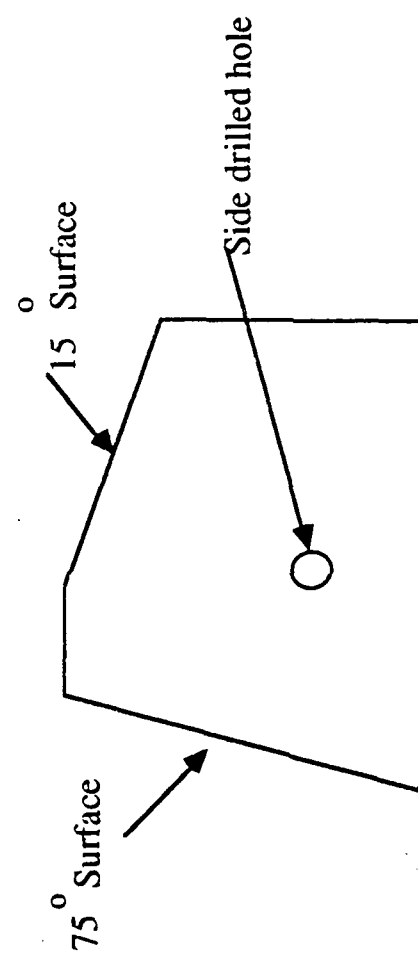


Figure 6.14 c A test sample prepared from the CCSS pipe section.

90° angled surfaces, have been used. A broad band 2.25 MHz contact transducer has been used for the experiments. A side drilled hole has been used as a target. Signal-to-noise ratio as defined by (6.7) has been used as the grain noise evaluator. The processing has been for 16 filters of center frequencies as shown on the abscissa of Figures 6.15a to 6.15e and 6.16a to 6.16e.

$$\text{SNR} = \frac{\text{Maximum peak to peak amplitude of the target signal}}{\text{Maximum peak to peak amplitude of the grain cluster}} \quad (6.7)$$

For each signal obtained from the test block (one for each grain type and angle), the frequency diverse split time domain signals are obtained by the SSP technique. The signal-to-noise ratio (6.7) for each split time domain signal is calculated which has an additional advantage of reducing the effect of loss due to absorption because of the cancellation between the numerator and the denominator of (6.7).

The SNR values calculated for the equiaxial and columnar grains have been plotted in Figures 6.15 and 6.16 as a function of the center frequency of the bandpass filters. Figures 6.15a to 6.15e show the SNR curves for the equiaxial test blocks for 0°, 15°, 45°, 75° and 90° respectively. Figures 6.16a to 6.16e are the corresponding diagrams for the columnar grain samples. It can be seen from Figures 6.15 and 6.16 that the equiaxial and columnar grains have a dramatically different response to insonifications of different frequencies and angles of incidence.

Results of the grain characterizing study shown in Figures 6.15 and 6.16 display some interesting features. The SNR curves for the equiaxial grain sample are shown in Figures 6.15a to 6.15e, each one for a different angle of insonification. The curves in all the figures show similar trends indicating that the grain dimension is of similar order of magnitude in all the directions. On the other hand, the curves shown in Figures 6.16a to 6.16e (for columnar grains) exhibit completely different trends for each angle of insonification, indicating a difference in the grain dimension in the direction of wave propagation. Also, Figures 6.16a, 6.16b and 6.16c show peculiar 'spectral depressions' created by two neighboring peaks, especially Figure 6.16a for 0° incidence. It has been hypothesized that the peaks have been caused by higher modes of waves becoming

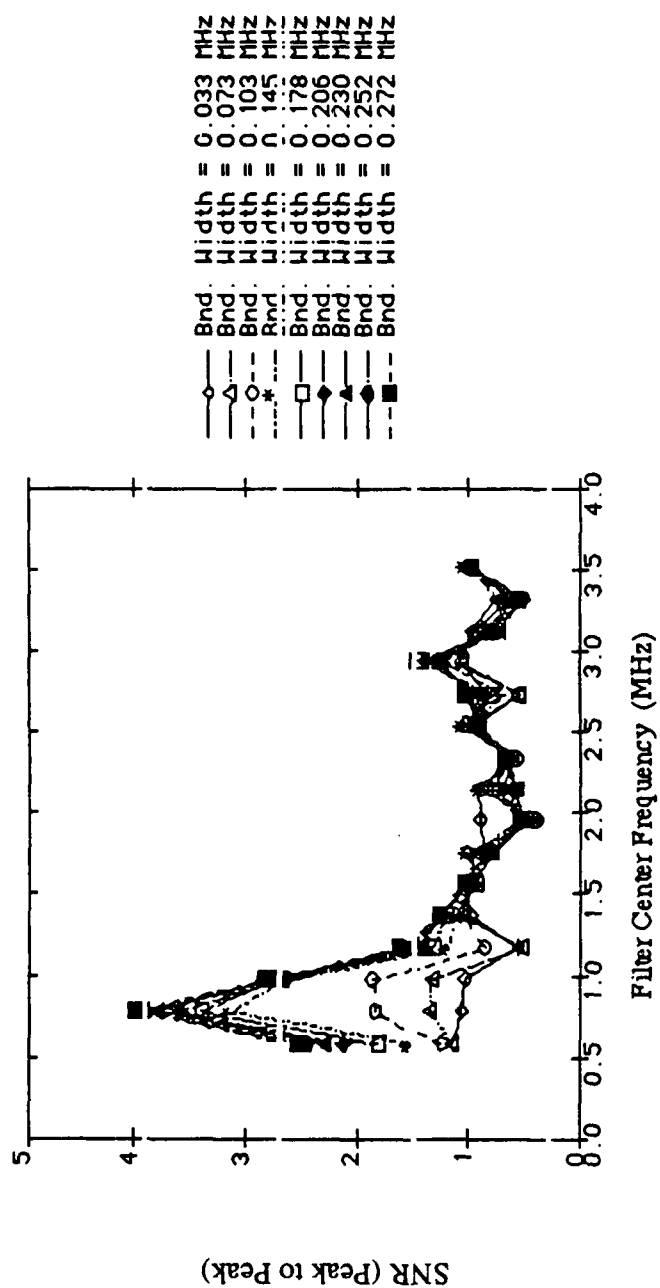


Figure 6.15 a Signal-to-noise ratio curves of the split time domain signals obtained for equiaxed CCSS for 0 degrees wave incidence.

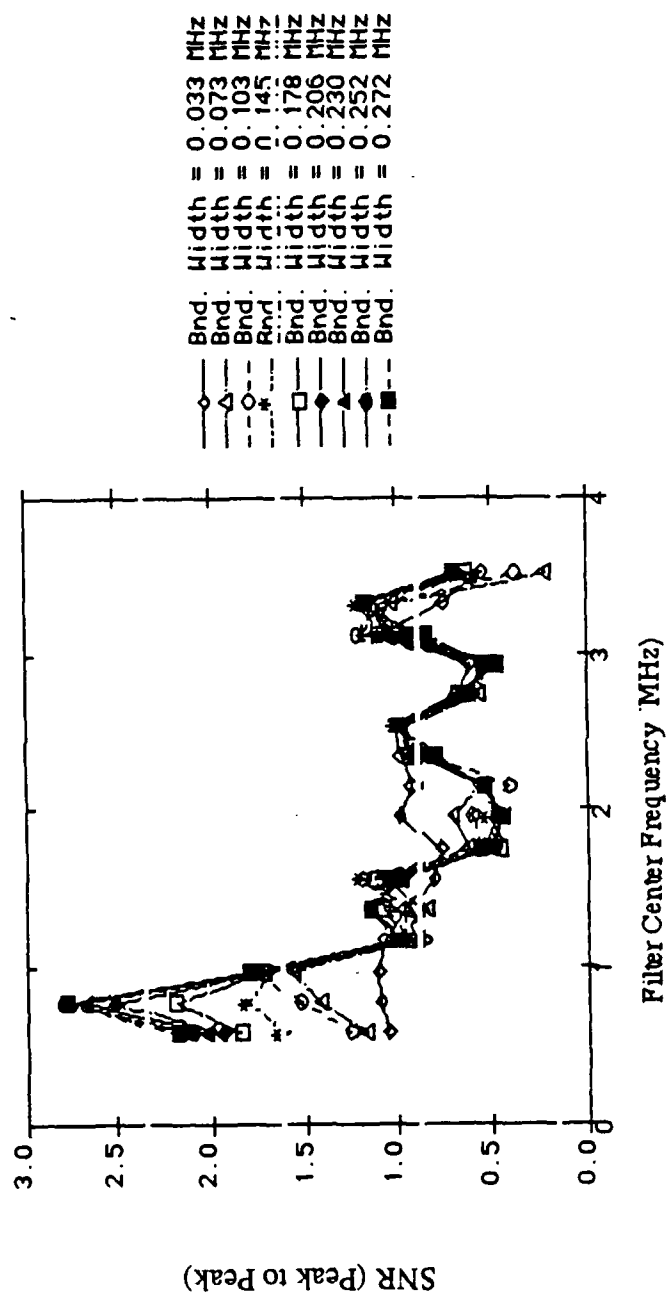


Figure 6.15 b Signal-to-noise ratio curves of the split time domain signals obtained for equiax grained CCSS for 15 degrees wave incidence.

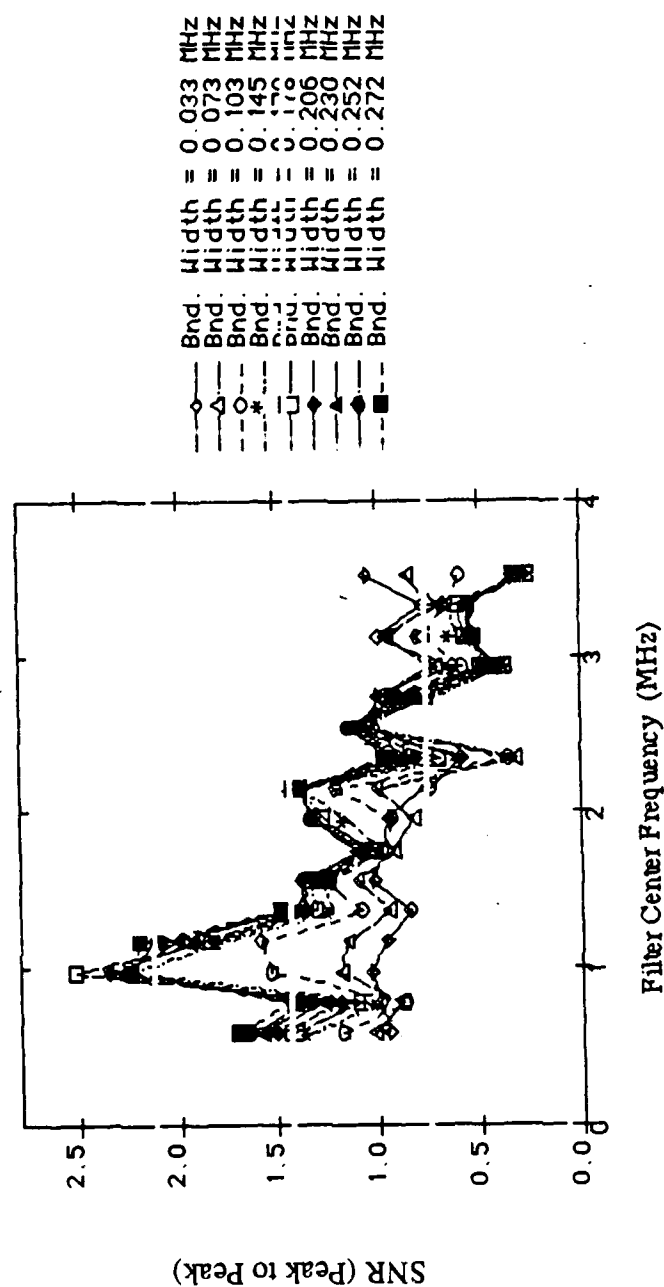


Figure 6.15 c Signal-to-noise ratio curves of the split time domain signals obtained for equiax grained CCSS for 45 degrees wave incidence.

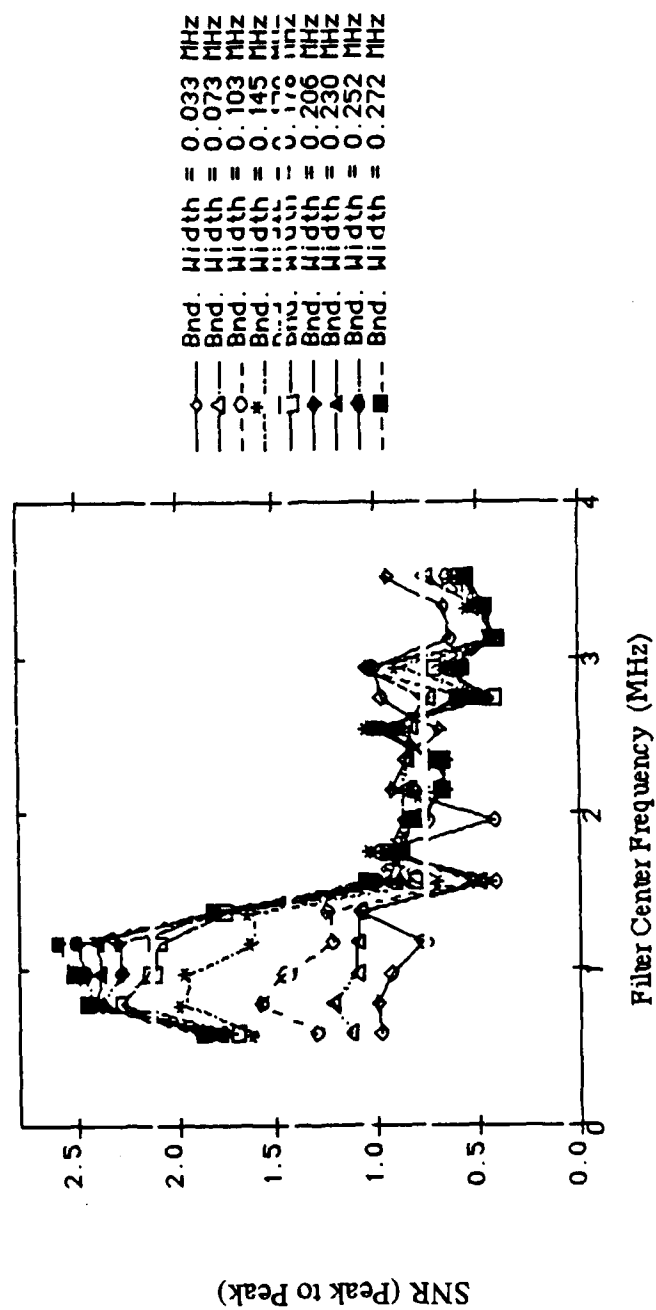


Figure 6.15 d Signal-to-noise ratio curves of the split time domain signals obtained for equiax grained CCSS for 75 degrees wave incidence.

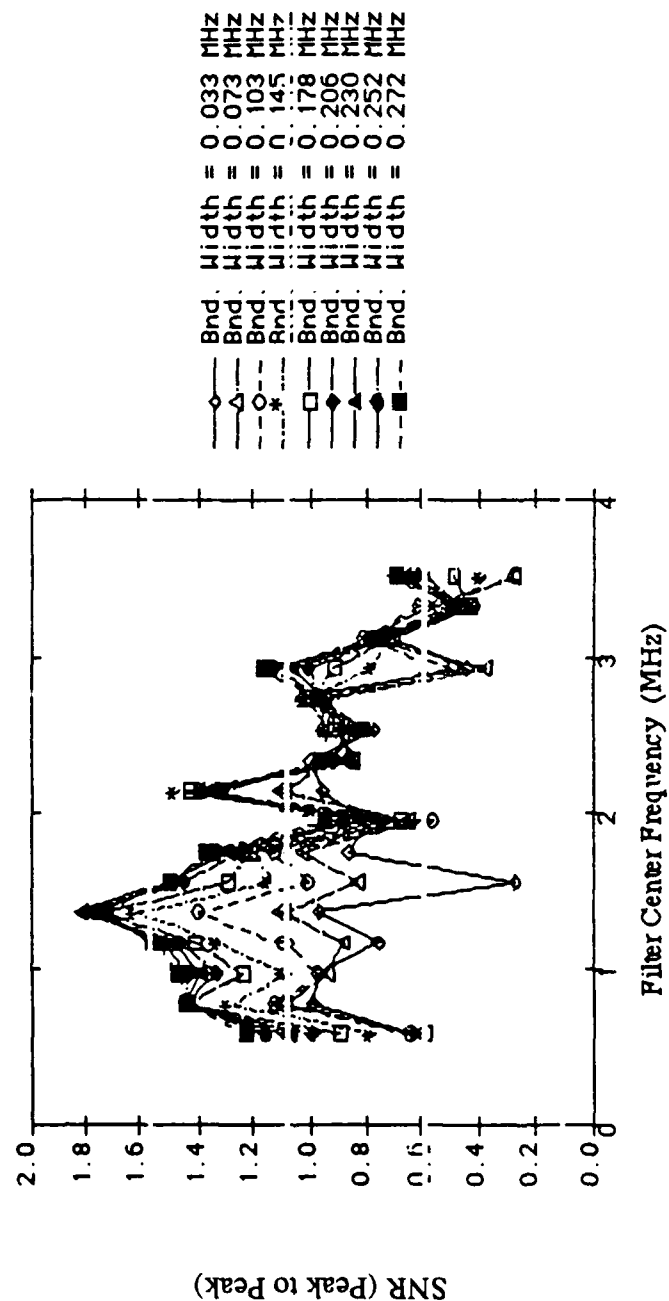


Figure 6.15 e Signal-to-noise ratio curves of the split time domain signals obtained for equiaxially grained CCSS for 90 degrees wave incidence.

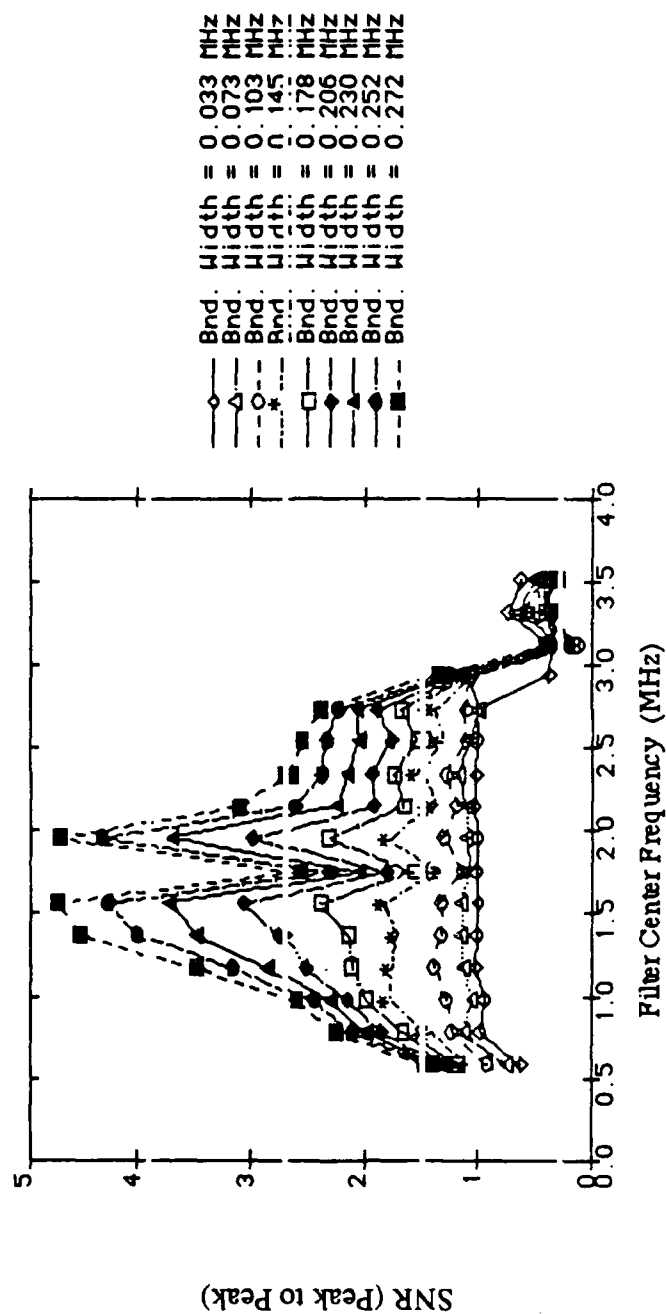


Figure 6.16 a Signal-to-noise ratio curves of the split time domain signals obtained for columnar grained CCSS for 0 degree wave incidence.

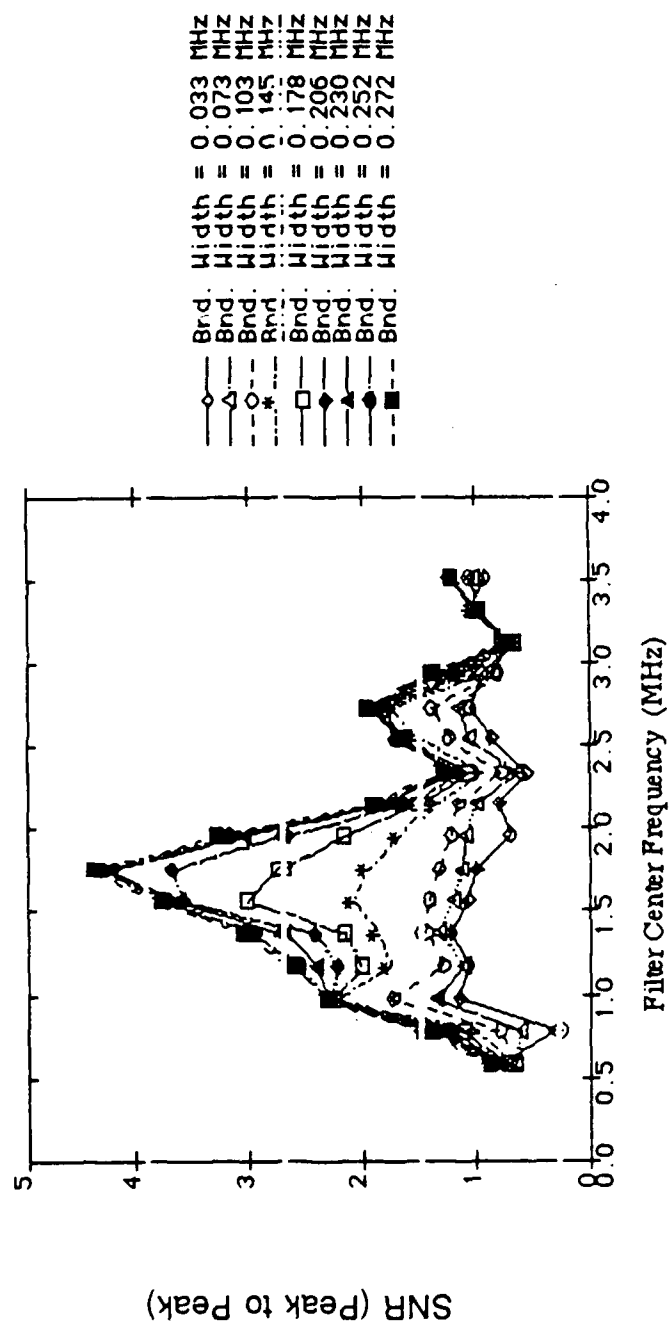


Figure 6.16 b Signal-to-noise ratio curves of the split time domain signals obtained for columnar grained CCSS for 15 degree wave incidence.

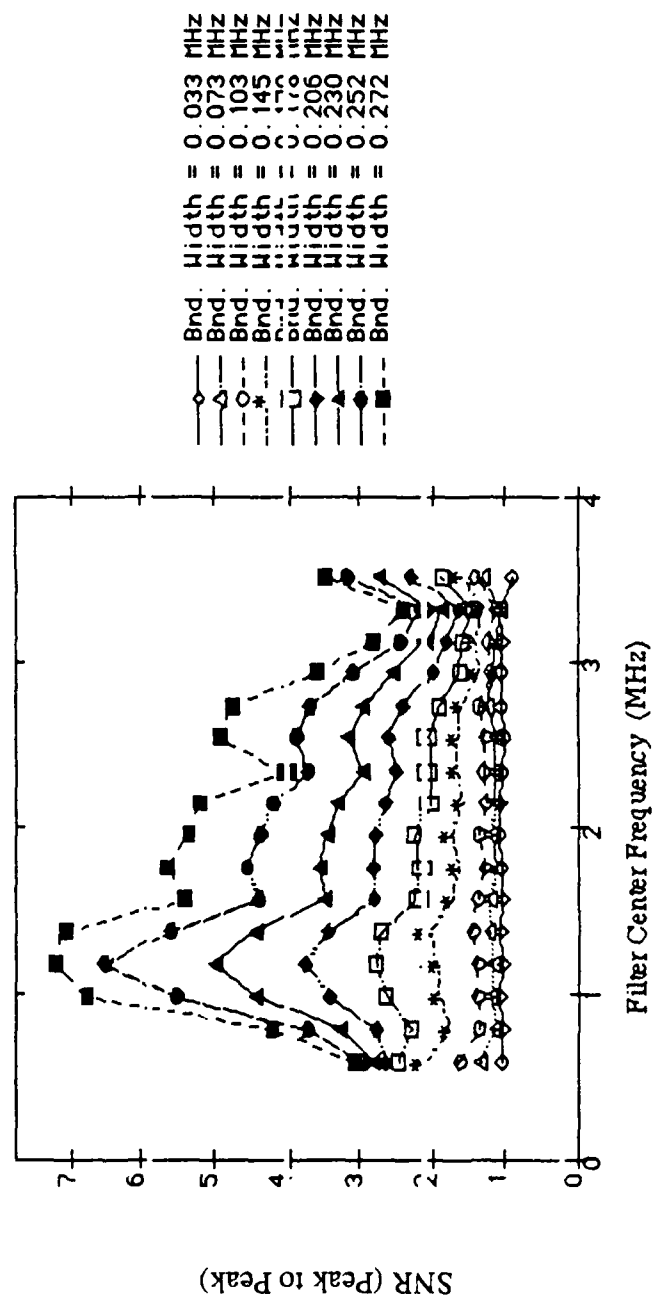


Figure 6.16 c Signal-to-noise ratio curves of the split time domain signals obtained for columnar grained CCSS for 45 degree wave incidence.

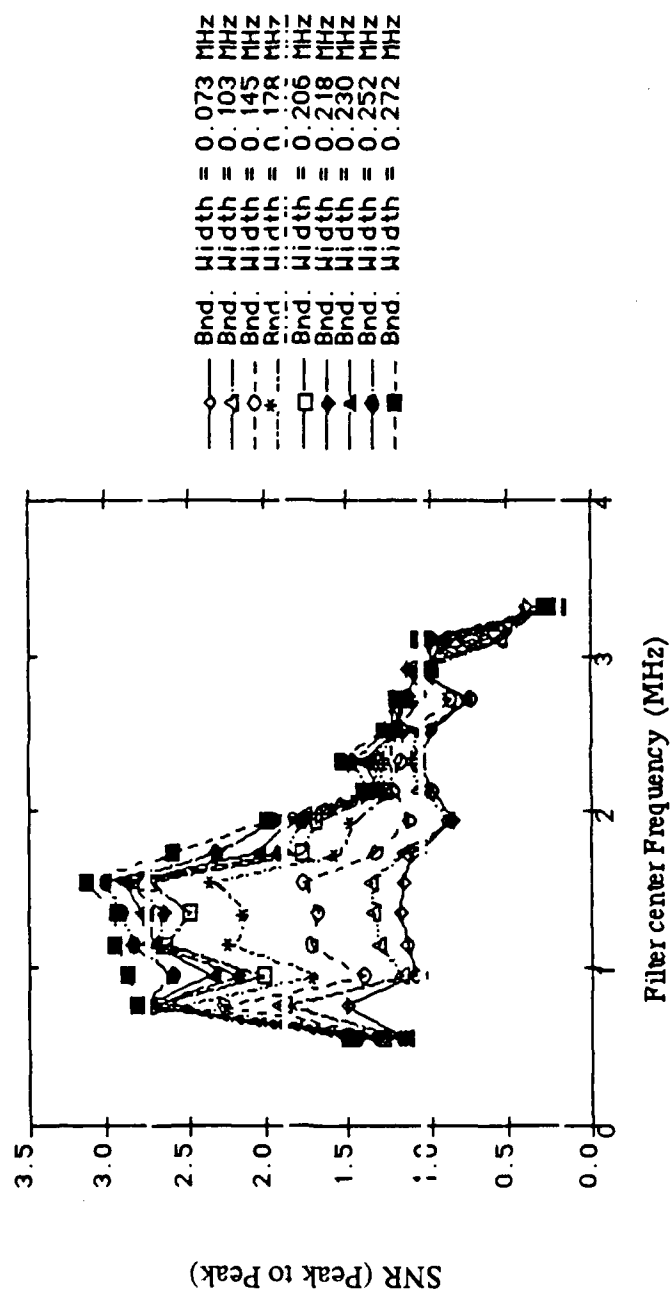


Figure 6.16 d Signal-to-noise ratio curves of the split time domain signals obtained for columnar grained CCSS for 75 degree wave incidence.

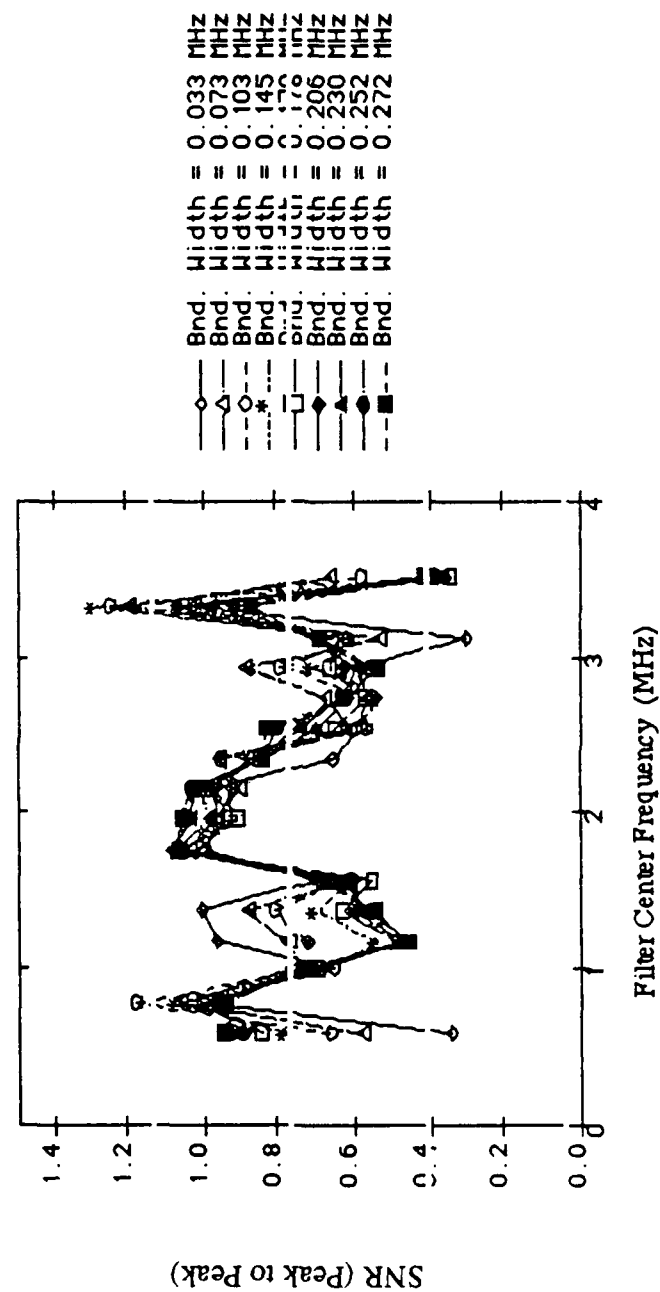


Figure 6.16 e Signal-to-noise ratio curves of the split time domain signals obtained for columnar grained CCSS for 90 degree wave incidence.

propagational in the 'ducts' (columnar grains) at the corresponding frequencies. The acoustic duct model suggests that the locations of the peaks in Figure 6.16a is proportional to the ratio between the cross sectional dimension of the columnar grains and the wavelength determined by the center frequency of the corresponding bandpass filter. It should also be pointed out here that the decrease in SNR due to a decreasing filter bandwidth is very much stronger for the columnar grains than for the equiaxed grains. However, since the columnar grains have irregular boundaries, further theoretical modeling and research with various frequencies and samples is necessary before a proper relationship between the grain dimension and the frequency can be defined. Nevertheless, the results in Figures 6.15 and 6.16 serve well to establish the feasibility of such a technique of grain characterization.

6.4 Discussion

There are several parameters like the bandwidth of the filters and the degree of overlap between the adjoining filters that are important for the processing technique. If the adjoining filters do not overlap, certain frequency components of the spectrum will be omitted from the processing resulting in poorer results. However, the bandwidth of the filters is also equally important. If the filters are too narrow relative to the bandwidth of the transducer, the performance of the technique will not show great improvements, even with a large overlap of the filters. Also, if the material being tested has high attenuation in the frequency range of the transducer, a narrow banded transducer or a lower frequency transducer might have to be used to retain the spectral components of the received signal in relation to the transmitted signal. There are other parameters like the total number of filters used, average size of the noise producing scatterers relative to the wavelength [44] etc., which will have some bearing on the results.

The results of the experiments presented in this chapter demonstrate the potential and the utility of SSP. However, it should be pointed out that SSP is not the panacea of all problems in ultrasonic nondestructive testing. It has been shown by others [2] that SSP is fairly insensitive to situations when the plane of the defect is not perpendicular to the direction of wave propagation. However, if the distance 'x' (Figure 6.17) through which one edge of the plane of the defect is displaced from the other edge is more than 3 to 4 times the wavelength, the technique will not be successful in SNR enhancement. However,

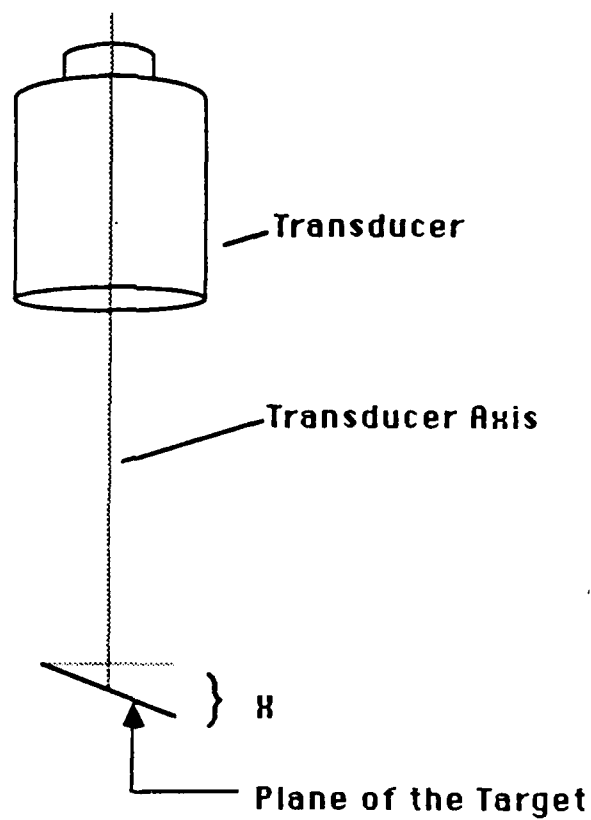


Figure 6.17 Schematic diagram showing a possible plane of orientation of a defect with respect to the axis of the transducer.

the drawback posed by the plane of the defect is characteristic of many of the ultrasonic techniques and is not specific to SSP alone. Nevertheless, the drawback could be overcome by inspecting the material using different angles of inspection if permitted by the geometry of the test specimen. Also, if the material is highly dispersive (about 8 to 10 percent or more) over the range of frequencies over which the bandpass filters are located, a simple application of the technique as discussed in this paper will not suffice. When the material is dispersive, it would be necessary to first determine the different velocities at each frequency of the filters and convert all the signals to a 'base' velocity using a ratio of the base velocity and the dispersive velocity of the individual filters. The same approach will have to be taken if the dispersion is due to the geometry of the test specimen instead of the physical property of the material being tested. It should also be remembered that the effect of dispersion, whether due to the geometry of the test specimen or the physical property of the material, is more severe for longer distances of wave propagation. Another limitation to the technique is from the size of the scatterers and the size of the target of interest relative to the wavelength. The scatterers should have a dimension equal to or smaller than the wavelength while the target should be at least 2 to 3 times the wavelength.

6.5 Summary

The split spectrum technique has indeed been demonstrated as an useful tool in ultrasonic NDE. Impressive results for a variety of engineering problems have been obtained. SNR enhancement in many engineering problems like CCSS, composite materials, welded joints and Zircalloy - Zirconium tubes has been obtained. Improvements in SNR ratio can be expected if physical considerations indicate that frequency dependent material noise is masking the reflector signal information. In addition to the SNR improvement, the material noise itself can be studied with this technique to obtain guidelines on grain structure and possible anisotropic material characteristics. The results presented in this chapter has shown that SSP has the potential to be an useful tool in grain characterization in materials like CCSS. However, further research is necessary for a better understanding of the relationship governing the wavelength - grain size interaction, especially in columnar grains.

The performance of the technique is dependent on a proper selection of such processing parameters as the number of filters, bandwidth etc. The implementation of the

technique will be successful if care is exercised in the selection of the processing parameters and if the technique is implemented with a careful consideration of the limitations discussed in this paper. Recent studies have shown that the number of filters is dependent on the bandwidth of the received signal and the total time duration of the signal (range). Also, the bandwidth of the filters should be at least three to four times the frequency separation between the adjoining filters.

7. SUMMARY, CONCLUSIONS AND FUTURE RESEARCH

This chapter summarizes the research work and conclusions of this dissertation and suggests possible directions for future research.

7.1 Summary

The second chapter of this dissertation provides a literature review about coherent noise in ultrasonic signals, speckle in ultrasonic images and methods of speckle reduction as proposed by various authors and researchers. A detailed literature review about SSP is also included based on which the objectives of this research work were developed.

The spectral splitting process has been formalized by modeling an ultrasonic signal as a time limited, band limited process which permits the use of the frequency sampling theorem to determine the total number of filters and their bandwidth. Experimental corroboration has been provided to support the theoretical modeling. Minimization algorithm was used for the experimental work done to support the theory. However, since the performance of the polarity thresholding algorithm modifies the parameter selection process, it was necessary to study the polarity thresholding algorithm to determine the performance limits of the algorithm.

Polarity thresholding algorithm has been analyzed to assess and to evaluate the performance of the algorithm and to establish the limits of performance. The problem has been approached by treating the signal as a stochastic process. A mathematical representation of the polarity thresholding algorithm has been presented using which the probability density function (pdf) of the output of the algorithm was derived. The derived pdf was used to calculate the theoretical SNR enhancement curves, the probability of false alarm, the probability of detection (POD) and the receiver operating characteristics (ROC) of the algorithm.

The sixth chapter of this dissertation has been dedicated to experimental work conducted to demonstrate the utility of SSP in various NDE applications. Signal-to-noise ratio enhancement in various materials like CCSS, composite material and Zircalloy tubes has been demonstrated. The potential of SSP as a tool for material characterization has been shown by experimentation.

7.2 Conclusions

The conclusions of this dissertation can be drawn under three categories: 1. Process modeling and parameter selection, 2. performance of the polarity thresholding algorithm, and 3. Utility of SSP.

7.2.1 Process modeling and parameter selection

1. The total number of filters to be used for 'optimum' SNR enhancement is given by the equation $N = BT$ where B is the available band width of the signal (ie., bandwidth of the received signal) and T is the total time duration of the signal being processed.
2. The ideal bandwidth of the theoretical SINC filters, for maximum SNR enhancement, is $2/T$ Hz where T is the total time duration of the signal. However, the bandwidth of the Gaussian filters used for the actual processing has been found to be at least 2 to 3 times the theoretical bandwidth.

The actual filter bandwidth is a function of the type and size of the scatterers present in the material as well as the size of the smallest anomaly to be detected. The filter bandwidth is inversely proportional to the size of the scatterers and directly proportional to the size of the smallest anomaly that is to be detected. Hence, it is obvious that the optimum filter bandwidth is a balance between SNR enhancement and the probability of detection. As a result, the 'optimum' filter bandwidth necessary for the processing should be determined for each type of material to be tested because the theoretical bandwidth ($2/T$ Hz) gives only an approximate starting point. Conceptually, the 'optimization' of the filter bandwidth can be achieved by using a reference block made of the same material being tested and containing 'pre-programmed' defects of required sizes situated at suitable depths.

3. The SNR enhancement deteriorates rapidly when fewer than the 'optimum' number of filters ($N=BT$) is used. However, SNR enhancement does not show any substantial deterioration, and might even show some improvement, when the

number of filters is increased beyond the 'optimum'. Nevertheless, it is not economical to use more than the optimum number of filters because of the excessive increase in the processing time.

4. The available bandwidth of the received signal is a function of the type and the size of the scatterers present in the material being tested. The selection of the bandwidth of the received signal to place the bank of filters is also influenced by the size, geometry and/or orientation of the target of interest. As a result, it is essential to 'tune' or optimize the processing parameters using a calibration block made of the same material as the test material and containing known defects of required size at specified depths.

7.2.2 Performance of the Polarity Thresholding algorithm

1. The SNR enhancement obtained by using the polarity thresholding algorithm is a function of both the number of filters and the input SNR. As a result, the maximum possible SNR enhancement as well as the number of filters necessary to achieve the maximum SNR enhancement are dependent on the input SNR.
2. The 'optimum' number of filters for use in conjunction with the polarity thresholding algorithm can be found either from Figure 5.2 (page 48) or by numerically solving (5.22) [page 47]. Thus, the 'optimum' number of filters to be used for the polarity thresholding algorithm is the minimum of the number of filters calculated from i. Figure 5.2 , and ii. Equation $N=BT$.
3. Polarity thresholding algorithm should not be used when the input SNR is less than or equal to unity because of a very high probability of losing the target altogether exists.
4. The filter bandwidth for the polarity thresholding algorithm is generally smaller than that required for minimization. A bandwidth of about $4/T$ Hz provides an excellent SNR enhancement. However, a larger bandwidth is necessary for increased probability of detection (POD) but at the expense of a decreased SNR enhancement.

Thus, the optimum bandwidth of the filters is a balance between the SNR enhancement and the probability of detection of the algorithm.

5. Polarity thresholding algorithm is best suited for use in conjunction with other SSP algorithms like minimization and provides a superior SNR enhancement than when either of the two algorithms is used by itself.
6. The probability of false alarm and the probability of detection of the algorithm are dependent on the total number of filters used for the processing.
7. The polarity thresholding algorithm is very severe in its present form thereby resulting in low POD for small input SNR values. However, lesser severe forms of the algorithm can be implemented by tolerating more than one polarity change.

7.2.3 Utility of Split Spectrum Processing

1. The potential of SSP in SNR enhancement and improvement of detectability has been conclusively demonstrated in various types of engineering materials.

Equiax grained CCSS poses the most challenging problem for SNR enhancement because the grain size is of similar order of magnitude as the wavelength in the material for frequencies in the range of one to five megahertz. Nevertheless, the experimental results presented in this dissertation has indeed shown that the SSP technique performs satisfactorily in equiaxed CCSS even when the input SNR is close to unity. Similar results have been presented for columnar grained samples also.

Results of SNR enhancement in Carbon-Epoxy composite material is also presented to demonstrate the versatile applicability of SSP. The result does show a remarkable SNR enhancement in Carbon-Epoxy composite materials.

Improved detectability and SNR enhancement has also been accomplished in a clad material using a Zircalloy tube clad internally by Zirconium. The results

demonstrate the utility of SSP in different engineering problems when coherent material noise is the source of difficulty.

2. Split spectrum processing has also been found to be very useful in speckle suppression and SNR enhancement in B-scan images. The lateral resolution in a B-scan image is unaffected by SSP while the axial resolution is affected resulting in sharper boundary detection.
3. Finally, the potential of SSP as a tool for material grain characterization has been demonstrated through experimentation. Although it is not possible to draw quantitative grain size estimation from the preliminary experimental data presented in this dissertation, the results prove the feasibility of using SSP for the determination of grain type and size. Further research is necessary before quantitative results can be obtained by this technique.

7.3 Future Research

Three important areas of SSP need to be researched further to harness the potential of SSP and to make the technique useful. They are, i. implementation of SSP through hardware, ii. implementing SSP in conjunction with Synthetic Aperture Focusing Technique (SAFT), and iii. SSP as tool for material characterization. These aspects are discussed next.

7.3.1 Hardware implementation of SSP

The split spectrum processing technique has been researched, developed and understood over the last one decade. However, the technique has remained in a research environment mainly because it is currently being implemented by software and hence is very time consuming. If the technique is to be accepted by the industry as a standard, it is critical to implement the techniques as close to 'real time' as possible. A 'real time' processing is possible only by a hardware implementation of the technique.

The SSP hardware circuitry can be analog, digital or a combination of the two. Systolic arrays, which are becoming popular in digital signal processing, appear to be a

good method of 'real time' implementation of SSP.

7.3.2 Split spectrum processing and SAFT

The Synthetic Aperture Focussing Technique (SAFT) is a well accepted and effective method of mimicking large apertures as well as coherent noise reduction. SAFT has the effect of improving lateral resolution and reduced noise level. At the same time, SSP sharpens the axial resolution and reduces coherent noise. Consequently, a combined implementation of SAFT and SSP should improve both axial resolution and lateral resolution while providing improved SNR enhancement. Further, various new algorithms like multiple sector maximization, multiple sector minimization etc. can be tried with a combined implementation of SAFT and SSP.

7.3.3 SSP as a tool for material characterization

The results presented in this dissertation prove the potential of SSP as a tool for material characterization. However, further research in theoretical and experimental aspects of physics and mechanics of wave propagation, scattering theory and the waveguide phenomenon is necessary before quantitative grain type and size estimates can be drawn using the SSP approach.

LIST OF REFERENCES

LIST OF REFERENCES

1. Rose J. L. and B. B. Goldberg, "Basic Physics in Diagnostics Ultrasound", John Wiley & Sons, New York, 1979.
2. Bilgutay N. M., "Split-spectrum Processing for Flaw-to-Grain Echo Enhancement in Ultrasonic Detection", Ph.D. Thesis, Purdue University, Laffayette, 1981.
3. Furgason E. S., V. L. Newhouse, N. M. Bilgutay and G. R. Cooper, "Application of Random Signal Correlation Technique to Ultrasonic Flaw Detection", Ultrasonics, Vol. 13, No. 1, pp:11-17, Butterworth Scientific, Guildford, U.K., January, 1975.
4. Bilgutay N. M., E. S. Furgason, and V. L. Newhouse, "Evaluation of Random Signal Correlation System for Ultrasonic Flaw Detection", IEEE Transactions on Sonics and Ultrasonics, Vol. SU-23, pp:329-333, September 1976.
5. Kraus S. and K. Goebbels, "Improvement of Signal-to-Noise Ratio for the Ultrasonic Testing of Coarse Grained Materials by Signal Averaging Techniques", Proceedings of the First International Symposium on Ultrasonic Material Characterization, pp:104, NBS, Gaithersburg, MD, June 1978.
6. Kennedy J. C. and W. E. Woodmansee, "Signal Processing in Nondestructive Testing", Journal of Testing and Evaluation, Vol. 3, No. 1, pp:26-45, January 1975.
7. Cutrona L. J., E. N. Leith, L. J. Porcello and W. E. Vivian, "On the Application of Coherent Optical Processing Techniques to Synthetic-Aperture Radars", Proceedings of IEEE, Vol. 54, pp:1026-1032, 1966.
8. Beasley E. W. and H. R. Ward, "A Quantitative Analysis of Sea Clutter Decorrelation with Frequency Agility", IEEE Transaction on Aerospace Electronic System, Vol. AES-4, No. 3, pp:468-473, May 1968.
9. Kock W. E., "Acoustic Holography", Physical Acoustics, Vol. X, Editors: W. P. Mason and R. N. Thurston, Academic Press, pp:297-384, 1973.
10. Corl P. D., G. S. Kino, C. S. DeSillets and P.M. Grants, "A Digital Synthetic

- Focus Acoustic Imaging System", Acoustic Holography, Vol. 8, Ed: A. F. Metherell, Plenum Press, New York, 1980.
11. Kino G. S., P. D. Corl, S. Bennett and K. Peterson, "Realtime Synthetic Aperture Imaging System", Proceedings of the IEEE Ultrasonics Symposium, pp: 722-731, 1980.
 12. Schmitz V., W. Miller and G. Schafer, "Classification and Reconstruction of Defects by Combined Acoustical Holography and Line-SAFT", New Procedures in Nondestructive Testing, Editor: P. Holler, Springer-Verlag, Berlin, Heidelberg, pp:95-104, 1983.
 13. Schmitz V., W. Muller and G. Schafer, "Flaw Sizing and Flaw Characterization With Holo-SAFT", Materials Evaluation, Vol. 42, April 1984, pp:439-443.
 14. Porcello, Massey, Innes and Marks, "Speckle Reduction in Synthetic Aperture Radars", Journal of the Optical Society of America, Vol. 66, No. 11, pp:1305-1311, November 1976.
 15. Newhouse V. L., E. S. Furgason, N. M. Bilgutay and J. Saniie, "Flaw-to-Grain Echo Enhancement", Proceedings of the Ultrasonic International Symposium, Butterworth Scientific, Guildford, U.K., pp:152-156, 1979.
 16. Goodman W., "Statistical Properties of Laser Speckle and Related Phenomenon", in Laser Speckle, Ed: J. C. Dainty, Springer-Verlag, New York, pp:9-75, 1975.
 17. Abbott J. G. and F. L. Thurstone, "Acoustic Speckle", Ultrasonic Imaging, Vol. 1, pp:303-327, 1979.
 18. Burckhardt C. B., "Speckle in Ultrasound B-Mode Scans", IEEE Transactions on Sonics and Ultrasonics, Vol. SU-25, No. 1, pp:1-6, January 1978.
 19. Parker D. L., T. A. Pryor and J. D. Ridges, "Enhancement of Two Dimensional Echocardiographic Images by Lateral Filtering", Computers and Biomedical Research, Vol. 12, pp:265-277, 1979.
 20. Parker D. L. and T. A. Pryor, "Analysis of B-scan Speckle Reduction by Resolution Limited Filtering", Ultrasonic Imaging, Vol. 4, pp:108-125, 1982.
 21. Wells P. N. T. and M. Halliwell, "Speckle in Ultrasonic Imaging", Ultrasonics, Butterworth Scientific, pp:225-229, September 1981.
 22. O'Donnell M., "Phase-insensitive Pulse-echo Imaging", Vol. 4, No. 4, pp:321-325, October 1982.

23. Dickinson R. J., "Processing of Ultrasound Images to Reduce Speckle", Proceedings of the IEEE Ultrasonic Symposium, October 1982.
24. Shattuck D. P. and O. T. von Ramm, "Compound Scanning With A Phased Array", Ultrasonic Imaging, Vol. 4, pp:93-107, 1982.
25. Maginin P. A., O. T. von Ramm and F. L. Thurstone, "Frequency Compounding for Speckle Contrast Reduction in Phased Array Images", Ultrasonic Imaging, Vol. 4, pp:267-281, 1982.
26. Wagner R. F., S. W. Smith, J. M. Sandrik and H. Lopez, "Statistics of Speckle in Ultrasound B-scans", IEEE Transactions on Sonics and Ultrasonics, Vol. 30, No. 3, pp:150-163, May 1983.
27. Smith S. W., F. F. Wagner, J. M. Sandrik and H. Lopez, "Low Contrast Detectability and Contrast/Detail Analysis in Medical Ultrasound", IEEE Transactions on Sonics and Ultrasonics, Vol. 30, No. 3, pp:164-173, May 1983.
28. Smith S. W. and R. F. Wagner, "Ultrasound Speckle Size and Lesion Signal to Noise ratio: Verification of Theory", Ultrasonic Imaging, Vol. 6, pp:174-180, 1984.
29. Patterson M. S. and F. S. Foster, "The Improvement and Quantitative Assessment of B-mode Images Produced by an Annular Array/Cone Hybrid", Ultrasonic Imaging, Vol. 5, pp:195-213, 1983.
30. Kerr A. T., M. S. Patterson, F. S. Foster and L. F. Van-der-Wal, "Speckle Reduction in Pulse Echo Images by Using Phase Insensitive Summation and Multiplicative Techniques", Acoustical Imaging, Proceedings of the 14th International Symposium, April 1985.
31. Kerr A. T., M. S. Patterson, F. S. Foster and J. W. Hunt, "Speckle Reduction in Pulse Echo Imaging Using Phase Insensitive and Phase Sensitive Signal Processing Techniques", Ultrasonic Imaging, Vol. 8, No. 1, pp:11-28, January 1986.
32. Melton, Jr. H. E. and P. A. Magnin, "A-mode Speckle Reduction With Compound Frequencies and Compound Bandwidths", Ultrasonic Imaging, Vol. 6, pp:159-173, 1984.
33. Shankar P. M. and V. L. Newhouse, "Speckle Reduction With Improved Resolution in Ultrasound Images", IEEE Transaction on Sonics and Ultrasonics, Vol. SU-32, No. 4, pp:5437-543, July 1985.

34. Shankar P. M., "Speckle Reduction in Ultrasound B-scans Using Weighted Averaging in Spatial Compounding", IEEE Transactions on Ultrasonics, Ferroelectrics and Frequency Control, Vol. UFFC-33, No. 6, pp:754-758, November 1986.
35. Wagner R. F., M. F. Insana and D. G. Brown, "Progress in Signal and Texture Discrimination in Medical Imaging", Proceedings of SPIE, Vol 535, Applications of Optical Instrumentation in Medicine, pp:57-64, 1985.
36. Wagner R. F., M. F. Insana and D. G. Brown, "Unified Approach to the Detection and Classification of Speckle Structure in Diagnostic Ultrasound", Proceedings of SPIE, Vol 556, International Conference on Speckle, pp:146-152, August 1985.
37. Insana M. F., R. F. Wagner, B. S. Garra, D. G. Brown and T. H. Shawkar, "Analysis of Ultrasound Image Texture via Generalized Rician Statistics", Proceedings of SPIE, International Conference on Speckle, Vol. 556, pp:153-159, August 1985.
38. Bamber J. C. and C. Daft, "Adaptive Filtering for Reduction of Speckle in Ultrasonic Pulse-echo Images", Ultrasonics, pp:41-44, January 1986.
39. Trahey G. E., S. W. Smith and O.T. von Ramm, "Speckle Reduction in MEDical Ultrasound via Spatial Compounding", SPIE Medicine XIV PACS IV, pp:626-651, 1986.
40. Trahey G. E., J. W. Allison, S. W. Smith and O. T. von Ramm, "A Quantitative Approach to Speckle Reduction via Frequency Compounding", Ultrasonic Imaging, Vol. 8, pp:151-164, 1986.
41. Furgason E. S., N. M. Bilgutay, B.B. Lee and V. L. Newhouse, "Random Signal Correlation and Split Spectrum Processing", Proceedings of the First Workshop on Nondestructive Evaluation of Titanium Alloys, Edited by O. P. Arora, H.H. Chaskelis and N. K. Batra, Office of Naval Research, Arlington, VA 22217, pp:169-179, December 1980.
42. Newhouse V. L., N. M. Bilgutay, J. Saniie and E. S. Furgason, "Flaw-to-Grain Echo Enhancement by Split Spectrum Processing", Ultrasonics, Vol. 20, pp:59-68, 1982.
43. Draheim W. A. and E. S. Furgason, "A Two Dimensional Approach to Clutter Rejection in Ultrasonic Images", Proceedings of the IEEE Ultrasonics Symposium, pp:1000-1004, 1983.
44. Bilgutay N. M. and J. Saniie, "The Effect of Grain Size on Flaw Visibility

Enhancement Using Split-spectrum Processing", *Materials Evaluation*, Vol. 42, pp:808-814, 1984.

45. Brase J., R. McKinney, K. Blaedel, J. Oppenheimer, S. Wang and J. Simmons, "An Automated Ultrasonic Test Bed", *Materials Evaluation*, Vol. 42, pp:1619-1625, 1984.
46. Newhouse V. L., P. Karpur, J. L. Rose and I. Amir, "A New Technique for Clutter Reduction in Ultrasonic Imaging", *Proceedings of the IEEE Ultrasonics Symposium*, Vol. 2, pp:998-1003, October 1985.
47. Amir I., "Clutter Suppression and Texture Estimation in Non-Destructive Evaluation", Ph.D. Dissertation, Drexel University, Philadelphia, 1986.
48. Baligand B., M. Grozellier and D. Romy, "Improvement of Ultrasonic Examination of Austenitic Steels", *Materials Evaluation*, Vol. 44, pp:577-581, April 1986.
49. Amir I., N. M. Bilgutay and V. L. Newhouse, "Analysis and Comparison of Some Frequency Compounding Algorithms for the Reduction of Ultrasonic Clutter", *IEEE Transactions on Ultrasonics, Ferroelectrics and Frequency Control*, Vol. UFFC-30, No. 4, pp:402-411, July 1986.
50. Bencharit U., J. L. Kaufman, N. M. Bilgutay and J. Saniie, "Frequency and Spatial Compounding Techniques for Improved Ultrasonic Imaging", *Proceedings of IEEE Ultrasonics Symposium*, 1986.
51. Li Y., "Two Signal Processing Techniques for the Enhancement of the Flaw-to-Grain Echo Ratio", Master's Thesis (in Chinese), Academia Sinica, China, 1985.
52. Li Y. and C-F Ying, "Two Signal Processing Techniques for the Enhancement of the Flaw-to-grain Echo Ratio", *Ultrasonics*, Butterworth Scientific, Vol. 25, pp: 90-94, March 1987.
53. Rose J. L., P. Karpur and V. L. Newhouse, "Utility of Split Spectrum Processing in Ultrasonic NDE", accepted for publication in *Materials Evaluation*.
54. Shankar P. M., P. Karpur, V. L. Newhouse and J. L. Rose, "Split Spectrum Processing: Analysis of the Polarity Thresholding Algorithm for Improvement of Signal-to-noise Ratio and Detectability in Ultrasonic Signals", submitted to the *IEEE Transactions on Ultrasonics, Ferroelectrics and Frequency Control*.
55. Papoulis A., "The Fourier Integral and its applications", McGraw-Hill, New York, 1962.

56. Skudrzyk E., "The Foundations of Acoustics", Springer-Varlag, New York, 1971.
57. Eeyszig E., "Advanced Engineering Mathematics", Second Edition, pp:473-475, John Wiley and Sons, Inc., New York, 1968.
58. Newhouse V. L., J. L. Rose, P.Karpur and P. M. Shankar, "SplitSpectrum Processing: Performance of the Polarity Thresholding Algorithm in Signal-to-noise Ratio Enhancement in Ultrasonic Applications", Proceedings of 'The Review of Progress in Quantitative NDE', June, 1987.
59. Whelan A. D., "Detection of Signals in Noise", Academic Press, New York, 1971.
60. Van Treas H. L., "Detection, Estimation and Modulation Theory", Part I, New York, Wiley, 1968.
61. Karpur P., P. M. Shankar, J. L. Rose and V. L. Newhouse, "Split Spectrum Processing: Optimizing the Processing Parameters Using Minimization", Ultrasonics, Vol. 25, July 1987, pp:204-208.
62. Rose J. L., "Elements of a Feature Based Ultrasonic Inspection System", Materials Eveluation, Vol. 42, February 1984, pp:210-218.
63. Nestleroth J. B., J. L. Rose, M. Bashyam and K. Subramanyam, "Physically Based Ultrasonic Feature Mapping for Anomaly Classification in Composite Materials", Materials Eveluation, Vol. 43, April 1985, pp:541-546.
64. Papadakis E. P., "Ultrasonic Attenuation Caused by Scattering in Polycrystalline Metals", Journal of the Acoustical Society of America, Vol.37, pp:711-717, 1965.
65. Saniie J. and N. M. Bilgutay, "Quantitative Grain Size Evaluation Using Ultrasonic Backscattered Echoes", Journal of the Acoustical Society of America, Vol. 80, December 1986, pp:1816-1824.
66. Morse P. M. and K. V. Ingard, "Theoretical Acoustics", McGraw Hill Book Company, New York, 1968.
67. Meeker T. R. and A. H. Meitzler, "Guided Wave Propagation in Elongated Cylinders and Plates", in 'Physical Acoustics', Vol. 1-Part A, edited by W. P. Mason, Academic Press, New York, 1964.
68. Jeong Y. H., "An Ultrasonic Material State Classifier for Elastically Anisotropic Materials", Ph. D. Dissertation, Drexel University, Philadelphia, 1986.
69. Kanefsky M. and J. B. Thomas, "On Polarity Detection Schemes with Non-

Gaussian Inputs", Journal of the Franklin Institute, Vol. 280, No. 2, pp:120-138, August 1965.

70. Wolff S. S., J. B. Thomas and T. R. Williams, "The Polarity-Coincidence Correlator: A Nonparametric Detection Device", Transactions of I. R. E. on Information Theory, Vol. IT-8, pp:5-9, January 1965.
71. Krautkramer J. and H. Krautkramer, "Ultrasonic Testing of Materials", Third Edition, Springer-Verlag, New York, 1983.
72. Shankar P. M., U. Bencharit, N. M. Bilgutay and J. Saniie, "Grain Noise Suppression in NDE Through Bandpass Filtering", submitted to Materials Evaluation.
73. Karpur P., P. M. Shankar, J. L. Rose and V. L. Newhouse, "Split Spectrum Processing: Determination of the Available Bandwidth for Spectral Splitting", Submitted to Ultrasonics, Butterworth Publishers.